

Mapping the Jurassic/Cretaceous lithological units in the Buëch area in France using Sentinel-2 and ASTER

MSc Thesis
Adomas Liepa

Department of Physical Geography
Faculty of Geosciences
Utrecht University

Supervisors:

Dr. Steven de Jong

Dr. Wiebe Nijland



November 2019 – April 2020

Table of Contents

Abstract.....	1
1. Introduction.....	2
1.1 General background.....	2
1.2 Approaches in spectral mapping.....	3
1.3 Challenges in identification and mapping of minerals using imaging spectroscopy	4
1.4 Research objectives and questions.....	5
1.5 Outline of the thesis	5
2. Study area	7
2.1 Site location and description	7
2.2 Geological setting	7
2.3 Climatic setting.....	9
3. Data and Methodology.....	9
3.1 Fieldwork and sample collection	9
3.1.1 Description of lithological units.....	9
3.1.2 Field data collection and sample locations	13
3.2 Image spectroscopy.....	14
3.2.1 Imaging spectroscopy principle	14
3.2.2 PSR+3500 spectroradiometer	15
3.2.3 Building spectral libraries.....	16
3.3 Satellite data	18
3.3.1 Sentinel-2 and ASTER.....	18
3.3.2 Imagery selection.....	21
3.3.3 Image pre-processing.....	21
3.4 Spectral mapping techniques	25
4. Results	28
4.1 Spectral signatures of lithological groups	28
4.2 Comparison of spectral mapping	29
4.3 Comparison of spectral libraries	36
4.4 PSR+ spectroradiometer performance	38
5. Discussion.....	41
6. Conclusion	49
References:.....	51
Appendix A - full lithological maps of the study area.....	57
Appendix B - fresh and weathered rocks	64
Appendix C - results using different mapping techniques.....	66

Abstract

Spaceborne remote sensing performs a significant role today in geological mapping, interpretation and analysis of large areas in a rapid and cost-efficient manner. Spaceborne satellite imagery have been successfully utilized in lithological mapping of arid areas, however, similar approaches for lithological mapping in semi-arid regions with high degree of structural complexity, vegetation and topographic effects are yet to be developed. The primary objective of this study is to combine field-based spectroscopic research with geological remote sensing in obtaining representative lithological maps of the Buëch area in South-East France. To achieve this aim Support Vector Machine (SVM) classifier and Spectral Angle Mapper (SAM) were used on Sentinel-2 and ASTER imagery. Spectroscopic examination of field samples enabled the creation of spectral endmembers representative for the area and detection of local weathering mechanisms. The results derived from SVC classifier showed great pattern-recognition ability and more accurate classification of different lithological groups. SAM derived thematic mapper demonstrated the ability to correctly classify a great portion of blue marl outcrops, by recognising the lack of spectral response displayed by blue marls as being the distinctive indicator of the class. Using and evaluating different satellite imagery shows that Sentinel-2 allows better mapping in this semi-arid area, indicating that the higher spatial resolution of Sentinel-2 has an edge over the higher spectral resolution in the SWIR range of ASTER for this specific setting and methodology. The study has shown that field-based spectroscopic research complements geological remote sensing well. The limiting factor in achieving better classification is the spectral and spatial properties of the satellite imagery. Therefore, future research should consider the integration of hyperspectral data and assimilation of geomorphic products to increase the accuracy of lithological unit discrimination.

Key words: Geological mapping, Image spectroscopy, SVM, SAM, ASTER, Sentinel-2, France

1. Introduction

1.1 General background

Geologic maps provide valuable insight into Earth's structural and mineralogical composition (Nahmi et al., 2017; Fal et al., 2019). These maps are an essential part of solving issues centered around Earth resources, environment, land-use planning and hazards (Rajesh, 2014). Field geological research has for a long time been the primary method in obtaining geologic maps. However, satellite imagery obtained from spaceborne optical sensors in the late 1970s (Bishop et al., 2018) enabled the field of applied geology to enter a new era (Nahmi et al., 2017). Nowadays, remote sensing has been often utilized as an initial step in geologic exploration of the surface (Unger & Sikhegyi, 2004). Application of remote sensing allow us to learn new techniques in identifying different lithological units and apply these in areas featuring dense vegetation or difficult accessibility while simultaneously increasing the surveying scale.

Solid knowledge and understanding of rocks, soils, minerals and their spectral nature in the electromagnetic (EM) spectrum exist (Kruse, 2010). When a rock or a mineral is subjected to light, the interaction between the matter and the EM radiation from the light source results in selective absorption and transmission (Van der Meer & de Jong, 2006). In image spectroscopy, each objects specific response to the subjected radiation from a light source results in a spectral signature unique to that object (Fal et al., 2019). That is why rocks, minerals and other material have characteristic electromagnetic spectra (Krishnamurthy & Sreenivasan, 2005). The relationship between the wavelength and intensity of electromagnetic radiation is what we now know as the spectral signature of an object (Gupta P R., 2017). These spectral signatures, also referred to as "reflectance spectra" have been successfully utilized in obtaining structural information of the Earth's surface (Rudorff et al., 2011; Parashar et al., 2016; Kruse, 2010).

Airborne sensors have greatly evolved and are now capable of providing spectral measurements that were until recently only feasible by field spectrometry (Van der Meer & de Jong, 2006). The emergence of spaceborne sensors unveils a range of new possibilities for surface mapping.

Since the year 2000, Advanced Spaceborne Thermal Emission and Reflectance Radiometer (ASTER) emerged as the "work horse" of geological remote sensing research (Van der Meer et al, 2014; Abrams, 2000; Cudahy & Hewson, 2002; Yamaguchi et al, 2003). Rowan & Mars (2003) successfully discriminated the major lithological units in the Mountain Pass, California by applying spectral-matching algorithms. Employment of spectral analysis algorithms such as spectral angle mapper (SAM) over traditional methods such as maximum likelihood classifier (MLC) has shown to be advantageous in lithological classification by Qui et al. (2006). Gomez et al. (2005) displayed the capabilities of ASTER in classifying lithological units based on geological maps in Namibia. Inclusion of laboratory-derived reflectance of rock samples in spectral lithological analysis in Oscar II Coast Area, Antarctic

Peninsula was successfully demonstrated by Haselwimmer et al. (2009). The potential of ASTER in lithological mapping has been well documented and proven to be advantageous.

The launch of Sentinel-2 in 2005 provided the remote sensing community with a new tool to analyze the Earth's surface. The potential of multispectral instrument onboard Sentinel-2 for geological studies was first assessed by Van der Meer et al. (2014). He derived Sentinel-2 band ratios as an analogue of ASTER band ratios and applied them as proxies for mineral mapping. Van der Meer et al. (2014) demonstrated a high-quality correspondence between Sentinel-2 and ASTER bands, and concluded that these proxies can be utilized in mineral mapping. A comparison between ASTER and Sentinel-2 in terms of lithological unit classification using knowledge-based approach was demonstrated in North-East Greenland (Salehi et al., 2019). The importance of Sentinel-2 imagery in geological mapping was shown by applying spectral matching algorithms in Tafilalet basin, Morocco (Fal et al., 2019). Application of Sentinel-2 imagery for the purposes of lithological mapping has been shown to be capable of producing excellent geological maps (Nahmi, et al., 2017). The capabilities of Sentinel-2 and ASTER for geological mapping has been the subject of numerous comparative research papers and their potential has been greatly analyzed in various settings.

1.2 Approaches in spectral mapping

Spectral mapping can be defined as the extraction of qualitative and quantitative knowledge from remotely-sensed reflectance and emittance spectra, based on the wavelength- and albedo-dependant features of the object (Mustard and Sunshine, 1999). Spectral mapping is synonymous with spectral processing and spectral analysis. It is comprised of all methods and techniques for classification, characterization, detection and recognition of objects in a hyperspectral as well as multispectral scenes (Chang, 2003, 2007; van der Meer & de Jong, 2006, Kruse 2010, 2012).

Spectral mapping begins with appropriate selection of satellite imagery. Satellites differ in mission objectives, spectral bands, revisit times and many other distinctive features. Therefore, in addition to research objective, the selection of satellite data depends on data availability, situational circumstances and satellite capabilities as well.

Open-source satellite data comes in various formats. Whether the data comes as a series of digital numbers, radiance or reflectance, it has to be processed and prepared prior to further analysis. Pre-processing aims at preparing the data by compiling, subsetting, correcting and transforming it to contain information solely relevant to further analysis (Guyon, 2008; Hastie et al., 2009). Pre-processing includes use of various digital enhancement techniques, radiometric correction, atmospheric correction, noise reduction methods and masking of secondary objects such as clouds, ice, vegetation and water.

Once the satellite data is prepared, the focus shifts towards gathering of input data and selection of processing methods. Laboratory-based spectra are ideally absent of interferences and complexities caused by weathering, water, vegetation, organic matter or soil cover. In contrast, in situ spectra are often subjected to these disturbances (Gupta P R., 2017). The degree of similarity between laboratory spectra and in situ spectra depends highly on the surrounding conditions of the samples on which the in-situ spectra have been acquired. The detailed spectra obtained from controlled conditions in the laboratory or in situ rock samples are collected and used to build spectral libraries. The components of spectral libraries, also known as *endmembers*, are used as reference spectra in algorithms such as Spectral Angle Mapping (SAM) and Support Vector Machine (SVM) classifier.

1.3 Challenges in identification and mapping of minerals using imaging spectroscopy

In order to reproduce promising lithology mapping results, many conditions should be met: (1) the study site should be relatively vacant of vegetation, with vegetation ideally taking up less than 30 % per pixel, (2) the subject lithological units should be exposed and the outcrop should preferably be larger than the pixel size of the sensor, (3) secondary effects such as weathering should only have a minor influence, (4) the spectral signatures of the targeted units should have a high albedo relative to the background and be spectrally unique for each unit to ensure separability, and (5) the satellite data used should be of very high quality (Van der Meer & de Jong, 2006). Majority of examples showing the promising results of mineral and lithological mapping meet most, if not all of the conditions listed.

A significant challenge in obtaining similar quality results in semi-arid areas featuring less favourable conditions lies in reduction of the vegetation effect. Vegetation in high resolution satellite imagery often make up a considerable part of a pixel, making mapping of lithology in the area difficult. In areas with significant changes between seasons, vegetation introduces data availability constraint and limits the usable data. In Southern France where the study area is situated, the summer seasons feature most precipitation and respectively vegetation growth. Hence the satellite imagery from the summer months will have a greater vegetation effect, providing greater interference with spectral mapping. In addition, the masking of weathering effects as well as lichens cover of the outcrops prove to be of high importance (Van der Meer & de Jong, 2006). The success of lithological mapping using space-based optical sensors relies on both the quality of the sensor and the characteristics of the study area. Therefore, availability of satellite data and the time of data acquisition serve as important factors in lithological mapping.

1.4 Research objectives and questions

A study area was selected with lithological formations dating back to Middle-Upper Jurassic and Lower Cretaceous periods. The Buëch area in South-East France shows geological faults and folding in a complex way. The area's unique setting is suitable for field-based geological research and spectral analysis of different lithological units. Combination of field work, laboratory work and access to remote sensing tools provide a great opportunity to thoroughly examine the study area. Therefore, the primary objectives of this project are to:

- *Map the Jurassic/Cretaceous lithological units in the Buëch area using Sentinel-2 and ASTER.*
- *Build a spectral library of the lithological formations in the Buëch area in France.*
- *Examine the extent of which fieldwork data and satellite data can complement each other.*

Several research questions are formulated to aid in accomplishing these goals:

- *How well can the lithological formations and structural geology be mapped using satellite observations in the optical domain between 400 and 2500 nm?*
- *How well can spectra in the optical domain between 400 and 2500 nm be used to separate the lithological formations?*
- *What effects do the surface conditions such as weathering, moisture and lichens have on the spectral signatures in the area?*
- *Can the lithological formations be accurately mapped using spectral library derived from rock samples in the area?*

1.5 Outline of the thesis

The first part of the thesis (chapter 2) provides an overview of the study area. The aim of the chapter is to provide a general description of the area, its geological setting and climatic conditions. It gives the reader an insight into the conditions of the present day landscape and acts as a prelude for further explanation of the lithological units observed and their origin. The following chapter (chapter 3) is reserved for the methodology followed in this project. Chapter 3 is divided into 4 parts which are dedicated to: (i) fieldwork and field sample collection, (ii) image spectroscopy and examination of field samples, (iii) satellite data and pre-processing steps associated with it, and (iv) spectral mapping techniques.

In Chapter 4, the key findings are presented. This chapter includes the comparison between spectral libraries and lithological maps derived using different methods and techniques. A discussion of the findings is then presented in the subsequent chapter. Chapter 5 focuses on the significance of the findings and their importance in the bigger picture. It discusses the performance of various spectral

mapping methods, the process of field work and highlights a few shortcomings associated with the project. The outlook and recommendations for further research on the topic is incorporated into the chapter as well. Concluding remarks are then presented in the last chapter of the main body (chapter 7).

Three appendixes are presented in the end containing extended lithological mapping results (Appendix A), additional spectral comparison of weathered and fresh rock samples (Appendix B), and lithological mapping results obtained using other spectral mapping techniques (Appendix C).

2. Study area

2.1 Site location and description

The study area is centered around the village Serres in south-east France (Figure 1). The area covers a section of the river Buëch basin, which originates in the Devoluy mountains north of Serres. The river flows through Serres and into the river Durance near Sisteron, 20 kilometres south of Serres. The area is part of the department *Hautes-Alpes* and is known as Préalpes du Sud. The department of *Hautes-Alpes* is a mountainous region with the average elevation of 1000 meters above sea level and high degree of local elevation differences. Similar landscape characteristics are observed in the study area.

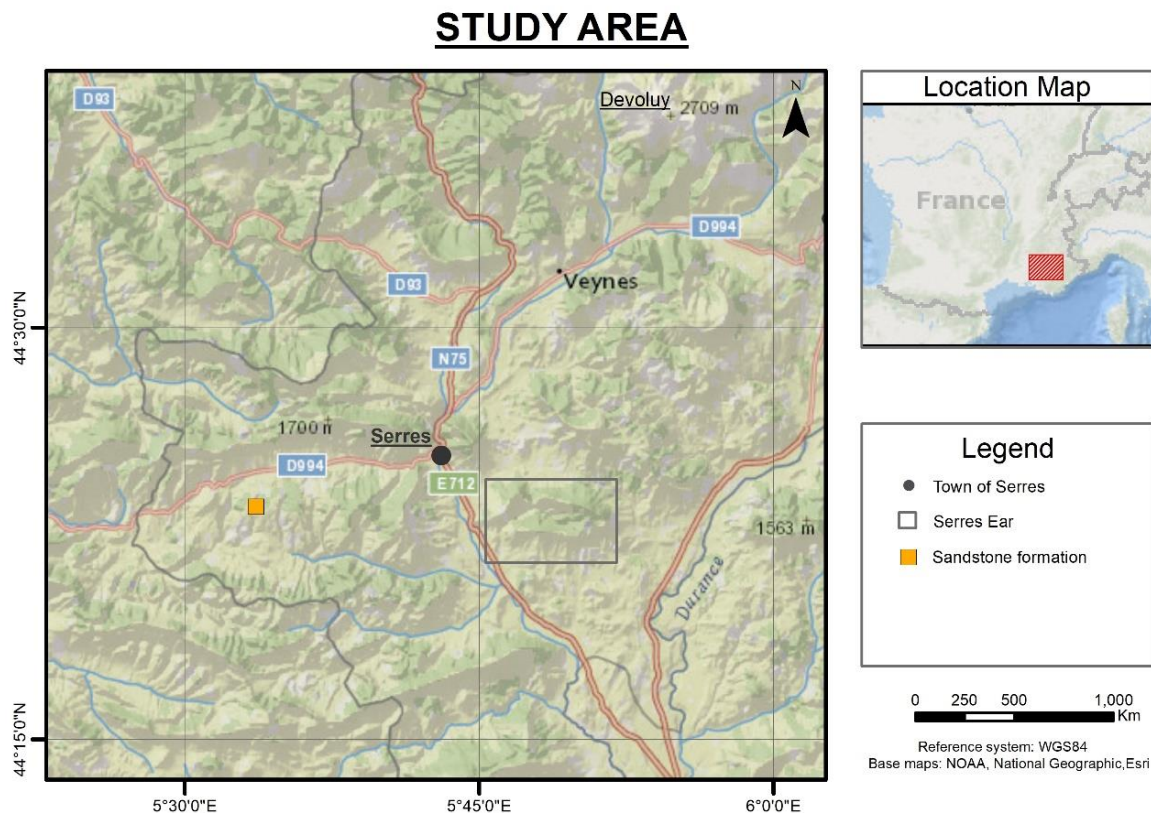


Figure 1: Study area

2.2 Geological setting

The relief of Préalpes du Sud has a pronounced structure largely due to the Alpine orogeny phases, which occurred in Miocene (30 – 2.6 Ma). The lithological formations in the Buëch area display geological faulting and folding in a complex way. The rock formations in the area can be summarized as a result of two folding phases: (1) an East-to-West folding axis which originates from the late Cretaceous to Eocene (70 – 34 Ma), and (2) a South-to-North strike, which took place from the end of Miocene to early Pliocene (10 – 5 Ma.).

The area is made up of mainly two sedimentary components: (1) hard and resistant limestone units from Late Kimmeridgian and Tithonian (“Calcaire Tithonique”) and the Lower Cretaceous (“Hauterivian-Barremian”), and (2) a number of softer marls, predominantly from the Bathonian-Oxfordian (“Terre Noires”) and Aptian-Albian (“Marnes Bleus”). The larger geological formations in the area feature the resistant limestone layers on top of the ridges. Hence, the limestone formations in the area tend to be prominent in the higher elevations, while complex softer marl formations are more dominant in the lower elevations (Figure 2). A notable geological formation formed by the Late Cretaceous limestone is the mountains north of Serres – Devoluy. Other notable lithological units in the area include sandstone formations close to Saint André-de-Rosans (yellow square in Figure 1), the marl conglomerates near Montmaur (North-East of Serres), the green and red marls located along the D937 (North-East of Serres) and the gypsum outcrops along the road to Saint Genis (South of Serres).

In addition to rock formations, loose sedimentary deposits, such as Quaternary deposits are present in the study area. These deposits are comparatively young and consist predominantly of glacial and glaciofluvial sediments transported by several Durance glaciers (Gidon et al., 1991). Other geological formations such as periglacial alluvial fans, colluvium, glacis and river terraces are also present in the area. Sediments deposited in Holocene era at the hill bases (colluvium) and river deposits (alluvium) seem to be of local importance. These geological formations make up several alluvial fans which range in size.

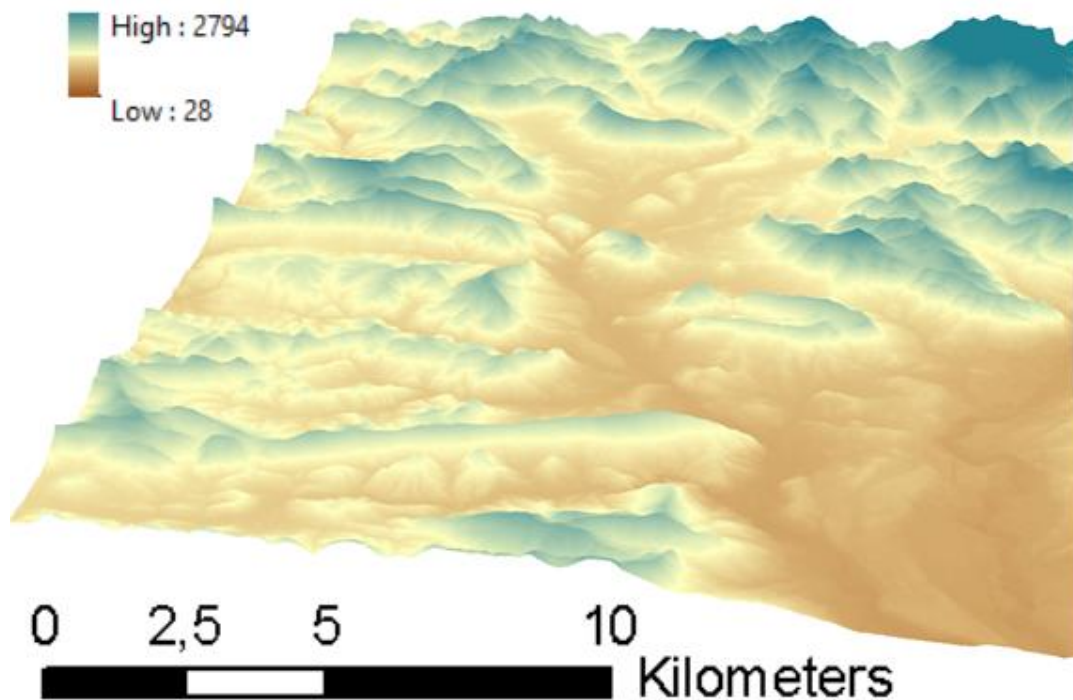


Figure 2: Digital elevation model of the study area.

2.3 Climatic setting

The climate of the study area is largely governed by Mediterranean influences. The summer period consists of 2-5 months and is relatively dry. This time of the year is characterised by atmospheric high pressure areas. The mean annual temperature lies around 12 °C, but it is important to note that the area experiences large temperature variation between summer and winter periods (Figure 3). Due to the mountainous setting, the elevation differences between the valleys and ridges can reach up to 1000 meters. This causes large climatic variability within small distances. The local conditions of valleys and mountain ridges are strongly governed by location and orientation relative to the sun. The annual precipitation is in the 700 – 900 mm range and is distributed fairly even throughout the (Figure 3).

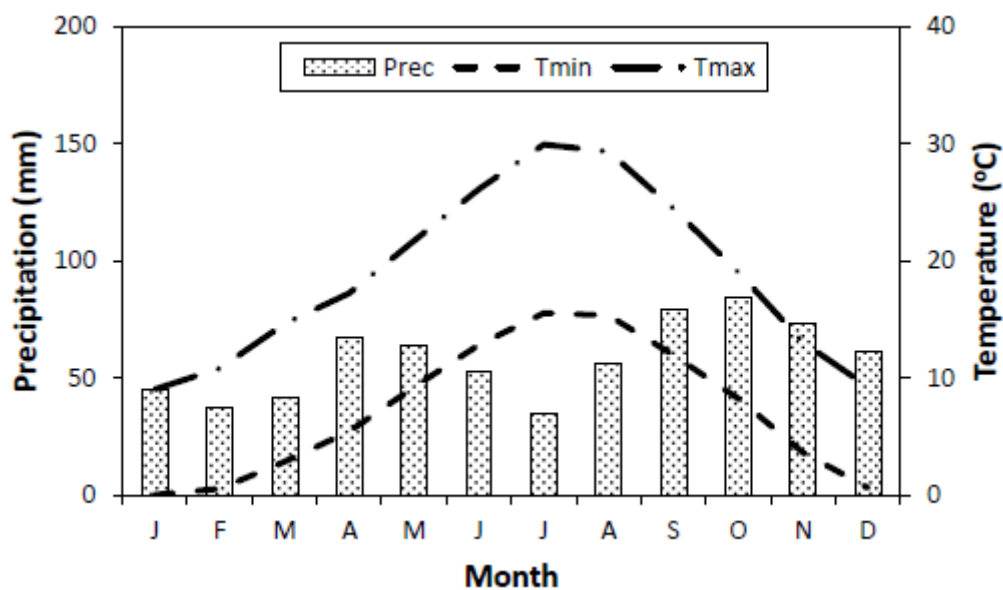


Figure 3: Annual rainfall and temperature in St. Auban d'Oze, 13 km northeast of Serres (Source: Météo France, 2017).

3. Data and Methodology

3.1 Fieldwork and sample collection

3.1.1 Description of lithological units

During the Jurassic period (201.3 – 145.0 Ma) the study area was submerged. In the Middle to Late Jurassic the area experienced large depositional rate which deposited thick layers of dark marl. Locally named 'Terres Noires', 'Argovien' and "Sequanien", these marl formations are highly erodible and large outcrops are observed throughout the landscape, making these marls the dominant lithological formation in the area (Gidon et al., 1991). The folding phases, predominantly in Miocene deformed these marls to irregular forms of synclinal and anticlinal sequences. Lateral thickness of the lithological units vary spatially.

During Kimmeridgian and Tithonian stages (157.3 – 145.0 Ma) large limestone sequences were deposited. These limestones are highly resistant to erosion and are locally known as ‘Calcaire Tithonique’ (Gidon et al., 1991). Limestone and marl alternating sequences were deposited during Early Cretaceous period (145.0 – 100.5 Ma).

The majority of outcrops present on the surface in the study area date back to Middle-Late Jurassic and Early Cretaceous (Gidon et al., 1991). Lithological units are categorized into 5 groups based on spectral signatures of rock samples collected in the field, along with geological knowledge of different formation. The groups are created to insure higher chance of spectral separability and detection. The description of the lithological units is listed in table 1.

Local name	Period	Stage	Description
“Terres Noires”	Middle-Late Jurassic	Bathonian – Early Oxfordian	Sequences of marl, limestone and calcareous marl. Older parts being sandier, but more resistant to erosion.
“Argovien”	Late Jurassic	Middle Oxfordian	Limestone and marl alternations.
“Sequanien”	Late Jurassic	Late Oxfordian – Early Kimmeridgian	Similar to “Argovien” with the lower part of the sequence being dominated by marls and upper by limestone.
“Calcaire Tithonique”	Late Jurassic	Late Kimmeridgian – Early Tithonian	Alternations of dominant limestone and subordinate marl.
“Calcaire Tithonique”	Late Jurassic	Late Tithonian	Limestone bed with spatial variation in thickness. Bears ammonite fossils and locally occurring conglomerates.
	Early Cretaceous	Berriasian	Argillaceous limestones with situational marl layers. Ammonite-bearing.
	Early Cretaceous	Valanginian	Marl alternations with occasional ammonite-bearing calcareous marls.
	Early Cretaceous	Hauterivian - Barremian	Monotone, ammonite-bearing limestone alternations with thin marl beds in between.
“Marnes Blues”	Early Cretaceous	Aptian – Albian	Marls with a slight blue tone, containing some argillaceous limestones.
	Early-Late Cretaceous	Cenomanian	Sandstone formations west of Serres

Table 1: Overview of lithological units and groups.

A colour code, unique to each group is assigned and is correlated with the classification colours in the lithological maps derived. The green group consists of “Berriasian”, “Valanginian”, “Hauterivian” and “Barremian” (Figure 4). These Early-Cretaceous marl-limestone alternations are in abundance in large parts of the Serres ear and West of Serres. Lithological units featuring dominant limestone layers formed during Kimmeridgian and Tithonian are assigned the colour red. Locally known as “Calcaire Tithonique” this group often lays on top of major geological formations in the area, providing them with recognisable ridges (Figure 4). Marl-dominated formations dating back to Late Jurassic are

grouped together and given a brown colour (Figure 5). This group includes all dark marl formations dating to Middle-Late Jurassic. Group three is the dominating lithological unit in the lower elevations and is in large abundance throughout the study area (Gidon et al., 1991). The last groups, four and five, are assigned to blue marl and sandstone outcrops West of Serres (Figure 6). Even though these two rock types are less frequent in the area, an exception was made due to their visual distinction. Bluish marls are separated from the other marl sequences and are assigned the blue colour. Sandstone outcrops are not widely observed throughout the area, but the continuity and extent of the singular outcrop in the West makes it an interesting target in comparing spectral mapping capabilities of Sentinel-2 and ASTER. Hence this sandstone outcrop is the last group and is given an orange colour.

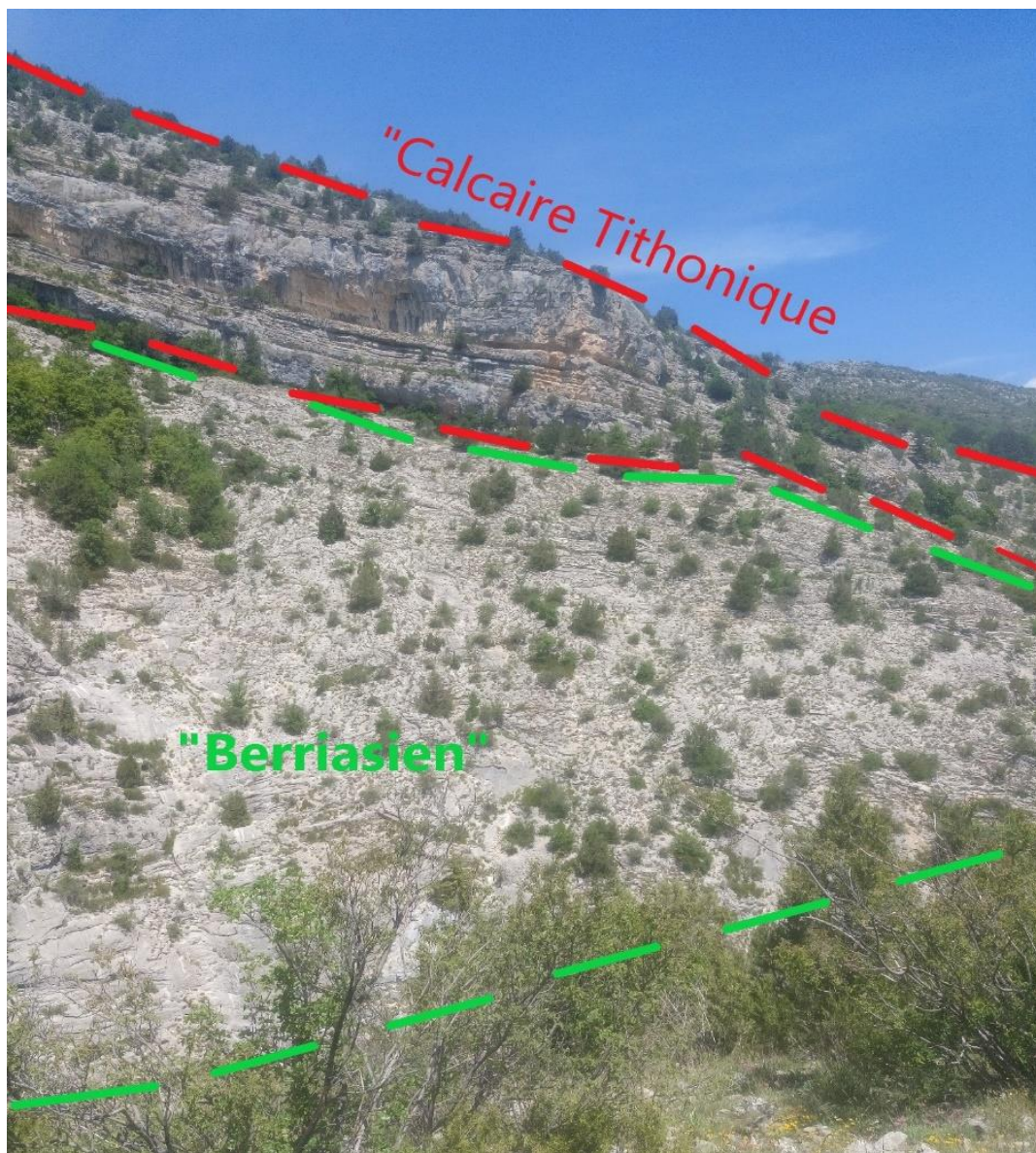


Figure 4: "Calcaire Tithonique" and "Berriasien" units observed inside Serres Ear. Picture taken at sample location 35.



Figure 5: Dark marl outcrop north of Serres. Picture taken at sample location 8.



Figure 6: Sandstone outcrop with blue marls seen in the distant valley. Picture taken at sample location 25.

3.1.2 Field data collection and sample locations

A field campaign was organized to collect rocks for construction of weathered and fresh spectral libraries of the area. A field plan was made on a day-to-day basis taking into consideration the weather conditions and logistics. Sample locations were chosen based on the accessibility of the outcrops and their potential representability of the lithological units (Figure 7). GPS coordinates were notated and other geological information was documented to ensure least amount of error. A selection of rocks with visible weathered and fresh surfaces are included in Appendix B.

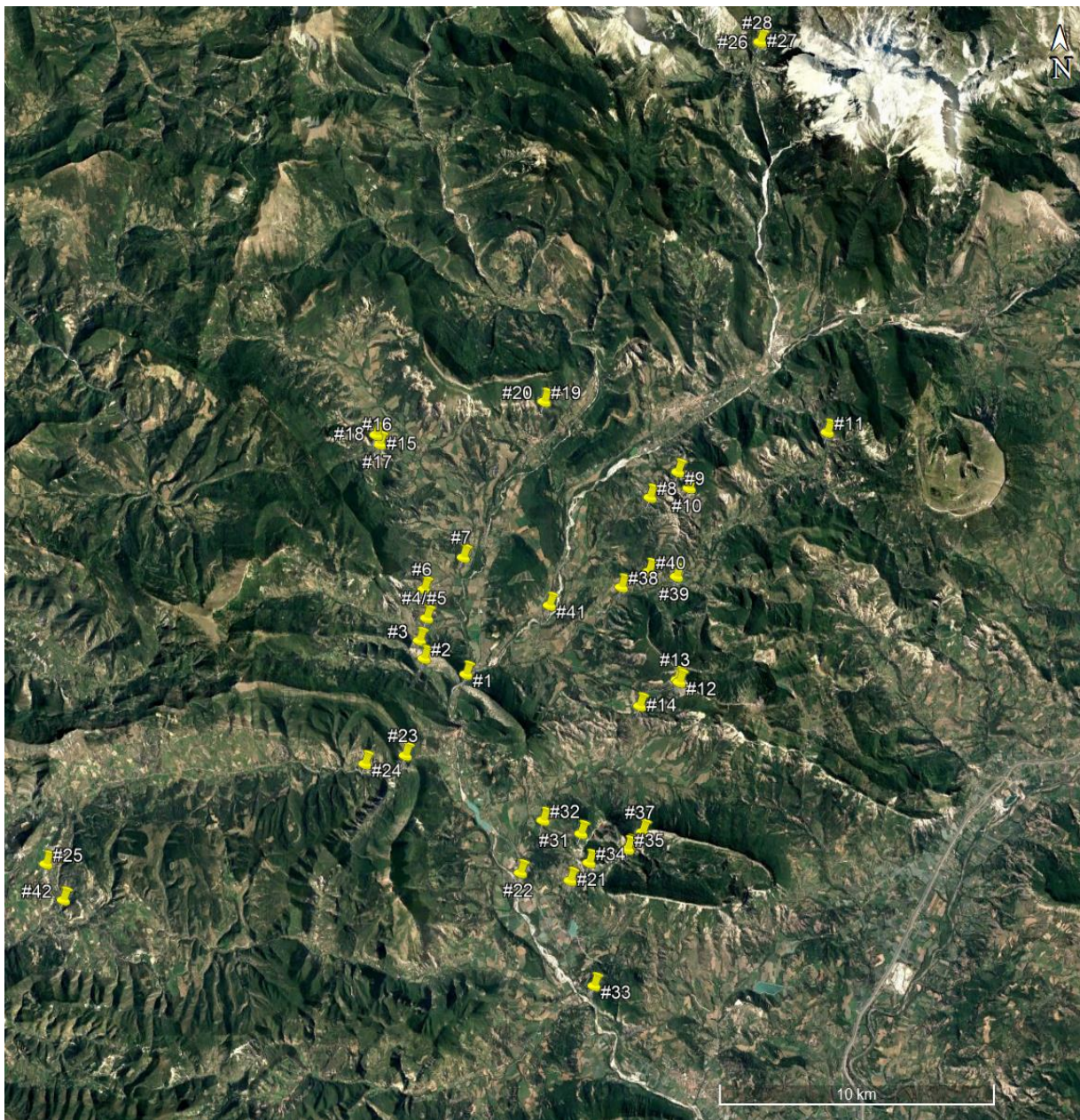


Figure 7: Satellite image with marked sample locations (Source: Google Earth Pro).

3.2 Image spectroscopy

3.2.1 Imaging spectroscopy principle

The appearance of soils and rocks across the electromagnetic (EM) spectrum is dictated by the mineral physics (Kruse, 2010). The identification of rocks and soils are made available by the absorption of radiation at specific wavelengths. Terrestrial substances such as hydrocarbons, minerals and rocks display characteristic absorption features (Kruse, 2010; Asadzadeh & Filho, 2016). These diagnostic features appear in the visible-near infrared (VNIR) (350 – 1000 nm), short-wave infrared (SWIR) (1000 – 2500 nm), mid-infrared (MIR) (3000 – 5000 nm), and longwave infrared (LWIR) (8000 – 14000 nm).

In the context of geology, molecular vibrations at wavelengths less than 1000 nm provide recognition of iron-rich (Fe^{+3}) minerals. The geological formations in the study area originate from marine sediment. Marine sedimentary rocks tend to contain little iron which is why reflectance of the rocks around 400 – 1000 nm spectral range show little features (Figure 8). The absence or presence of water, hydroxyl and carbonate dictate the diagnostic absorption features in the SWIR spectral range (Van der Meer & de Jong, 2006). Soils and rocks show an almost monotonic increase in reflectance with wavelength, although with dips situated approximately 1400 nm and 1900nm due to water content (Richards & Jia, 2006). Such moisture absorption bands are almost inconspicuous in very dry rocks and sediments, such as sandstone in figure 8. Clay-bearing rocks and soils have been documented in having hydroxyl absorption features centered at 2200 nm (Richards & Jia, 2006) and carbonate sedimentary rocks display absorption features at approximately 2300 nm, owing to CO_3^{-2} ion (Van der Meer & de Jong, 2006).

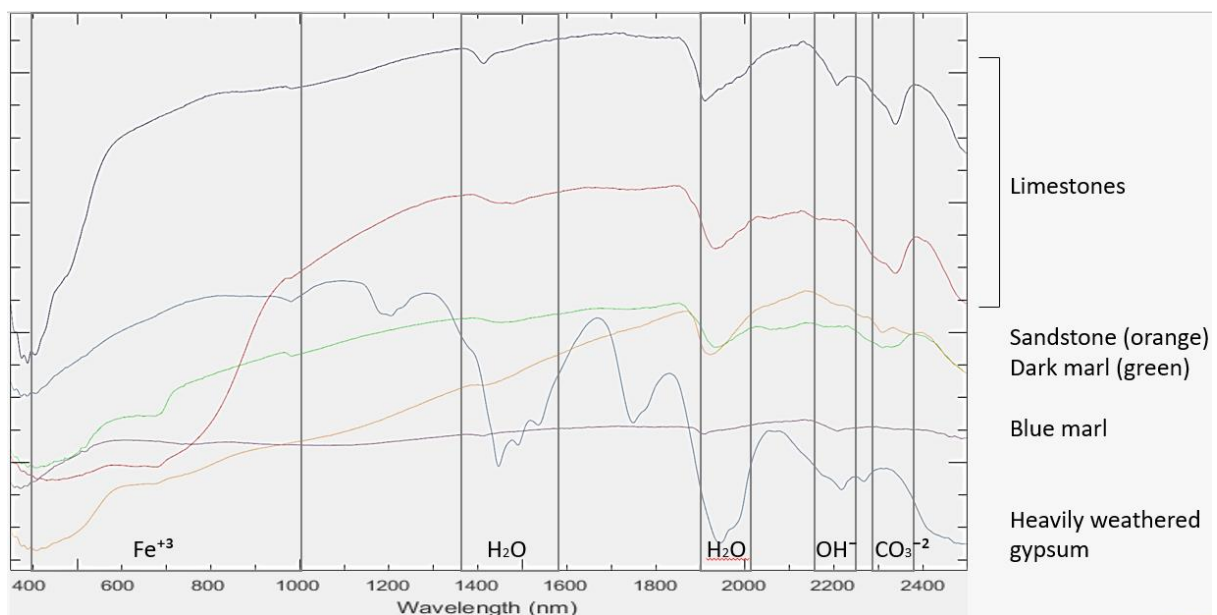


Figure 8: Most important absorption features in VNIR and SWIR for geological and mineralogical studies.

3.2.2 PSR+3500 spectroradiometer

A PSR+3500 spectroradiometer was used to measure spectral reflectance signatures of the samples collected in the study area. This spectroradiometer is a high resolution/high sensitivity spectroradiometer with both fiber mount Field-of-View (FOV) and directly attachable lens options which provide flexibility for varying target sizes. The PSR+ features a spectral range of 350 – 2500 nm and enhanced spectral resolution to allow high resolution scans with excellent signal-to-noise ratio (Spectral Evolution, 2012). There are three detectors measuring the spectral range. Table 2 shows the three detectors, their representative type and spectral resolutions at Full Width Half Maximum (FWHM).

Detector	Type	Range, nm	Spectra resolution at FWHM
1	512 element Si photodiode array	350 - 1000	3 nm at 700 nm
2	256 element extended InGaAs photodiode array	970 - 1910	8 nm at 1500 nm
3	256 element extended InGaAs photodiode array	1900 – 2550	6 nm at 2100 nm

Table 2: Overview of PSR+ detectors and their specifications (Source: Spectral Evolution 2012).

PSR+ spectrometer has various setup options to fit different spectra acquisition conditions. The use of a tripod to hold the spectrometer stationary and vary the distance between the PSR+ spectrometer and the sample, enables the user to vary the contact surface for spectral measurements. The spectrometer setup in the laboratory can be seen in figure 9. The figure shows the PSR+ spectrometer in the center, with white reference palette to the right and the fiber mount FOV lens attached to the spectrometer via optical cables.



Figure 9: Initial setup of the spectrometer.

3.2.3 Building spectral libraries

Spectroscopic measurements of field and laboratory samples are essential components of hyperspectral and multispectral remote sensing analysis (Zhou & Wang, 2017). Various important spectral libraries exist and are widely accessible such as U.S. Geological Survey (USGS) spectral library (Clark et. al., 2003) and ASTER spectral library (Baldrige et. al., 2009). While these libraries provide a great amount of spectral information for remote sensing analysis, they also come with some disadvantages in terms of practical application.

Standard, laboratory-derived spectral libraries oftentimes measure samples in powder state to increase the pure features of the material (Van der Meer & de Jong, 2006). Such powders may diminish and mask the characteristic absorption features of rocks, in turn obstructing their identification. Another important drawback with using pure materials is the reduction of weathering effect (Zhou & Wang, 2017). Surface rock interactions with the environment can produce mineral coatings which obscure the original parent rock and alter its surface composition (Younis et al., 1997). With advances in remote sensing leading to improvements in accuracy and availability of satellite imagery, an increase in false identification using standardized, laboratory-based spectral libraries can also occur (Zhou & Wang, 2017). This arises when spectral libraries of pure materials are used in identifying weathered surfaces. Hence, the standardized spectral libraries are convenient, but are disadvantageous in geologic mapping.

Zhou & Wang (2017) quantified weathered deformation by dividing the rock coatings into two groups: (1) biogenic, which refers to coatings from lichens and mosses, and (2) non-biogenic coatings which result from oxides, nanocrystalline iron and clay interactions with the material. The second group is prominent in arid and semi-arid regions. If the rock is severely exposed to weathering, these types of coatings can dictate the spectral signature of a rock.

In semi-arid regions, such as Serres, weathering deformation can change the shape and occurrence of diagnostic absorption features of a rock. In addition, mechanical weathering can alter the albedo which results in altering of overall reflectance. Therefore, it is essential to better understand the spectral differences between weathered and fresh materials. Comparative research on exposed and fresh surfaces is scarce. In order to successfully correlate satellite imagery to surface geology, strong knowledge on spectral features of weathered rock surfaces is required.

Measurement method selection

Five different setups were analysed on six selected samples to determine which setup is optimal to use for all rock samples. Two Field of View (FOV) lenses of 4° and 8° were used with the contact distance of 10 and 15 cm respectively between the spectroradiometer and the sample surface were used,

as well as the contact probe. Figure 10 shows measurement of a limestone sample from the study area using the beforementioned setups.

Contact probe was selected after taking the potential external light interference, light leakage, contact surface size and mobility into account. The contact probe is easy-to-use and ideal for reflectance measurements. It contains a built-in, 5-watt tungsten halogen bulb and a scratch-resistant window which is surrounded by protective rubber to ensure minimal light leakage from the built-in light source and minimal interference from external environment. Due to its mobility, it is capable to be placed on rugged surfaces in a manner most suiting for the user.

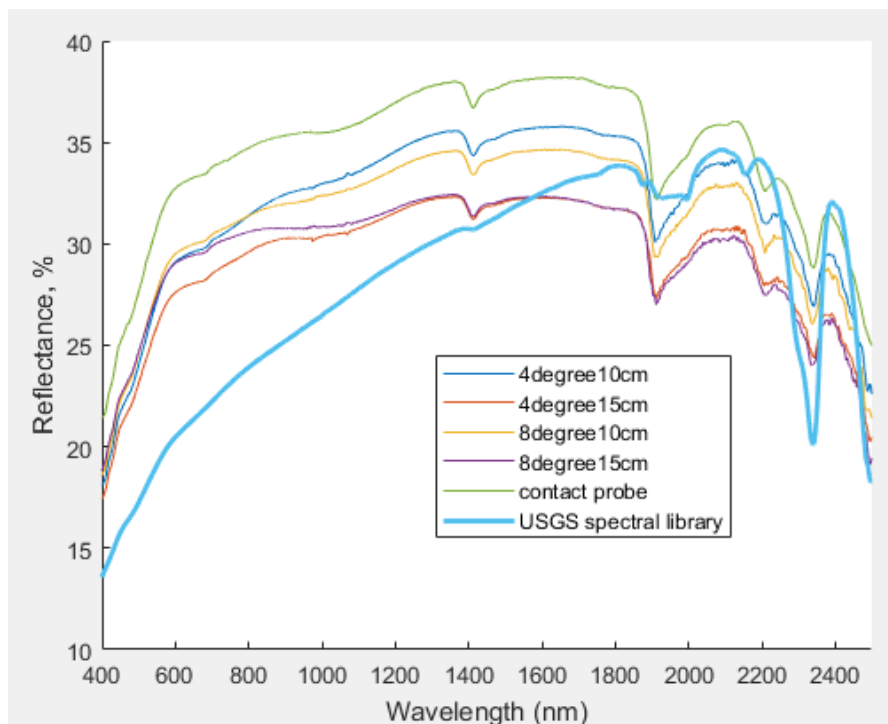


Figure 10: Comparison of different setups for measuring limestone in addition to spectral signature of limestone from USGS.

After measuring all the rock samples and storing the data of the weathered surfaces, the rocks were prepared for measurements of the fresh surfaces. In order to achieve this, a diamond saw was used to cut the rocks and expose the surfaces unaffected by the climatic elements. The diamond saw uses water for lubrication to minimise dust and rock particles during the sawing process. This results in the samples being wet. Water content affects greatly the spectral signatures of samples and therefore the samples had to be dried. Drying the rock samples at 60 °C for 24 hours was recommended. The decision was made to dry the samples in an oven with 60 °C for an hour and then leave it overnight. The oven drier loses heat at a slow rate, hence drying the samples long after the oven is switched off. When the samples had lost most of its water content, the measurements with the same setup were executed to build a spectral library of fresh rock surfaces.

Removal of organic material from rock surfaces

Organic material such as lichen and algae can alter the spectral response of rock surfaces. An experiment was made to see if washing the rock samples with vinegar had an effect on the spectral responses of sampled rocks. Five samples were selected (#25, #27, #32, #42 and dolomite). Samples were washed and left to dry overnight for 20 hours. Figure 11 shows a rock sample in vinegar after 30 seconds. The bottom of the box contains dissolved rock particles and the rising bubbles are the result of acidic vinegar reacting with calcite in the rock sample.



Figure 11: Example of a rock sample submerged in vinegar.

3.3 Satellite data

3.3.1 Sentinel-2 and ASTER

Sentinel-2

Sentinel-2 is a constellation of two satellites launched by European Space Agency in efforts to provide continuity to the on-going multispectral observations by SPOT and LANDSAT missions. The two satellites are designed to have a short revisit time and therefore are phased 180⁰ from one another. The orbit is sun-synchronous and at the altitude of 786 kilometres. All of this results in a revisit time of 5 days at the equator. Sentinel-2 satellites each carry on board a single Multi-Spectral Instrument (MSI) which samples a total of 13 spectral bands. With its high revisit frequency and 13 spectral bands (Table 3), Sentinel-2 provides valuable data for land and ocean studies.

Subsystem	Band no.	Spectral Range (nm)	Central Wavelength (nm)	Spatial resolution (m)
VNIR	B1	422 – 464	443	60
	B2	458 – 523	490	10
	B3	543 – 578	560	10
	B4	650 – 680	665	10
	B5	698 – 713	705	20
	B6	733 – 793	740	20
	B7	773 – 793	783	20
	B8	785 – 899	842	10
	B8A	855 – 875	865	20
SWIR	B9	935 – 955	945	60
	B10	1360 – 1390	1375	60
	B11	1563 – 1657	1610	20
	B12	2098 - 2283	2190	20

Table 3: Spectral characteristics of Sentinel-2 (Source: sentinel.esa.int, 2019).

The Multi-Spectral Instrument on board Sentinel-2 satellites provides a range of publicly accessible products. One of such products is Level-1C data. Level-1C is the initial data used for this study. It provides Top-Of-Atmosphere (TOA) reflectance and includes land, water and cloud masks.

ASTER

In December of 1999, NASA launched the TERRA platform to a near polar, sun-synchronous orbit. Terra platform orbits at an altitude of 705 km and has a revisit time of 16 days. The platform is equipped with several remote sensing devices such as MODIS, CERES and MISR. Another imaging device on board was a high resolution instrument – ASTER. The Advanced Spaceborne Thermal Emission and Reflection Radiometer (ASTER) is a multispectral imaging sensor containing 14 spectral bands. These spectral bands are categorized into: (i) VNIR containing 3 bands with 15-meter spatial resolution, (ii) SWIR consisting of 6 bands with 30-meter spatial resolution, and (iii) 5 bands in the Thermal InfraRed (TIR) of 90-meter spatial resolution (Table 4). Only VNIR and SWIR ASTER bands that coincide with spectral range of Sentinel-2 have been considered for further processing.

Subsystem	Band no.	Spectral Range (nm)	Central Wavelength (nm)	Spatial resolution (m)
VNIR	1	520 – 600	556	15
	2	630 – 690	661	15
	3N	780 – 860	807	15
	3B	780 – 860	804	15
SWIR	4	1600 – 1700	1656	30
	5	2145 – 2185	2167	30
	6	2185 – 2225	2209	30
	7	2235 – 2285	2262	30
	8	2295 – 2365	2336	30
	9	2360 - 2430	2400	30
TIR	10	8125 – 8475	8291	90

	11	8475 – 8825	8634	90
	12	8925 – 9275	9075	90
	13	10250 – 10950	10657	90
	14	10950 - 11650	11318	90

Table 4: Spectral characteristics of ASTER (Source: asterweb.jpl.nasa.gov, 2014).

Sentinel-2 features 13 spectral bands with VNIR bands having 10-meter spatial resolution and bands in the SWIR region having 20-meter resolution. ASTER contains 6 SWIR bands, enabling spectral mapping of surface mineralogy due to their relatively narrow spectral resolution (Mars & Rowan, 2010). The difference between the two sensors can be viewed as their separate advantage and disadvantage. Figure 12 shows the spectral bands of ASTER overlaid over Sentinel-2 spectral bands. ASTER sensor contains an array of narrow bands in SWIR, which aid in mineralogical remote sensing. The biggest disadvantage in using Sentinel-2 for geological remote sensing is its lack of such narrow spectral bands in the SWIR region. Sentinel-2 sensor on the other hand, features multiple narrow bands in VNIR region, which allows detection of iron-bearing minerals.

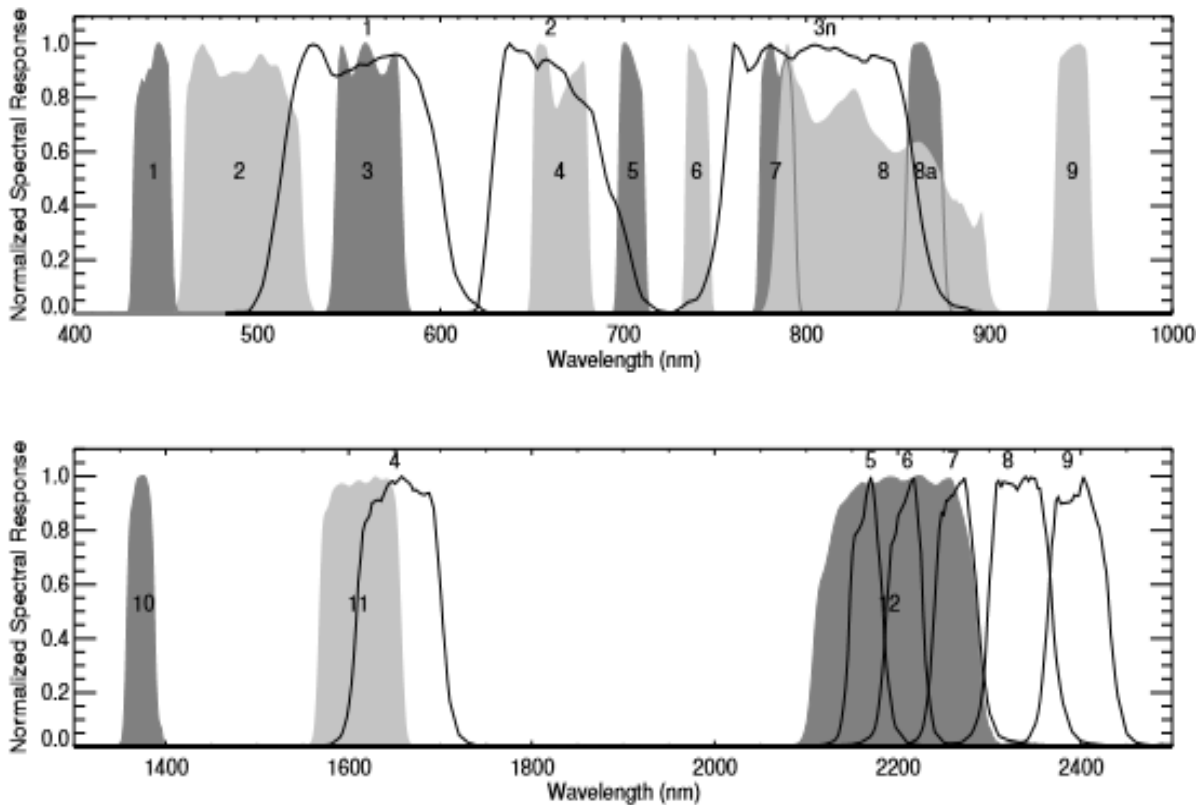


Figure 12: Comparison of Sentinel-2 (shadows) and ASTER (line) spectral bands. Figure above covers 400 - 1000 nm wavelength region and figure below shows 1000 - 2500 nm region (Van der Werff et al, 2018)

3.3.2 Imagery selection

Satellite scenes were selected via Earth Explorer website (URL: <https://earthexplorer.usgs.gov/>). A polygon was drawn over the region of interest and criteria such as cloud cover, time of acquisition and atmospheric disturbances were taken into account. Sentinel-2 contains a great amount of recent images, therefore an image captured on the 30th of May 2018 was chosen to represent the time of fieldwork in the area. Two granules at level-1C, with Top of Atmosphere (TOA) were selected. The two granules overlap and are projected with UTM coordinates at the 31N zone. The cloud cover is 52.5 % and 20.3% respectively. Fortunately, most of the cloud cover is outside the region of interest.

Same criteria were subjected to ASTER image selection. However, due to ASTER SWIR malfunctioning in 2008, the scene options have greatly reduced. A decision was made to aim at selecting a scene with most favourable surface conditions. Two granules were selected with the date of acquisition being the 21st of April 2015. The two ASTER granules overlap as well and are projected in the same, UTM 31N zone system. The cloud cover is 27 % and 8 % respectively. The clouds in these scenes are in the form of snow and are further North in the granule.

3.3.3 Image pre-processing

ASTER imagery was pre-processed in ENVI 5.5 using the conventional, manual methods found in the environment. Image pre-processing for Sentinel-2 imagery was performed in Sentinel Application Platform (SNAP). SNAP is an environment which includes all Sentinel Toolboxes and allows for more efficient management of Sentinel products. It is an ideal platform for Earth Observation processing and analysis. SNAP is open source and contains various third party plugins of which, two were used for the pre-processing of Sentinel-2 images in this study.

Atmospheric correction

Atmospheric correction re-scales the raw radiance data to reflectance by calibrating for influences caused by the atmosphere (Van der Meer & de Jong, 2006). In doing so all spectra are shifted to nearly equal albedo. The resulting data contains pixels which are defined by a reflectance spectrum. These reflectance spectra are directly comparable with the reflectance spectra of rocks from the field of study.

Sentinel-2 and ASTER images of the area are Level-1C and Level-1T products respectively. Sentinel-2 data is in Top-Of-Atmosphere (TOA) reflectance. In order to remove the atmospheric effects and obtain reflectance values from the earth's surface (BOA), atmospheric correction must be made. ASTER imagery on the other hand comes in the form of radiance. Sensor data is radiometrically calibrated but requires atmospheric correction as well.

The processing tool used to perform atmospheric correction for Sentinel-2 is Sen2Cor. Sen2Cor is a processor developed specifically to obtain Bottom-Of-Atmosphere (BOA) reflectance values from Top-Of-Atmosphere (TOA) reflectance of the Sentinel-2 Level-1C data (Pflug et. al., 2016). The processing relies on 2 key auxiliary data: Digital Elevation Model (DEM) and Radiative Transfer Look-Up Tables (Louis et. al., 2016). In using this data, the tool derives the Cloud Detection and Scene Classification. The processing continues with computation of Aerosol Optical Thickness (AOT) and the content of water vapour (WV). Finally, the processing ends with TOA to BOA conversion (Figure 13).

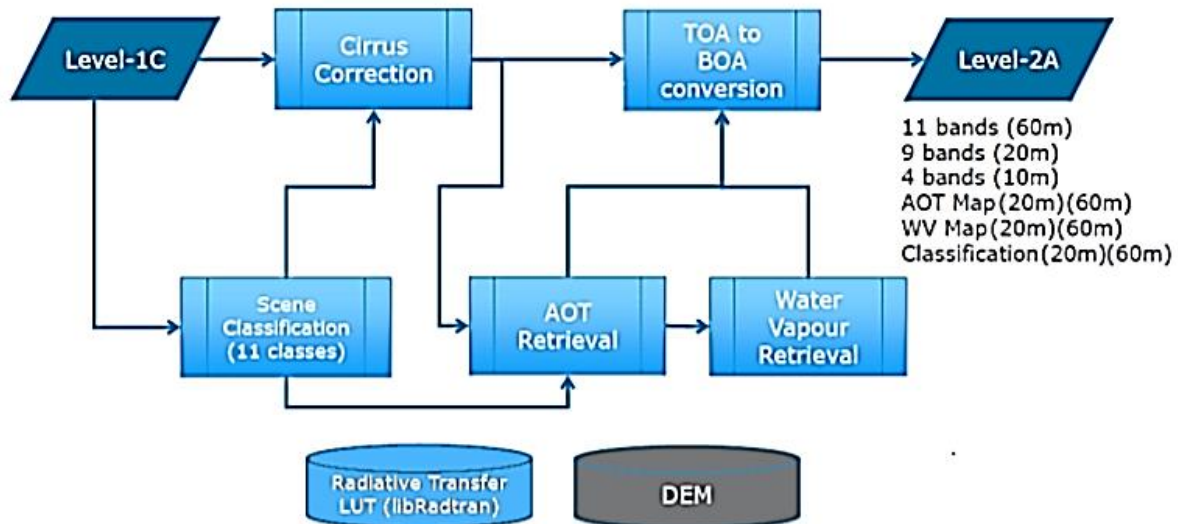


Figure 13: Key processing steps in Sen2Cor (Source: Louis et. al., 2016)

Log Residuals Correction tool was applied on ASTER data to obtain reflectance data. Logarithmic residuals tool removes the solar irradiance, gain from the instrument, atmospheric transmittance, albedo effects and topographic effects. The transformation is made by first dividing the original input spectrum by the spectral geometric mean and then dividing the resulting values by the spatial geometric mean. The spectral mean is the mean value of all spectral bands for each pixel and it is used to remove the topographic effects. The spatial mean accounts for the atmospheric transmittance, solar irradiance and instrument gain. It is defined as the mean of all pixels for each spectral band. Log Residuals transform is beneficial for further analysis of absorption features in hyperspectral data (Green & Craig, 1985).

Mosaic and subset

After the images have been atmospherically corrected, a region of interest around the study area is established. In doing so, the spatial subset can be chosen and the necessary images can be mosaicked. This improves the computational speed by only focusing further analysis exclusively on the study area. Figure 14 shows a Sentinel-2 satellite image of the study area ready for masking and further processing.



Figure 14: Sentinel-2 true color (RGB: [B4,B3,B2]) image of the study area after initial pre-processing. Town of Serres in the red rectangle.

Resampling

The resolution of the bands does not change during the atmospheric correction. The output data from Sen2Cor processor and Log Residual Correction provides us with the Level-2A data. The next step in pre-processing of satellite data is to increase resolution of the 20-meter and 60-meter spectral bands of Sentinel-2 image down to 10-meter spectral resolution and resampling the 30-meter spatial resolution of ASTER SWIR bands to 15-meter resolution.

In case of Sentinel-2, this can be achieved using Sen2Res tool from ESA. An advantage of using this processor is that while other resampling techniques utilize a panchromatic band, Sen2res extracts the information from the 4 bands of Sentinel-2 image that contain 10-meter spectral resolution. It essentially builds a model of information that is specific to the 10-meter bands such as the colour of the pixel and how information is related and shared between the spectral bands. Applying this model to the SWIR spectral bands enables the bands to maintain their reflectance and consistency between neighbouring pixels (Brodu, 2016).

The SWIR bands of ASTER featuring 30-by-30-meter pixel resolution are resampled to match the VNIR spectral resolution of 15 meters. This was achieved using nearest neighbour resampling method.

MNF transform

Minimum Noise Fraction transformation was used to reduce noise and inherent dimensionality of the image data. Minimum Noise Fraction is a linear transformation consisting of two consecutive principal components analysis (PCA) rotations: (1) the first rotation utilizes the principle components (PCs) of the noise covariance matrix in order to rescale and decorrelate the noise, resulting in data containing noise with no band-to-band relation, (2) second rotation using the PCs from the original data after the noise whitening performed in the first rotation (Boardman and Kruse, 1994).

A forward MNF transformation was made and the resulting images were examined (Figure 15). The bands containing a great portion of noise were then excluded and the rest of the bands were converted back to original form by applying an inverse MNF transform. This results in reduction of computational requirements for further analysis.

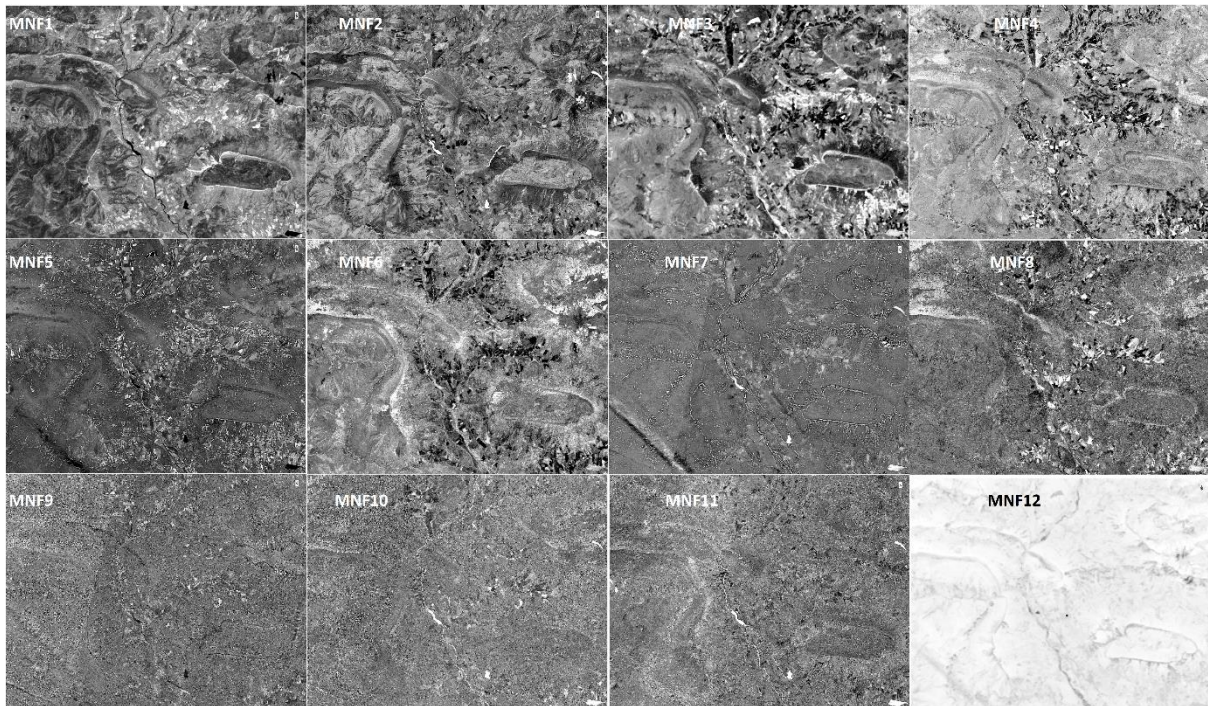


Figure 15: MNF bands after a forward MNF transform for Sentinel-2 image.

Masking

Raster masks were built to remove vegetation, cloud and shadows. The basis for the masks is the Normalised Difference Vegetation Index (NDVI). NDVI was calculated and using colour slicing, vegetation, shadows and clouds in the area were masked out. In addition to NDVI, other input bands were used to better exclude the agricultural crop, water and vegetation. The complexity of the study area makes it difficult to make a general set of rules to remove the unwanted surface features all-together, therefore in most important areas, separate subsets of smaller size were created to increase the accuracy of the masks. This ensures that the pixels selected to represent the lithological units have least amount of vegetation and are representative of the lithological units alone.

3.4 Spectral mapping techniques

The key to successful lithology mapping lies in utilising the advantages of optical sensor data, *a priori* knowledge of the area and appropriate selection of the mapping techniques, while simultaneously minimizing the drawbacks associated with the sensor data, data acquisition, terrain and mapping capabilities of the chosen algorithms.

Categorization of mapping methods can be made based on the resulting maps (Asadzadeh & Filho, 2016). Abundance maps provide the fractional amount of subject material present in each pixel. Such maps are meaningful when research focuses on the proportions of various endmembers in a pixel (Shao

et al., 2018). Band ratios (BR) and matched filtering (MF) are one of many techniques used in obtaining abundance maps (Van der Meer, 2012; Van der Werff, 2015). This study aims at mapping the pure lithological pixels and assigning them to correct lithological groups. Hence, instead of looking at abundances of materials, the priority is shifted to a more exact classification. This can be achieved by selecting representative samples either from the satellite imagery or a spectral library and using these as input (Weih & Riggan, 2010). The resulting maps are classifications of remaining image pixels into generated classes. Classification maps can be achieved by many algorithms, the two mapping algorithms used in this study fall in this category.

The selection of mapping techniques must also consider the specific conditions in the area that may pose an obstacle in obtaining realistic geological maps. The varying topography causes irregularities and shadows in areas directly behind higher-altitude formations. The agricultural crops and relatively dense vegetation in the area provide a wide range of diverse spectral pixel responses which may result in an increase of false-positives and misclassification.

Spectral Angle Mapper (SAM) and Support Vector Machine Classification (SVM) were chosen as the primary image processing techniques. In geological applications of remote sensing, Support Vector Machine technique is predominantly used in lithology classification (Cracknell & Reading, 2014; Mountrakis et al, 2011; Waske et al, 2009). The use of Spectral Angle Mapper in mapping lithological formations is well documented as well (Chen et al, 2007; Murphy et al, 2012; Fal et al, 2019). Both algorithms possess unique advantages and differ in their approach, which makes for an adequate comparison.

Spectral Angle Mapper (SAM)

Spectral Angle Mapper is a matching technique based on spectral similarity between a known reference spectrum and an unknown target spectrum (Asadzadeh & Filho, 2016). The algorithm determines the similarity by calculating the angle between the two spectra and treating them as vectors in a multi-dimensional space with dimensionality set to the number of spectral bands (Kruse et al., 1993). Due to its mathematical similarity approach, the Spectral Angle Mapper is relatively insensitive to illumination and albedo effects when used on calibrated reflectance data (Kruse et al., 1993). In lithology mapping, SAM algorithm is used by first assuming each lithological unit in the area having a unique spectral response (Debba et al. 2006; Rowan et al. 2000). Training samples are then provided to act as reference spectra for each lithological class. The reference spectra can be in a form of image-based regions of interest or spectral libraries (Kruse et al., 1993), making it suitable in comparing mapping results of laboratory-derived and image-derived reference spectra. SAM compares the angle between each pixel in the image scene with those of the training samples (Figure 16). Smaller angles indicate a better match and thus assignment of classes can be made. Image pixels which result in angles

exceeding the maximum specified angle threshold are not assigned to any class and are deemed unclassified.

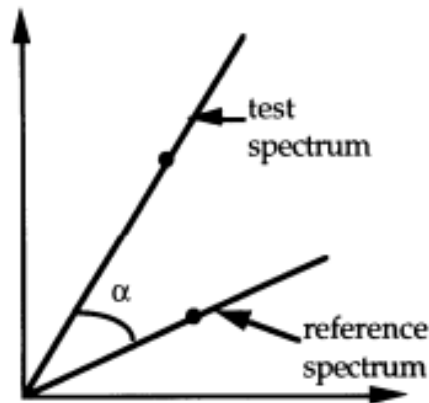


Figure 16: An example of SAM method to match a target spectrum with a reference spectrum by treating these as vectors (Kruse et al., 1993).

Support Vector Machine classifier (SVM)

Support Vector Machine (SVM) classifier is a machine learning algorithm based on statistical learning theory. It is a non-parametric method and works by constructing a hyperplane that most accurately divides the dataset into classes on an n-dimensional feature space (Cortes and Vapnik, 1995). To achieve this, it uses the training samples gathered from the scene image. This hyperplane acts as a *decision boundary* for classification of other samples in the dataset.

The discrimination between classes utilizes a kernel function which transforms low-dimension input space into a higher-dimension space. This implicit transformation enables a more accurate hyperplane to be generated to discriminate classes. Selection of the Kernel function is essential to obtain accurate SVM classification (Bachri et al., 2019). SVM algorithm in ENVI 5.5 software allows to choose between linear kernel (LN), sigmoid kernel (SIG), polynomial kernel (PL) or radial basis function kernel (RBF). Radial basis function kernel is advantageous due to its interpolation capabilities (Zhu et al, 2011) and is therefore selected as the input kernel function. The performance of SVM is highly dependent on kernel parameter choice (Bachri et al., 2019). The penalty parameter and the gamma kernel width are the parameters which need to be pre-determined by the user. The gamma kernel width dictates the order of non-linearity of the SVM model. The penalty parameter dictates the margin of error to be tolerated in the training samples. Penalty parameter set to high would result in a few training errors, while a small value for penalty parameters would create a larger error margin and, therefore, increase the number of training errors. Yang (2011) has shown penalty parameter set to 100 and the gamma kernel width set to the inverse of the band numbers (Sentinel-2: 0.083; ASTER: 0.111) to yield optimal classification results.

A two-class example is shown in figure 17. The grey squares indicate the samples which when used, result in the largest distance between the two classes. These samples are called *support vectors*, hence the name of the classification method. The support vectors are the only samples in the training dataset that are related to the hyperplane. If the support vectors are moved, the hyperplane is shifted as well. If any other training samples are displaced, this has no effect on the boundary between the two classes. This makes the SVM method insensitive to outliers and makes the method less memory intensive. In addition, it has been found that SVM is less sensitive to the number of training samples used, compared to other machine-learning algorithms (Kumar et al., 2020).

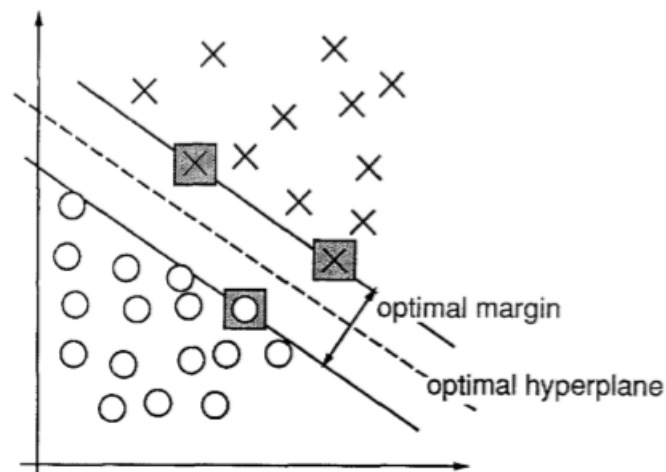


Figure 17: A 2D example of SVM with grey squares defining the margin of the optimal hyperplane separating the two classes (Cortes & Vapnik, 1995).

4. Results

4.1 Spectral signatures of lithological groups

The green group of limestone and marl alternations dating to “Berriasian”, “Valanginian”, “Hauterivian” and “Barremian” show distinctive absorption features at 670 nm and 950 nm (Figure 18). “Calcaire Tithonique” feature strong overall reflectance and distinctive absorption features in the SWIR spectral range. The carbonate absorption at 2300 nm is profound in both limestone groups. The lack of hydroxyl absorption around 2200 nm in “Calcaire Tithonique” as oppose to “Berriasien” could serve as an important difference between the two groups. Dark marls from Late Jurassic termed “Terres Noires”, show slight hydroxyl and carbonate absorption, but not as profound as the limestone units. Blue marls display little diagnostic absorption features, with a dip at 1900 nm owing to water content in the rocks and a small absorption at 2200 nm indicating presence of clay in the material. Sandstone is generally featureless with water absorptions at 1400 nm and 1900 nm dominating the spectral response.

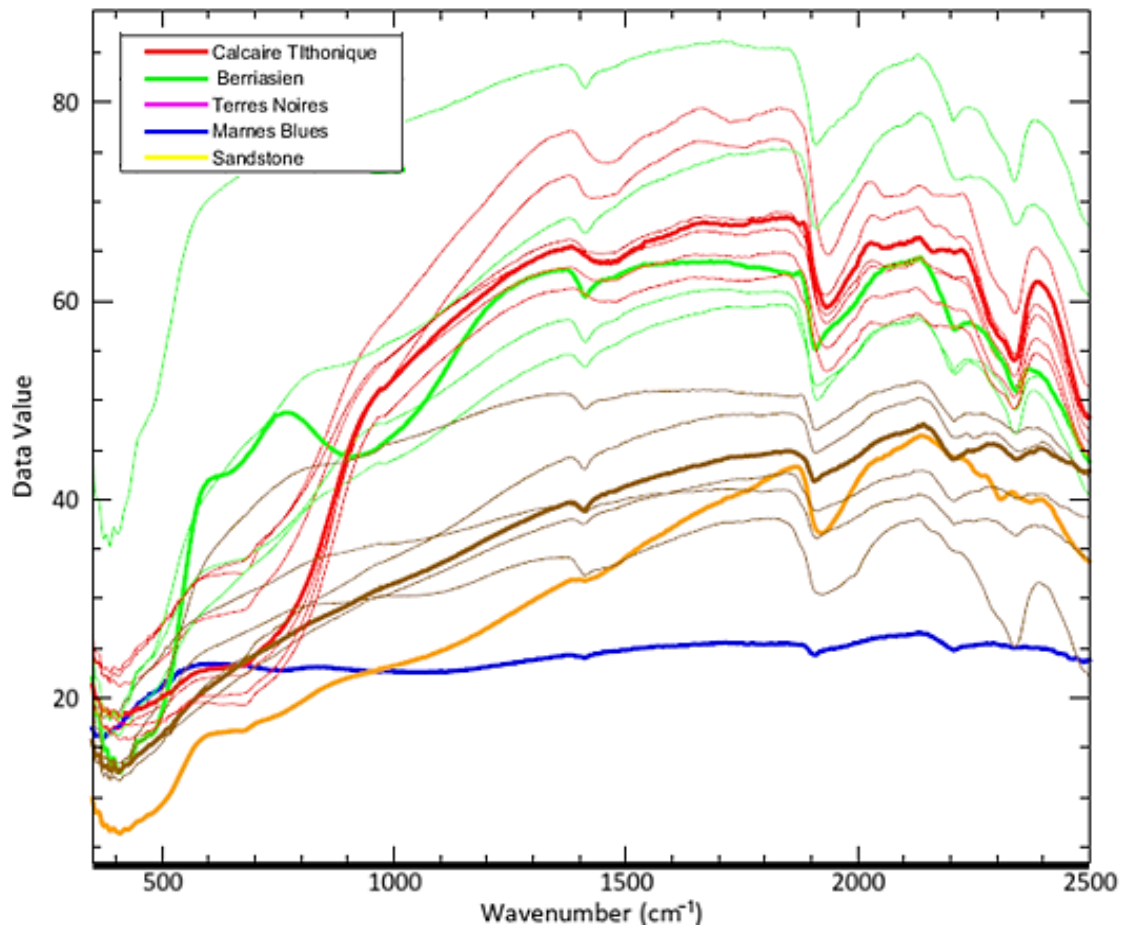


Figure 18: Spectral signatures of sampled rocks with colors indicating the lithological group.

4.2 Comparison of spectral mapping

Spectral mapping algorithms use different approaches in identifying and classifying the image pixels. Different approaches have unique advantages and disadvantages. Endmember similarity approaches such as SAM excel in mapping blue marl outcrops by recognising their lack of features as an indicator. However, the spectral similarity of limestone formations pose an obstacle and result in misclassifications. SVM algorithm uses a statistical approach and heavily relies on the accuracy of the training data. The distinction between spectrally similar groups has been made more accurately. The complex-patterns of dark marls have been identified as well. Overall, the SVM classifier has provided more accurate mapping results.

Three locations were selected comparing the spectral mapping results of Sentinel-2 and ASTER using SVM and SAM classifiers. These locations are chosen based on the outcrop visibility on the surface with the aim of displaying the classification outcomes on all lithological groups. Appendix A includes the full scale classification maps along with the geological map of the area.

Figure 19 and 20 show the performance of Sentinel-2 and ASTER nearby Serres. Dominant layer of steep, resistant limestone belonging to “Calcaire Tithonique” lithological group highlights the shape of the geological formation (Figure 4). The underlying lithological group, “Berriasian”, features a gentler slope which allows more vegetation to inhabit the area. Increase in vegetation result in decrease of pixels containing pure lithology, therefore the underlying layer becomes less visible in the classification. Outside the formation, less resistant marls allow the climatic forces to erode the surface and create small scale badlands. These basins are filled with eroded marl and low-laying colluvium (Gidon et al., 1991). The sediment in this area has a glacial origin and when mixed with marl, can create issues for classification.

Support Vector Machine (SVM) classifier has correctly identified the complex pattern of marls and limestones in Sentinel-2 imagery, with fewer misclassified pixels (Figure 19c). The misclassification appears in the bottom of the marl formations where glaciofluvial sediment mixes with eroded marls and results in pixels being classified as sandstone. Similar pattern recognition was achieved using Spectral Angle Mapper. Misclassification using SAM appears to be higher, with more parts of dark marl being classified as sandstone. The ridges around the geological formation are formed by “Calcaire Tithonique” with “Berriasian” situated beneath it. Discrimination between these two units is especially difficult giving their spectral similarity. SVM has somewhat distinguished pixels assumed to be “Calcaire Tithonique” and those assumed to belong to “Berriasian”. SAM could not distinguish the lithologies along the ridges and classified all pixels as “Calcaire Tithonique”. Whether that is false is difficult to conclude, knowing that a clear boundary between these two lithological units is not defined in the geological map (Figure 19e).

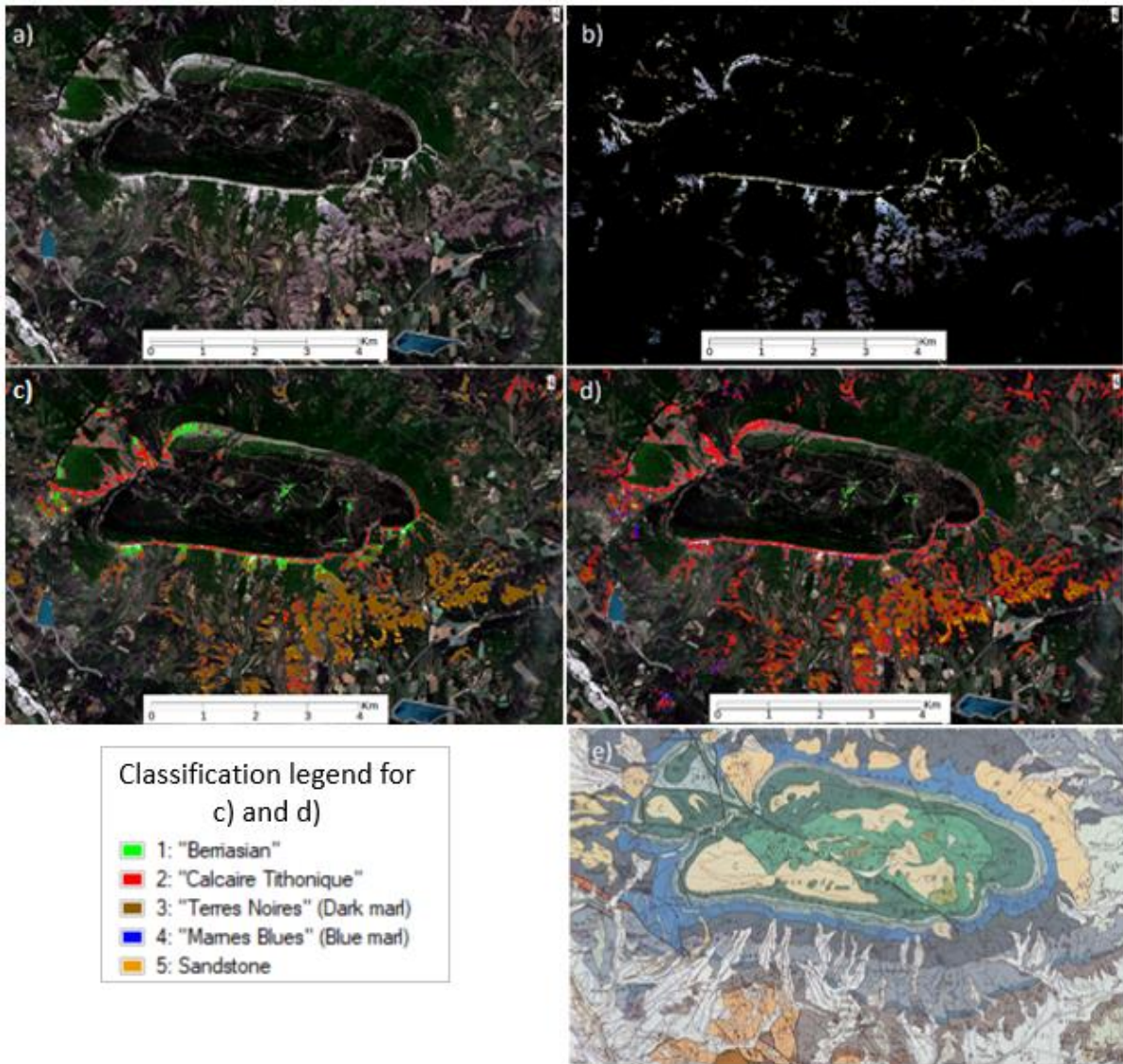


Figure 19: a) Sentinel-2 true color image of Serres Ear (RGB:[B4,B3,B2]), b) image after applied mask, c) SVM classification overlaid on true color image, d) SAM classification overlaid on true color image, and e) geological map.

Figure 20b shows the masked product of ASTER satellite image. Application of vegetation and shadow masks have removed a greater number of pixels, with the “Calcaire Tithonique” outline of the geological formation and some larger marl outcrops remaining visible. The complex nature of the geology in the area combined with coarser spatial resolution of ASTER result in much fewer pure lithological pixels. Both algorithms were capable of mapping the limestone ridges of the formation. The distinction between “Calcaire Tithonique” and “Berriasian” has not been defined along the ridges. SVM machine-learning algorithm has identified more presence of marls outside the formation than SAM (Figure 20c & 20d).

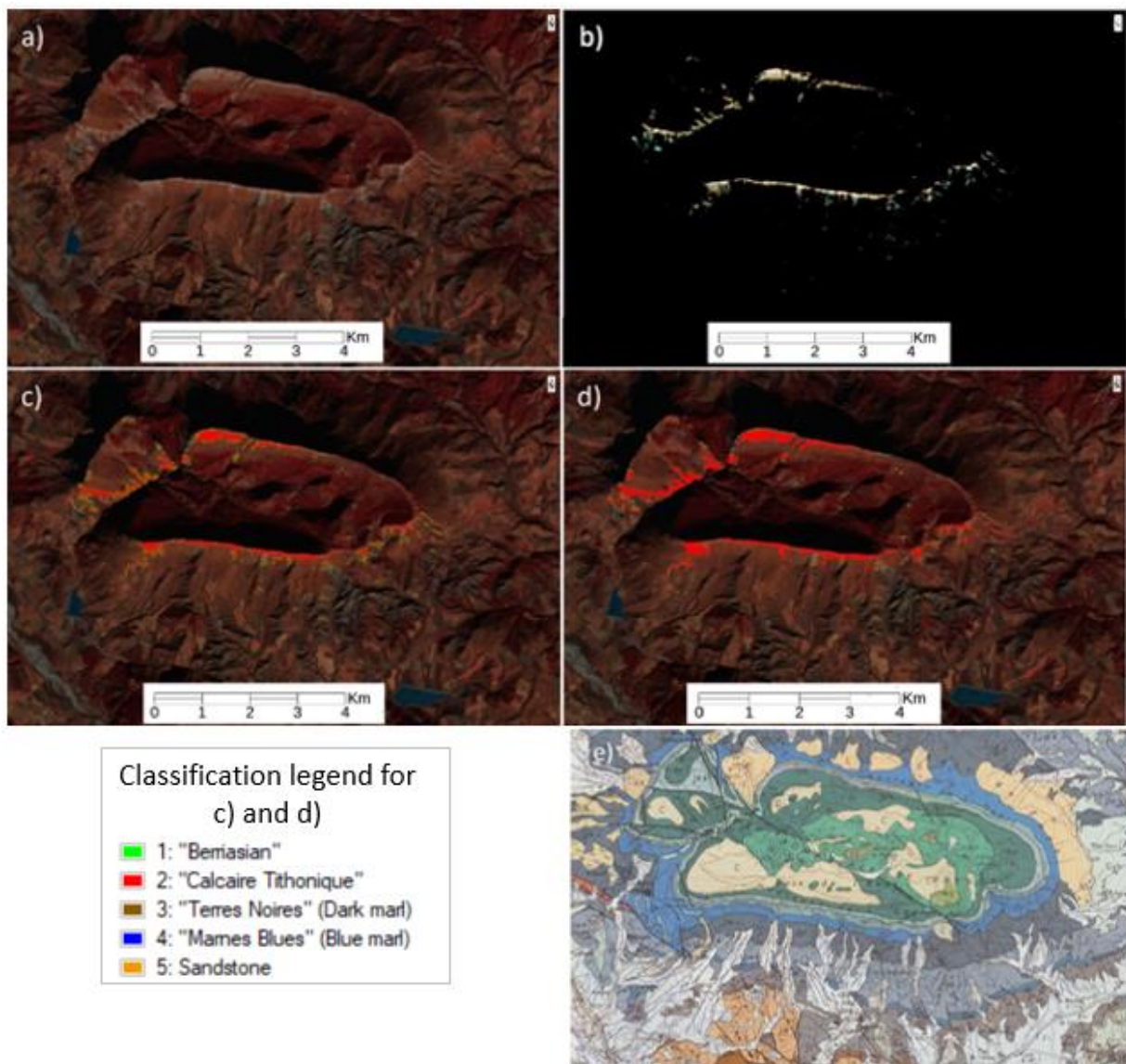


Figure 20: a) ASTER false color composite (FCC) image of Serres Ear (RGB: [B1,B2,B3N]), b) image after applied mask, c) SVM classification overlaid on FCC image, d) SAM classification overlaid on FCC image, and e) geological map.

The second location is situated north of Serres next to the small town of Aspres-sur-Buëch. A geological sequence similar to that of Serres Ear is visible here, with the strong resistant limestone on top and erosive badlands situated on the gentler hillsides below. The badlands contain minimal vegetation and clearly display the sedimentary marl beneath the vegetated surface. Sentinel-2 and ASTER original images of this site (Figure 21a & 22a) show a colour change occurring within the badlands. The geological maps (Figure 21e & 22e) confirm this change as being two different geological units of “Terres Noires” on top and “Argovien” below. While both sequences are grouped as the same lithological unit for the purposes of this project, the site location provides with a great opportunity to see pattern recognition abilities of SVM and SAM classifiers.

The spatial resolution of Sentinel-2 again shows more pure lithology pixels compared to ASTER (Figure 21b & 22b). The Support Vector Machine classifier is able to identify the marl pattern with less misclassification compared to SAM. The bottom of the formation where eroded material mixes with sediment again causes an issue for SVM with some areas being classified as sandstone. The same occurs on the top ridges of the badlands, where brighter pixels associated with “Argovien” get classified as “Calcaire Tithonique”. Generally, this misclassification is less severe than in the case of SAM. Here, the edges of the badlands result in brighter marl being mistaken for overlaying limestone. To the western side of the formation, spectral similarity between blue and dark marls result to some parts of the dark marl outcrops being classified as blue marls (Figure 21d). In the case of SVM classifier (Figure 21c), similar misclassification occurs between dark marls and more limestone-dominant “Berriasian”.

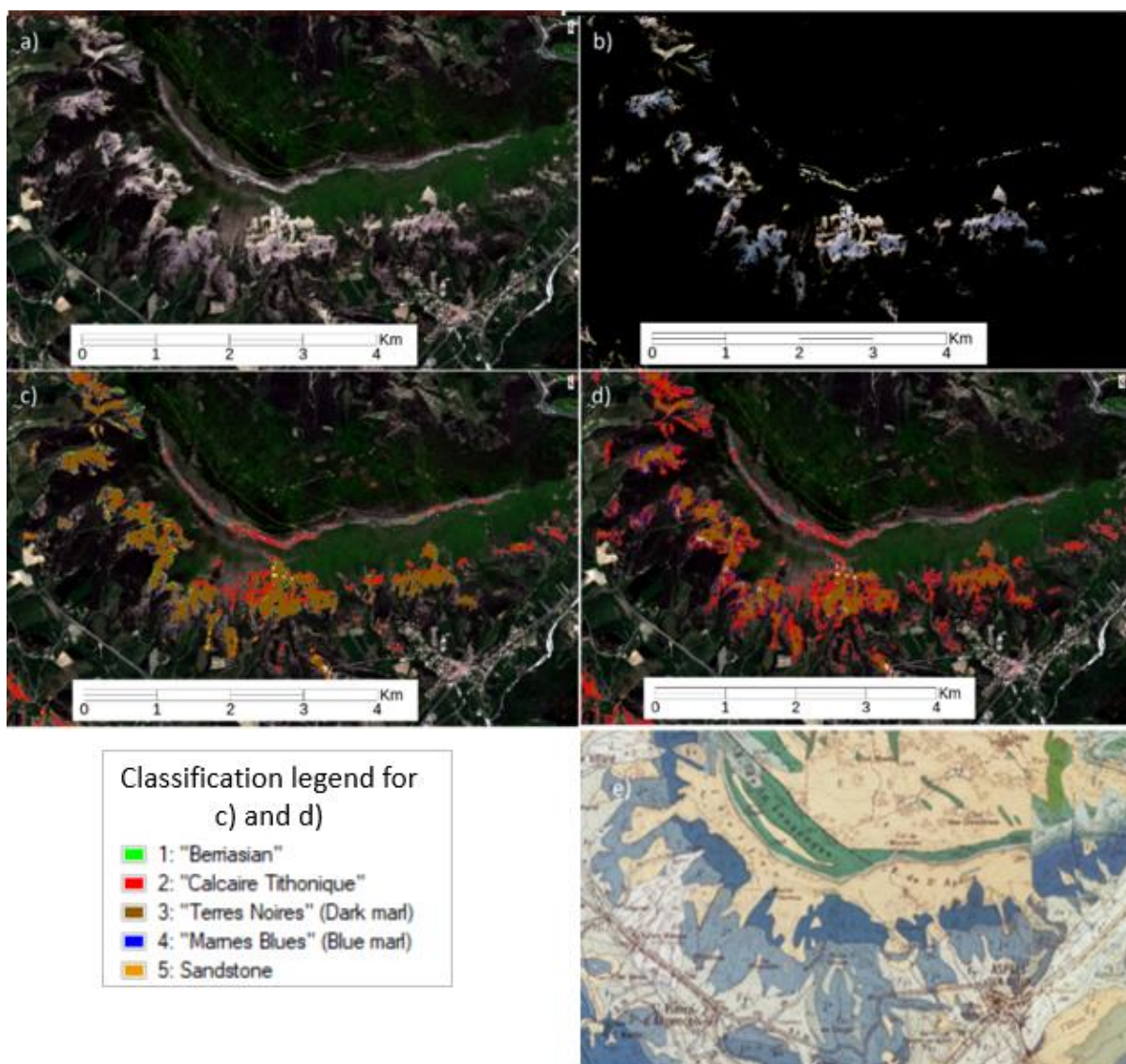


Figure 21: a) Sentinel-2 true color image north of Serres (RGB: [B4,B3,B2]), b) image after applied mask, c) SVM classification overlaid on true color image, d) SAM classification overlaid on true color image, and e) geological map.

Figure 22a shows the same location using ASTER imagery and winter conditions. The steeper ridges cause less recognition of pixels containing only rock. Spectral Angle Mapper and Support Vector Machine classifiers both struggle slightly with discrimination between the two limestone units of “Calcaire Tithonique” in red and “Berriasian” in green (Figure 22c & 22d). Spectral Angle Mapper seems to perform better, which can be explained by Support Vector Machine algorithm not having enough coherent points to establish a pattern in the ridges and badlands. The marl badlands location contains less misclassification compared to images from Sentinel-2.

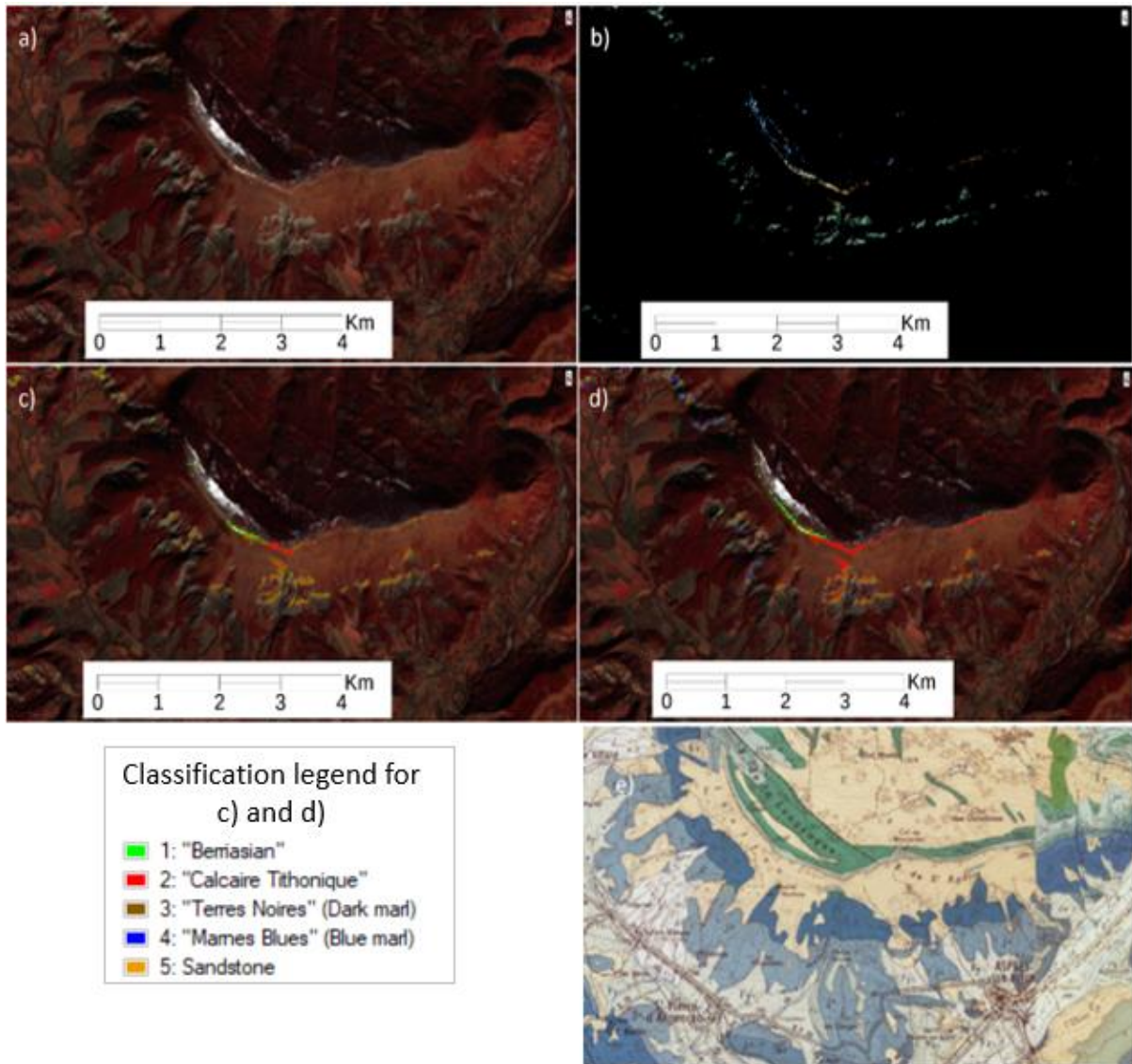


Figure 22: a) ASTER FCC image north of Serres (RGB: [B1,B2,B3N]), b) image after applied mask, c) SVM classification overlaid on FCC image, d) SAM classification overlaid on FCC image and e) geological map.

Figure 6 shows the sandstone outcrop situated west of Serres with visible blue marl outcrops spread out over the valley. The Sentinel-2 image of this location is displayed in Figure 23a. The pixel diversity and complex topography create a difficult scene to classify. Sandstone formation appears clearly in both SVM and SAM classifications (Figure 23c & 23d). The underlying blue marl seems to be an issue for

SVM (Figure 23c). The brighter edges of the ridges, along with singular lighter spots are assigned the green class, which judging by the geological map seems plausible. However, the abundance of blue marls has not been recognized in SVM and larger blue marl outcrops are classified as dark marls. Spectral Angle Mapper seems to perform better in differentiating between different marl formations (Figure 23d). However, the spectral similarity between “Calcaire Tithonique” and “Berriasian” cause an issue in areas with complex clusters of pixels. Another issue occurs in areas where high-altitude objects, i.e. airplanes, have diluted the spectral response of the pixels. This is observed next to the sandstone formation, creating an issue for both matching algorithms and result in misclassification near the sandstone outcrop.

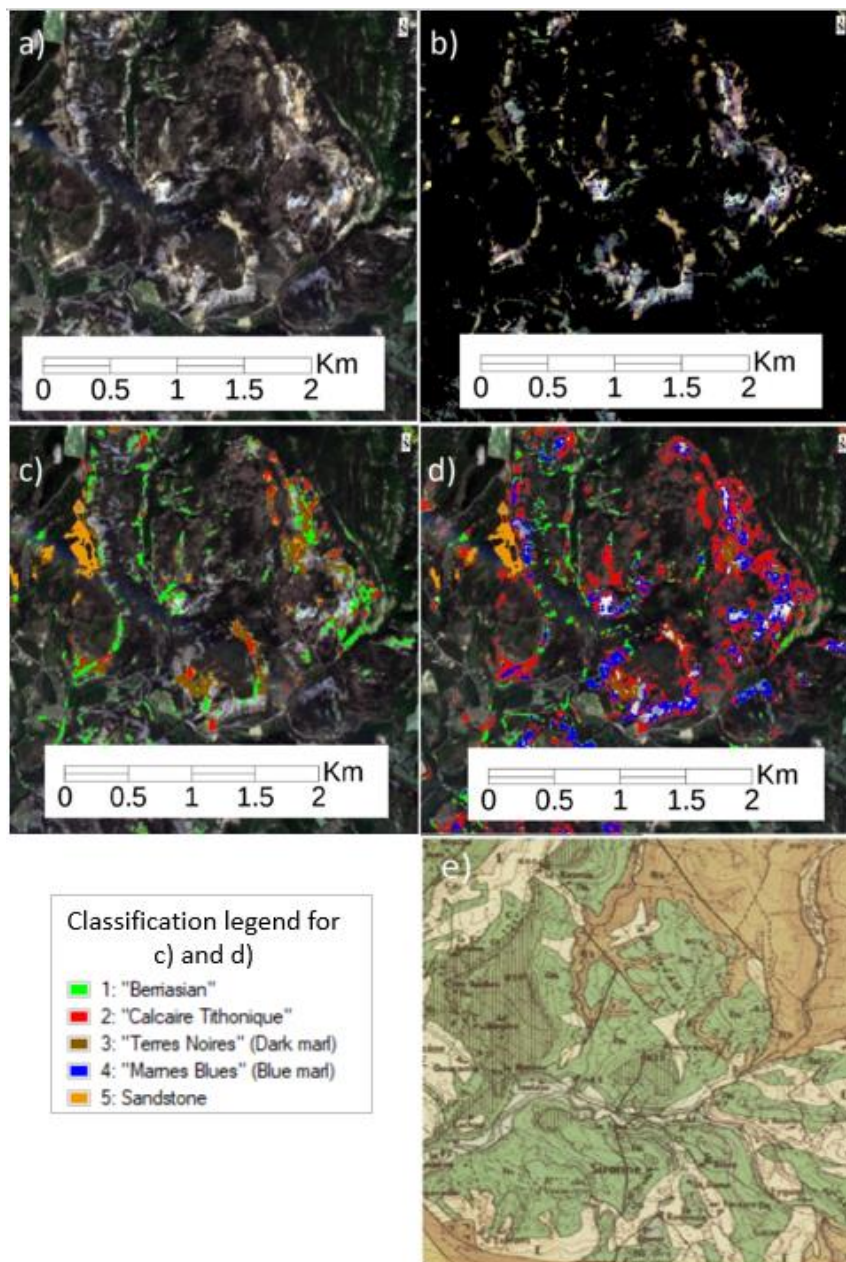


Figure 23: a) Sentinel-2 true color image of sandstone outcrop West of Serres (RGB: [B4,B3,B2]), b) image after applied mask, c) SVM classification overlaid on true color image, d) SAM classification overlaid on true color image, and e) geological map.

Figure 24 shows the same location captured using ASTER. The sandstone outcrop marked with an orange rectangle does not show significant spectral difference from surrounding vegetation, which results in sandstone outcrop being fully masked out under pre-processing (Figure 24b).

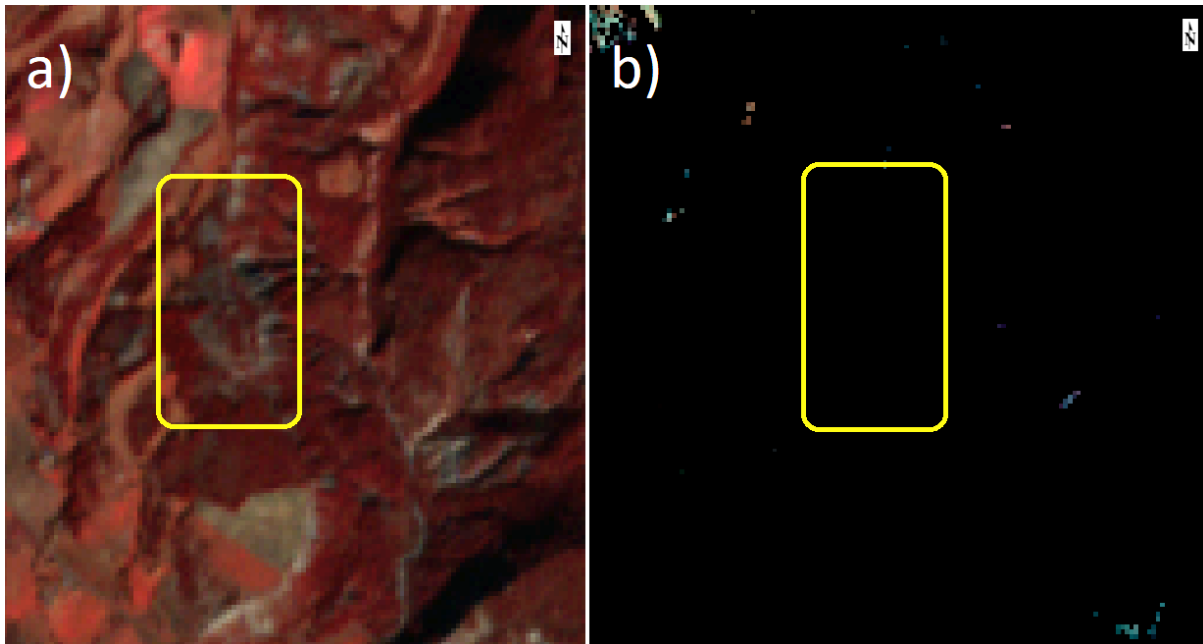


Figure 24: The same sandstone outcrop in ASTER FCC imagery showing the outcrop disappearing after masking.

4.3 Comparison of spectral libraries

Exposure to weathering over a substantial period of time has an effect on spectral brightness, intensity of diagnostic absorption features and spectral slope (Zhou & Wang, 2017). Spectral change has been measured by comparing the weathered sample with its fresh content (Figure 25). Positive values indicate areas where fresh samples have lower overall reflectance. In many cases the fresh material shows higher overall reflectance in the VNIR range (350 – 1000 nm) resulting in negative values in the figure.

Although it is difficult to draw a clear relationship between the lithological group and the degree of spectral change, overall biggest spectral differences have been observed in “Berriasian”, depicted in the figure 25 as green. Samples attributed to “Berriasian” limestones feature spectral differences reaching 50% at SWIR spectral range. Dark marls depicted in purple show least spectral change difference throughout the measured spectrum, with changes ranging from 0 % to 30 %. This lithological group also shows least variation near the characteristic absorption bands of water and carbonate. “Calcaire Tithonique” displays a significant difference between fresh and weathered signatures.

In terms of absorption features, a decrease in water absorption at approximately 1400 nm and 1970 nm were observed in all fresh samples. Calcium carbonate content of sample rocks is seen more clearly

in fresh material of “Calcaire Tithonique”, resulting in spikes near characteristic absorption features of calcite. The spikes are especially large at 2300 nm, indicating an increase of carbonate detected in the rock. Hydroxyl absorption feature at 2200 nm has remained unchanged in most measured samples with few samples showing a slight decrease. Sandstone and blue marls show an overall decrease in reflectance, but maintain the same depth, shape and form of characteristic absorption features as their weathered counterparts. Due to lack of absorption features in blue marl, the spectral change between weathered and fresh samples does not change significantly close to water and diagnostic mineral spectral bands.

It is important to note that marls themselves are too brittle to contain a large enough solid samples for weathered-fresh comparison. Hence, only the limestone layers within marl formations are examined. These limestones show considerably less weathering effect than the limestones of “Calcaire Tithonique” and “Berriasien”, which can be attributed to overlaying marl acting as a cover from weathering processes.

Spectral signatures and their differences between weathered and fresh surfaces for selected rock samples are shown in the Appendix B.

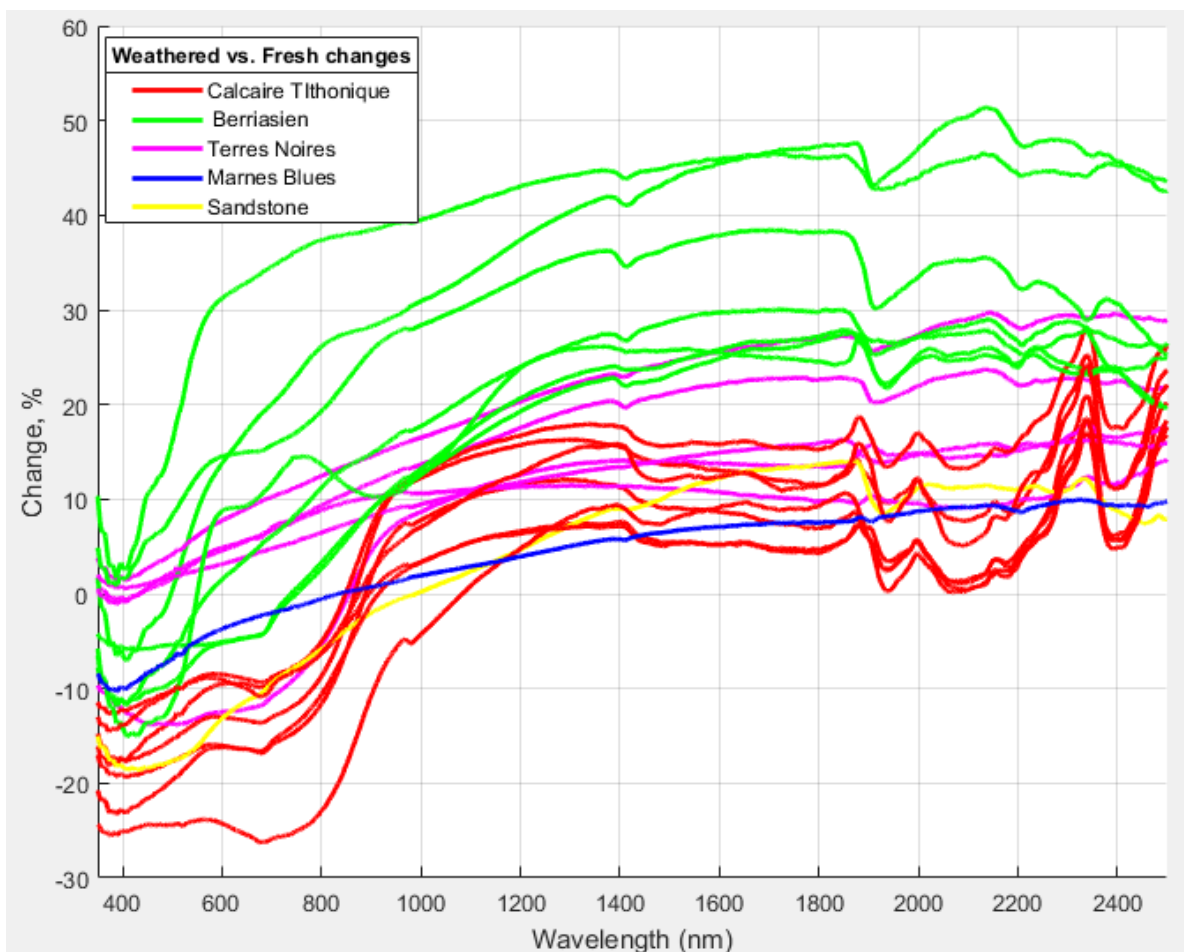


Figure 25: Spectral change of rock samples with color indicating the lithological group.

4.4 PSR+ spectroradiometer performance

Spectral radiance

Additional measurements were made to examine the performance of the spectroradiometer. Figure 26 illustrates the reference spectrum measured using PSR+ spectroradiometer in laboratory conditions. The first detector features peaks and troughs. This pattern differs from the smooth pattern observed in detectors two and three. The sudden transition between detectors is observed, marked with vertical black lines.

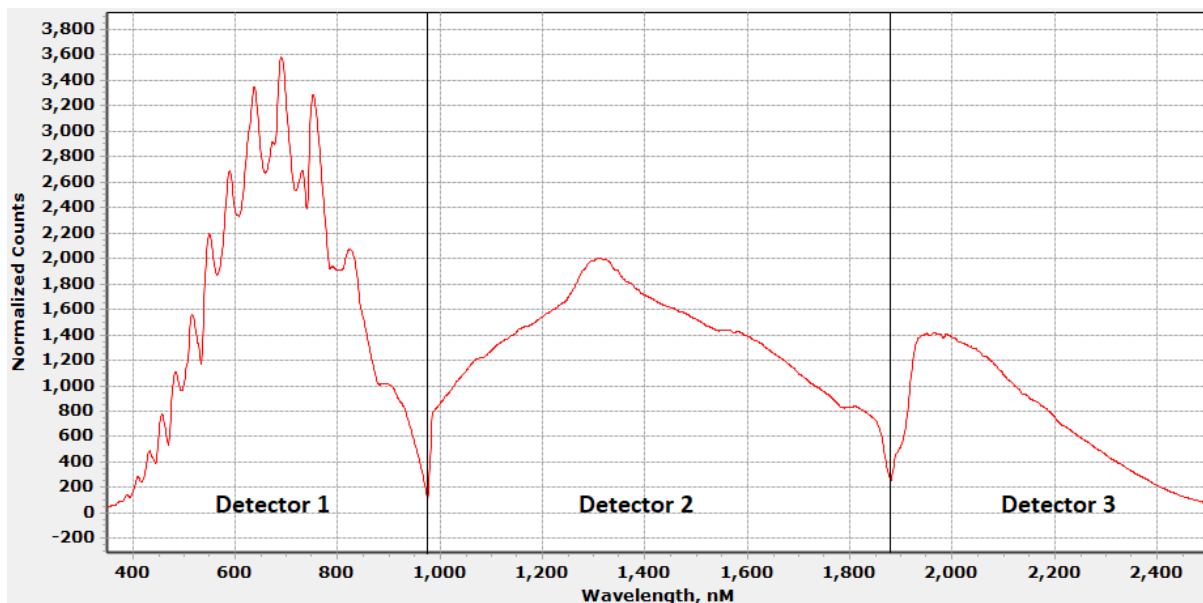


Figure 26: Spectral radiance curve of PSR+ spectroradiometer on the reference palette.

External light effects

Influence of light from the surroundings can heavily influence the measurements. To test if the light in the room has any effect, four measurements with light and four measurements without light were performed. The results show a small variation, however the same variation is observed measuring with constant conditions (Figure 27). The biggest error here does not exceed the inherent error margin of 0.5 % from the instrument. The implication of the experiment is that when contact surface between the probe and measured object is sufficient, the external light source has little to no effect on the results.

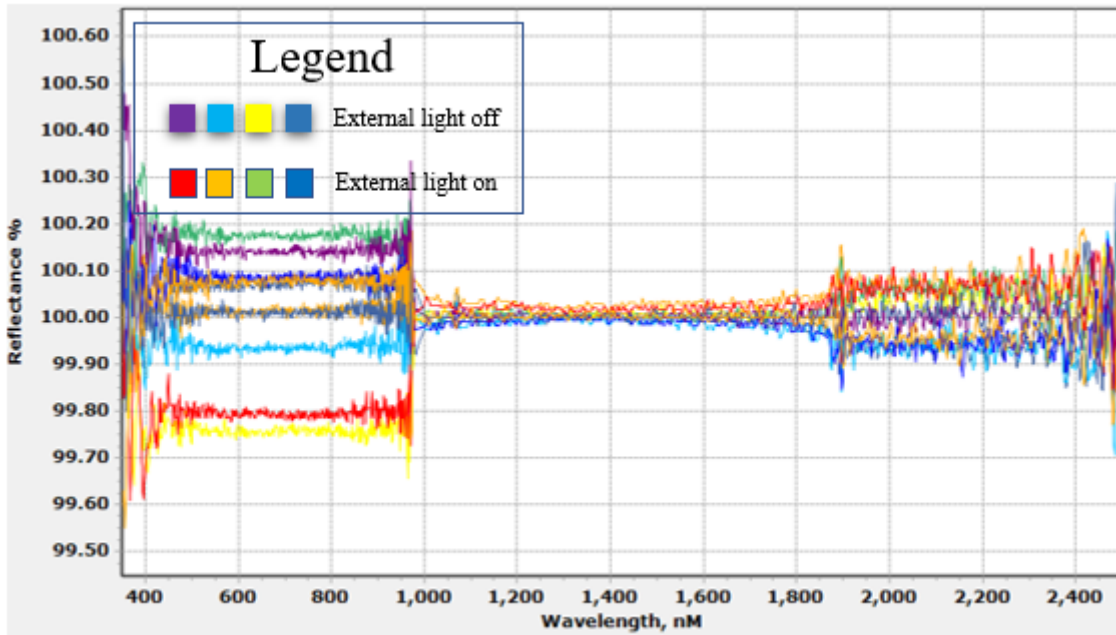


Figure 27: Measurements with external lights on (colours: red, orange, green, blue) and off (colours: yellow, purple, ocean blue, dark blue).

Contact surface

Figure 28 illustrates the effect of contact surface on measurements. Measuring sandstone with fully closed surface provides minimal light leakage insuring maximum possible albedo. This results in rock being “brighter” and in turn measured reflectance values being higher. This experiment provides an additional reason why using contact probe is advantageous over FOV lenses. Contact probe allows the user to control the contact surface between the spectrometer and sampled object, resulting in more accurate measurements.

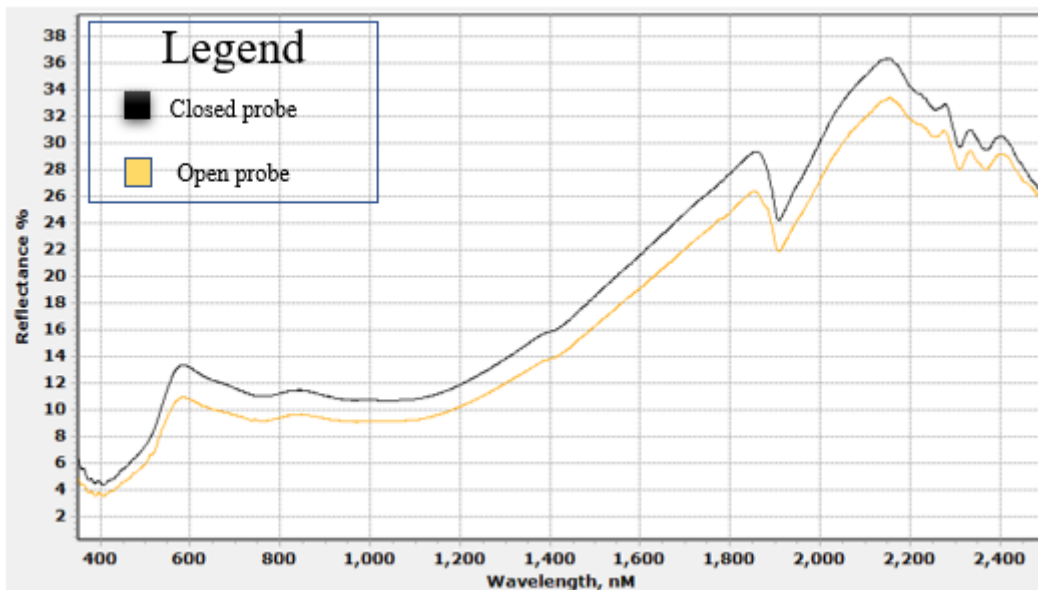


Figure 28: Measurement of sandstone with closed contact probe (black) and not fully closed contact probe (orange).

Drift in detector 1

During the measurement process, a drift in the first detector was observed resulting in a 0.5 % offset. Further tests were performed to examine if temperature from the light source, room lighting, optic cables or leakage of the light had an impact on the data. Additional measurements were performed to examine the heat effect exerted from the contact probe lens being closed and in contact with the reference palette. Repeated measurements were taken on a 1 minute interval for half an hour (Figure 29). If heat from the contact probe would have been the reason for the drift, a similar 0.5 % offset at any point in the experiment would have been observed. This however was not the case. While an upwards trend is observed in the first detector, it does not offset above 0.8 %. In order to minimise the error margin, every measurement of the sampled rocks were followed by a measurement on the reference palette.

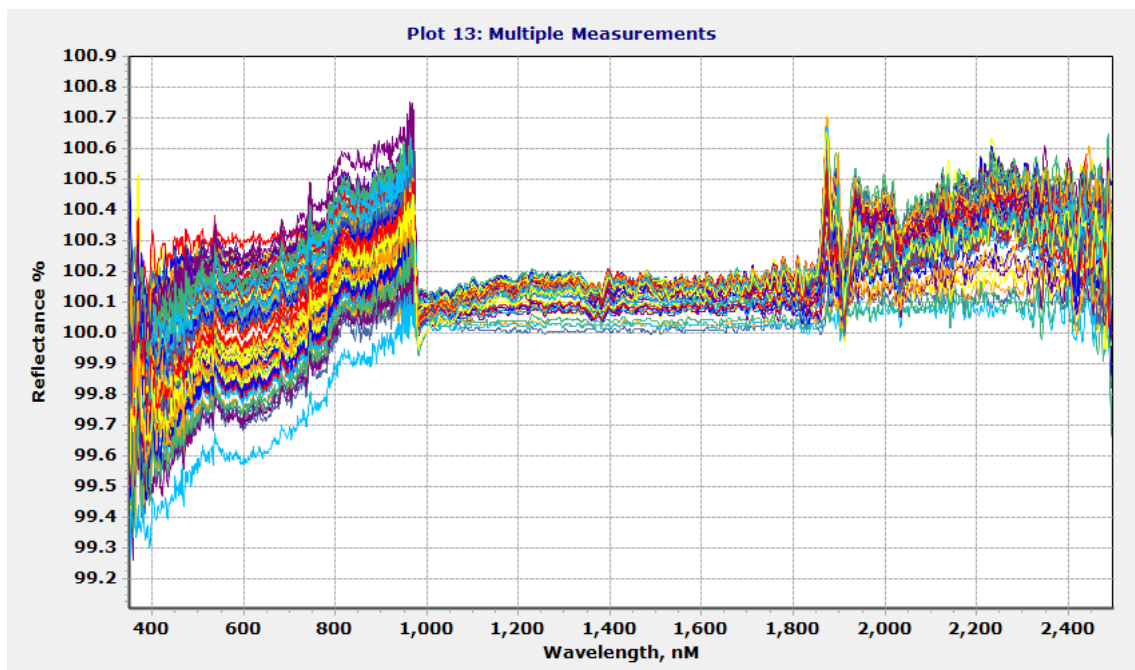


Figure 29: Experiment with closed contact probe and 1 minute measurement interval.

Overlapping fresh and weathered spectral signatures

Overlapping spectral signatures in visible and near infrared (VNIR) between fresh and weathered surfaces of the same samples were observed. A few theories were formulated to explain this anomaly. Presence of shadows or leakage of light can result in larger offsets between the three detectors. Such offsets are however minimal in the data, which rules out presence of shadows and light leakage as an explanation. Light leaking into the measurement from the outside can have an effect on the reflectance. But tests using contact probe with different light setups, such as with LED lights and tungsten lights show minimal effect.

Spectral measurements on samples washed with vinegar did not show any significant improvements (Figure 30). The overall reflectance decreased when the sample has been treated with vinegar and the same overlap is visible only at different wavelength due to the decrease in reflectance. The acidic vinegar reacts with carbonates such as calcite, this changes the chemical composition of the rocks slightly. This reaction could have a reverse effect on the objective – instead of improving the results, it reduces the representability of the samples.

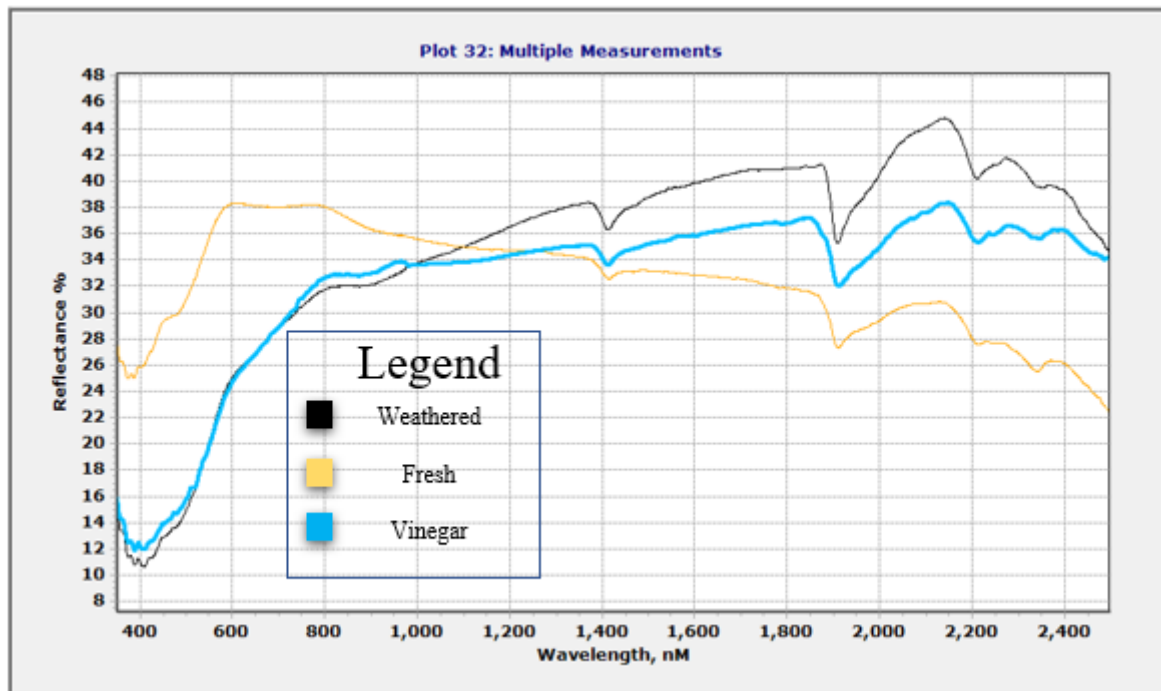


Figure 30: Spectral measurements of rock sample #27. Weathered surface in black, fresh surface in orange and vinegar treated sample in blue.

5. Discussion

Spectral mapping results

A major challenge observed in classifying lithological groups is recognition of different marls. In blue marl outcrops near the sandstone formation the complexity of patterns and diversity of pixel tones, created false classifications in both SVM and SAM (Figure 23). Spectral Angle Mapper has successfully located some of the outcrops, while other blue marls were assigned dark marl class.

Similar issue is observed in the case of limestone discrimination. The two limestone formations of “Calcaire Tithonique” and “Berriasian” appear near one another, share spectral similarity and the boundary between the two formations is unclear even in the geological maps. This creates an obstacle which SAM does not seem to tackle. This is imminent in Serres Ear where no discrimination between

lithological groups along the ridges seem to occur (Figure 19d & 20d). Taken the whole image scene into account, SVM algorithm yields a better separation between the lithological classes, indicates a strong pattern-recognition ability and appears to produce less misclassifications.

Selection of training data is a crucial part of supervised classification and hence is partially responsible in misclassifications. No more than 20 pixels were selected for each group. In doing so we assure more accurate representation of different classes. A larger training dataset was also tried, yet the results showed an increase of misclassification. More pixels resulted in less representative definitions of classes, making the classes more similar. Overall, SVM performs more favourably over SAM with limited reference data available.

The performance of spectral matching algorithms has been severely affected by the spectral and spatial resolutions of Sentinel-2 and ASTER. The lack of narrow spectral bands in the SWIR range prevented an effective use of Sentinel-2 high resolution imagery in combination with spectral signatures of the rock samples. An opposite is the case for ASTER, while it does have an immense potential for mineralogical approach and has been used for such applications prior to this research, here, the vegetation cover prevents a successful lithological matching based on rock composition.

Other spectral mapping techniques were examined, with another machine-learning technique showing potential in these conditions. Lithological maps derived by neural network (NN) algorithm yield promising results and are discussed in greater detail in appendix C.

Spectral changes in lithology

In semi-arid regions, such as the Southern France, the dominant weathering effect is the clay and iron oxide formation. The assimilation of atmospheric water into the material result in absorption features at 1400 nm and 1900 nm. Several samples show water-related absorption around 2200 nm, indicating a possible structural water being bounded with the crystalline lattice of the material. Measurements show the main spectral changes occurring in the 350 – 1000 nm (VNIR) and 1900 – 2500 nm range. The principal changes observed between weathered and fresh rock surfaces in the 350 – 2500 nm spectral range are connected to albedo of the material, existence and abundance of characteristic absorption features and slope difference.

In lithological remote sensing, the majority of misclassifications occur between materials exhibiting spectral similarities. Unfortunately, this is most often the case in real-life geological settings. The study area surrounding Serres is not an exception in this aspect. The diagnostic absorption features for different lithological units appear similar in intensity and overlap is common, making the endmembers for each class heavily correlated. Such spectral confusion prevents the identification and classification of lithological units by their mineral content.

In terms of usability of laboratory-derived spectral libraries, this project shows that in a scenario with complex and very similar geology between lithological groups, such libraries produce non-representative classification.

The most important reason for false identification of materials lies in the spectral and spatial resolution of the satellite imagery. Figure 31 shows a collection of satellites with their representative spectral bands. A selection of spectral signatures from the study area and atmospheric transmittance are overlaid in the background. A closer look at the signatures suggest that while Sentinel-2 does possess higher resolution imagery, the high-resolution spectral bands are in the VNIR range where the spectral signatures from the subject rocks are featureless. The distinctive spectral features of the subject rocks are located in the short-wave infrared (SWIR) range. Advanced Spaceborne Thermal Emission and Reflection Radiometer (ASTER) contains 5 bands in the short-wave infrared (SWIR) and seems to be the most promising satellite choice. However, the 15-meter spatial resolution of the spectral bands becomes a problem in regions with large vegetation and topographic effects.

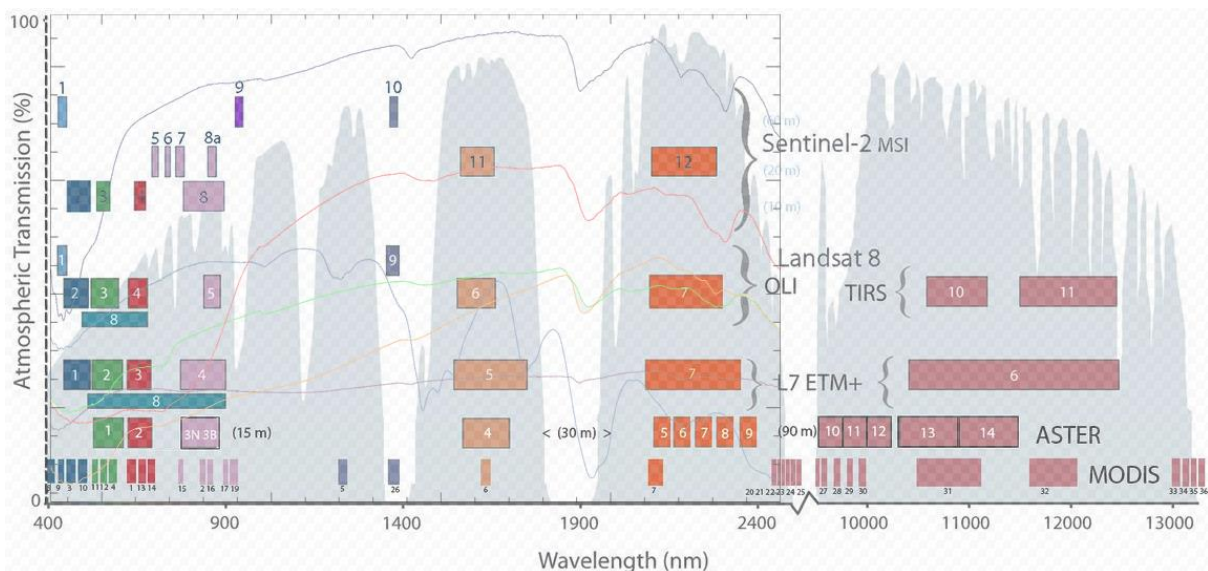


Figure 31: Comparison of satellite spectral bands in lithological spectral mapping perspective.

Spectral information necessary for successful classification

Ideally, the lithological classification would be based on the characteristic absorption features observed in the sampled rocks. The spectral band distribution in the satellite sensors provides an obstacle in using such method. However, this does not prevent supervised classifications such as SVM to form accurate definitions of classes from the training data to identify the lithological units.

The training pixels in SVM classifier are represented as pattern vectors which contain an array of numerical measurements for each band in the satellite image (Mountrakis et al., 2011). In addition to band-by-band numerical measurements, descriptive features based on spatial relationships between

pixels such as texture may be included in forming discriminative class definitions (Kupidura, 2019). Spectral variability of satellite image results in each pixel having a texture value which can be used in forming spatial relationships between pixels. Classification accuracy increases significantly with the addition of textural information in classification (Kupidura, 2019). An example can be used of the two marl lithological units - “Marnes Blues” and “Terres Noires”. Both classes display similar spectral characteristics, but the textural differences allow their complex patterns to be identified and distinguished from one another. More accurate overall classifications obtained by SVM classifier as oppose to SAM show that a combination of spectral and textural information yields better classification results compared to solely spectral similarity based classification in a setting with limited detectable absorption features.

Resampling of spectral libraries

PSR+ spectroradiometer measures the spectral response of an object in a 350 – 2500 nm spectral range. Spectral libraries of weathered and fresh rock samples need to be resampled to match the spectral range of Sentinel-2 and ASTER. This is done by importing the ASCII wavelength files from PSR+ spectrometer into ENVI 5.5 software and applying spectral resampling. Figure 32 shows the spectral profiles of weathered rock facies once they have been resampled to match Sentinel-2 and ASTER spectral ranges. The original spectral library shows distinctive absorption features which can be used for classification of sampled lithological units. However, resampling of spectral endmembers to Sentinel-2 spectral bands results in removal of characteristic absorption features. In the case of ASTER, spectral bands in SWIR range allow the spectral endmembers of rocks to retain some of their characteristic absorption features, such as hydroxyl absorption at 2200 nm and carbonate at 2240 nm. This shows that ASTER band distribution gives it an advantage in mineral mapping, given that the study area contains minerals diagnostic at SWIR spectral range.

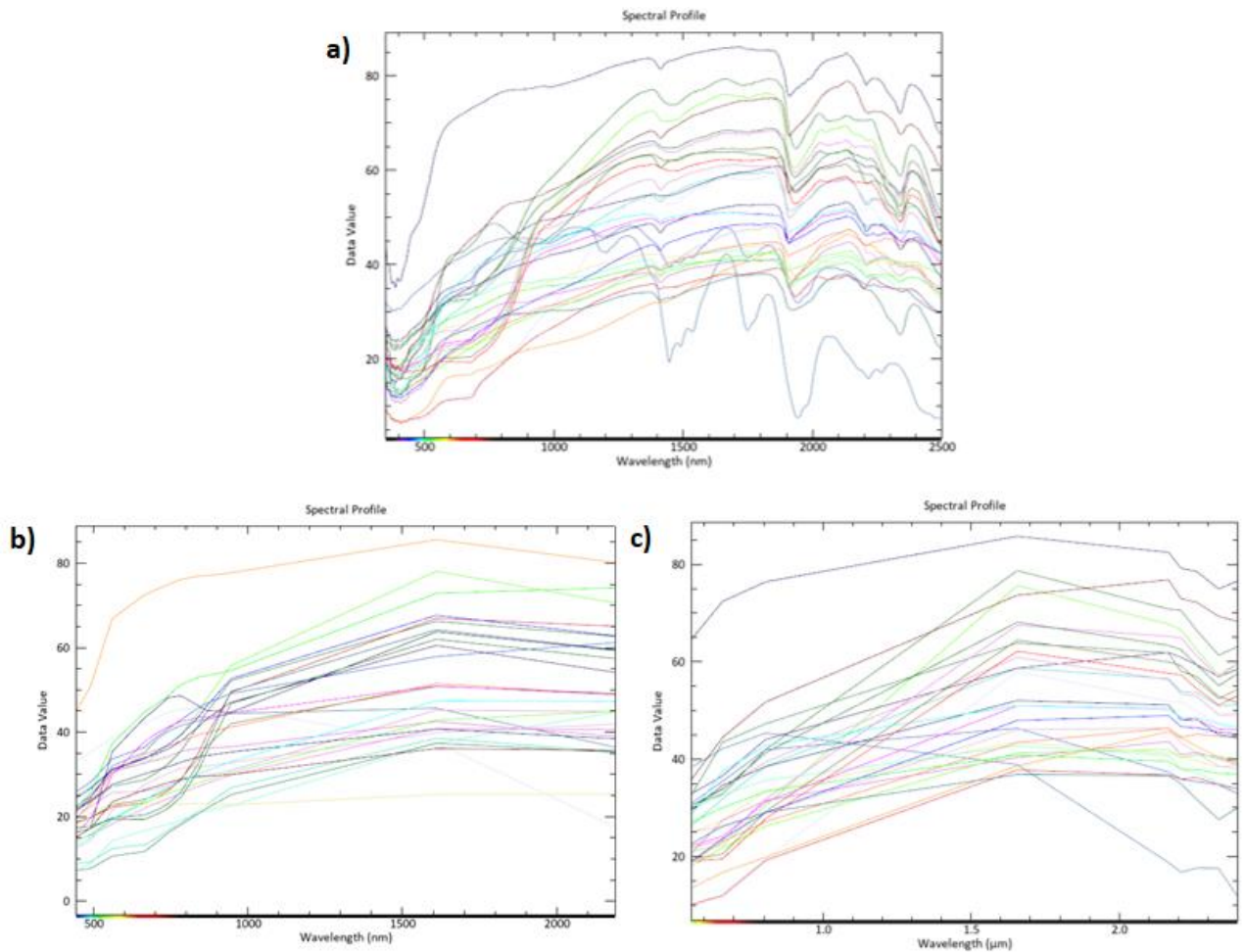


Figure 32: Spectral libraries of all weathered rock samples. Original measurements (a), resampled to Sentinel-2 (b) and resampled to ASTER (c).

Fieldwork and laboratory work

Fieldwork period had only few days with poor weather conditions. Outcrop accessibility governed and somewhat limited the sample site selection, but all major lithological units were sampled. UTM-coordinates, pictures and other geological information were notated and the field sample data was correlated with the geological maps to confirm the lithological class belonging to the samples. Fieldwork process was satisfactory and all fieldwork goals were achieved.

Laboratory measurements of the field samples were performed after the measuring setup was determined, spectroradiometer was examined and appropriate training on use of measurement processing data was given. Water absorption features were well documented in both weathered and fresh rock surfaces. Weathered samples were dried in room temperature for a day, prior to the measurement. Fresh samples were dried in a more intense conditions due to recent direct contact with water during sawing. Drying of the rocks produced different water absorption signals, with weathered material showing higher water content. This could have been adjusted by drying the samples in an

industrial oven, but was not applied in order to receive most accurate assessment of the actual field spectra.

The general performance of PSR+ spectroradiometer was quite good with satisfactory measurement results and few issues which were mostly nullified by making adjustments to the measurement process. Issues concerning the instrument itself such as the slight deviation in the first detector could not be resolved and had to be closely monitored during laboratory work and taken into account under discussion of the results.

Image quality

The objects at surface level contain good co-registration in the images by all spectral bands in Sentinel-2. However, the processing algorithms struggle in properly co-registering objects situated at higher altitudes such as planes and clouds (Clerc & MPC Team, 2020). According to the latest Sentinel-2 L1C Data Quality Report, the anomaly is caused by the spectral misregistration and results in discontinuity between detectors. This “rainbow” effect is observed in the Sentinel-2 image (Figure 33). This effect has impacted the mapping results close to the sandstone outcrop. An improvement would be to use satellite imagery absent of this anomaly, however such scene is not available taking into account other criteria such as cloud cover and time of acquisition i.e. closest to the field work time.

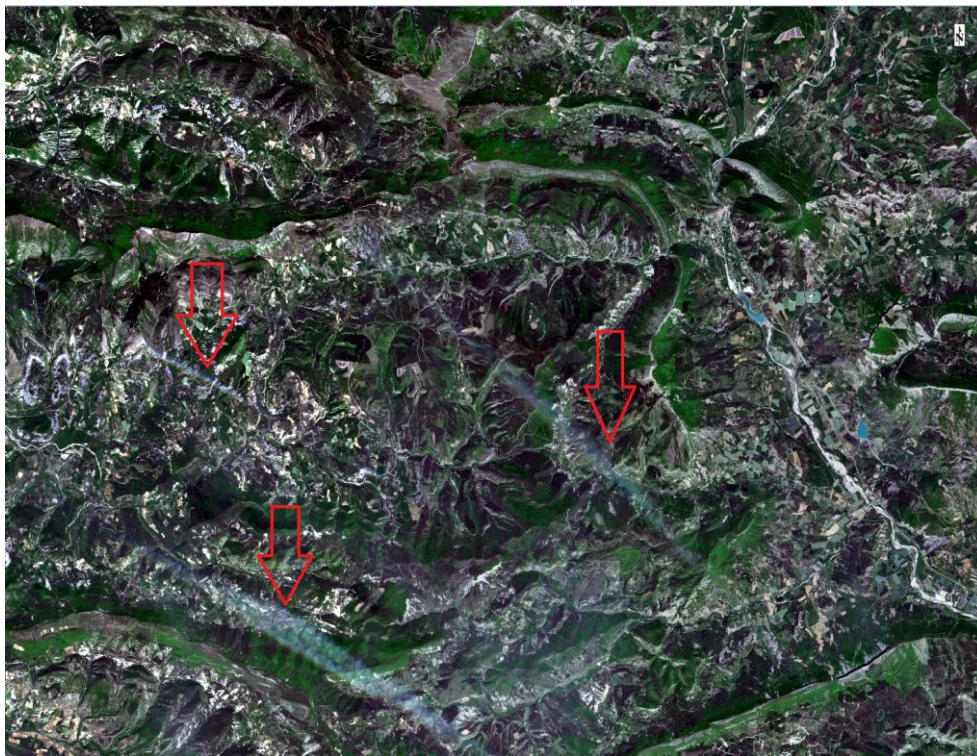


Figure 33: Examples of misregistration of high altitude objects in Sentinel-2 imagery (RGB: [B4,B3,B2]).

The study area is situated in a semi-arid region with strong influences from Mediterranean and Alpine weather systems. The climatic setting and human activity has resulted in large vegetation areas and agricultural fields. These conditions create issues for lithological mapping, especially in the summer. That is imminent in the case of Sentinel-2. As for ASTER imagery, the satellite data was acquired in winter, minimizing the vegetation effect. However, during the winter months, the sun pattern relative to Earth's rotation changes, providing more shadow during the acquisition of the images. The presence of shadows in lower elevations and water in the form of snow in the higher elevations have been the main limiting factors related to the study area for ASTER.

Pre-processing steps executed vary for the two satellite products. The newer Sentinel-2 contains specific processing algorithms designed to leverage the advantages of this satellite. In the case of ASTER, such satellite-specific processing techniques are absent with merely a handful of research papers focusing on ASTER data pre-processing for enhanced geological applications.

Outlook and recommendations for further research

Examining the results, a few recommendations could be made for further research. Classification and accuracy improvement could be achieved by upscaling from multispectral to hyperspectral imagery. Utilizing a high-resolution UAV imagery over the study area could be used for more accurate estimates of geological boundaries between lithological units. UAV imagery could be available on short-term, however it requires an on-site presence by the UAV operator. Spaceborne missions such as DLR EnMap (Guanter et al., 2015), ESA Copernicus CHIME (Rast et al., 2019) and NASA HypSIIRI (JPL, 2018) are planned but not yet in orbit. These missions will provide hyperspectral imagery in the near future which could complement the research done with existing spaceborne optical sensor data. Combination of spaceborne and hyperspectral imagery has been successfully used in achieving accurate lithological maps prior to this research (Van der Meer, 2012; Van der Werff, 2015).

Substantial understanding of different parameters and experience with training dataset inputs is required to obtain reliable SVM and SAM results. In terms of spectral processing, further improvements could be achieved by performing a more in-depth analysis of input parameters and their thresholds. While recommended values are derived, they are often generalized and may not provide favourable results for the specific conditions present in the study area.

Another point on future improvement concerns the hierarchy of project execution. The structure of this research included literature study, fieldwork, laboratory work and lithological mapping in that order. This resulted in classification methods being determined fairly late in the research. An argument could be made for more thorough examination of the satellite imagery and a primary selection of classification methods prior to fieldwork. This could lead to better fieldwork execution and improve

sample gathering. Blue marl formations could be used as an example. Blue marl outcrops are fairly distant from the fieldwork area. If knowledge on large misclassification of blue marl would be known prior to fieldwork, an extensive surveying and sampling of blue marl formations could have taken place. Furthermore, spectral measurements of weathered surfaces could be executed in the field during fieldwork. Field spectral measurements with the PSR+ spectrometer would increase the representability of measured weathered rock surfaces as oppose to transporting the samples in plastic bags back to the laboratory and measuring these samples several months later under different conditions.

Recommendations regarding the use of PSR+ spectrometer include measuring with a contact probe as opposite to other setups to reduce light leakage from build-in light source and light interference from the surroundings. In addition, it is recommended to let the spectrometer warm up for approximately 15 minutes once it has been started and execute a few test measurements on a reference palette to ensure the instrument is working properly.

The last recommendation concerns incorporation of digital elevation model and other morphological products to increase the textural understanding of the area. In this research, DEM was used solely for illustrational purposes, to improve the visualization of the study area. Inclusion of digital elevation model should provide valuable information on fault structures, as well as, geological boundaries and when draped over geological or lithological maps, could be used for accuracy assessment. Sample location data collected during fieldwork includes exact coordinates and elevation. A more precise accuracy assessment can then be performed by comparing the rock sample data with the geological maps draped over DEM. Similarly, the spectral mapping results could be draped over DEM and compared to the field samples.

Other geomorphic indexes, such as surface roughness (SR), surface index (SI) or hypsometric integral (HI), can provide useful information on landscape evolution. Surface roughness is described as the relationship between surface area and projected area. It is used as an indicator for surface deformations. Hypsometric integral has been demonstrated in accurately identifying the progression stages of landscape evolution (Othman & Gloaguen, 2013). As for surface index, it is a continuation of hypsometric integral and is used to distinguish between actively-deforming and more preserved landforms (Andreani et al., 2014). These indexes, if incorporated, should provide additional information on the structure and nature of the study area, as well as, improve classification between lithological units.

6. Conclusion

The primary objective of this study was to combine field-based spectroscopic research with geological remote sensing methods to produce representative lithological maps of the study area. The results of Spectral Angle Mapper indicate that this method did not take the spectral illumination into consideration and solely investigated the spectral similarity between training pixels and image pixels. In doing so, it introduced a potential classification error. However, SAM was able in correctly classifying a great portion of blue marl outcrops, indicating the lack of spectral response by blue marl as being an effective indicator. The results derived from Support Vector Machine classifier showed great pattern-recognition ability and more accurate classification of different lithological groups. Spectral similarities created problems for both methods in discriminating “Calcaire Tithonique” from “Berriasian” and “Terres Noires” from “Marnes Blues”, with occasional classifications of sandstone in areas containing loose sediment and debris. Thematic maps derived indicate the boundaries between similar geological units present most difficulties for classification methods. Unfortunately, the geological maps of the area contain uncertainties concerning boundaries between formations. This leaves with field observations and manual interpretation as being the most certain accuracy assessment method.

Spectral library of rock samples derived from the geological units dominating the landscape was successfully created. Spectral measurement products show high similarity in mineral composition and water absorption, with overall reflectance of materials and spectral changes between weathered and fresh samples serving as distinctive indicators. This project shows that in a scenario with complex and very similar geology between lithological groups, such libraries produce non-representative classification and should instead complement the pixel-based classification by supporting and assessing the results.

Exposed outcrops undergo a degree of change in terms of weathering. Weathering has altered the mineralogical composition of the surface material which resulted in spectral features being slightly obscured in comparison to the original, fresh material. Reflectance measurements show albedo increases in fresh spectra, indicating a brighter rock surface. Less water absorption and more profound mineral absorption features are observed with main spectral changes occurring in the 350 – 1000 nm (VNIR) and 1900 – 2500 nm range.

A comparison of products derived from ASTER and Sentinel-2 is a reoccurring theme in many geological remote sensing studies. An evaluation of Sentinel-2 and ASTER performance in semi-arid area with high degree of structural complexity, vegetation and topographic effects was executed. The results favour Sentinel-2, indicating higher spatial resolution having an edge over higher spectral resolution in the SWIR range for this specific setting and methodology. The study has shown that field-based spectroscopic research complements geological remote sensing well. The limiting factor in

achieving better classification is the spectral and spatial properties of the satellite imagery. Therefore, future research should consider the integration of hyperspectral data and assimilation of geomorphic products to increase the accuracy of lithological unit discrimination.

References:

- Abrams, M. 2000. The Advanced Spaceborne Thermal Emission and Reflection Radiometer (ASTER): Data products for the high spatial resolution imager on NASA's Terra platform. *International Journal of Remote Sensing*, vol. 21, pp. 847 – 859.
- Andreani, L., Stanek, K.P., Gloaguen, R., Krentz, O. & Domínguez-González, L. 2014. DEM-based analysis of interactions between tectonics and landscapes in the Ore Mountains and Eger Rift (East Germany and NW Czech Republic). *Remote Sensing*, vol.6(9), pp.7971 – 8001.
- Asadzadeh, S. & Filho, d. S.C.R. 2016. A review on spectral processing methods for geological remote sensing. *International Journal of Applied Earth Observation and Geoinformation*, vol.47, pp. 69 – 90.
- Bachri, I., Hakdaoui, M., Raji, M., Teodoro, A.C. & Benbouziane, A. 2019. Machine Learning Algorithms for Automatic Lithological Mapping Using Remote Sensing Data: A Case Study from Souk Arbaa Sahel, Sidi Ifni Inlier, Western Anti-Atlas, Morocco. *International Journal of Geo-Information*, vol. 8, pp. 248.
- Baldrige A.M., Hook S.J., Grove C.I. & Rivera G. 2009. The ASTER spectral library version 2.0. *Remote Sensing of Environment*, vol.113(4), pp. 711 – 715.
- Boardman, J. W., and Kruse, F. A. 1994. Automated spectral analysis: a geological example using AVIRIS data, north Grapevine Mountains, Nevada. *ERIM Tenth Thematic Conference on Geologic Remote Sensing, Environmental Research Institute of Michigan, Ann Arbor, MI*, pp. I-407 - I-418.
- Brodu, N. 2016. Super-resolving multiresolution images with band-independent geometry of multispectral pixels. *Institute of Electrical and Electronics Engineers*, vol.55(8).
- Bureau of Geological and Mining Research, BRGM. Carte Géologique de la France (1:50.000): 868 (Luc-en-Diois, 1970), 869 (Gap, 1971), 892 (Seres, 1967), 893 (Laragne Monteglin, 1991).
- Chang, C.I. 2003. Hyperspectral Imaging: Techniques for Spectral Detection and Classification. *Kluwer Academic Publishers, New York*.
- Chang, C.I. 2007. Hyperspectral Data Exploitation: Theory and Application. *John Wiley & Sons*.
- Chen, X., Warner, T. A., & Campagna, D. J. 2007. Integrating visible, near-infrared and shortwave infrared hyperspectral and multispectral thermal imagery for geological mapping at Cuprite, Nevada. *Remote Sensing of Environment*, vol.110, pp. 344 – 356.
- Clark R.N., Swayze G.A., Livo K.E., Kokaly R.F., Sutley S.J., Dalton J.B., McDougal R.R. & Gent C.A. 2003. Imaging spectroscopy: Earth and planetary remote sensing with the USGS Tetracorder and expert systems. *Journal of Geophysical Research: Planets* vol.108, pp. 5131.

- Clerc, S. & MPC Team. 2020. L1C Data Quality Report. Sentinel 2, ESA report, issue 47.
- Cortes, C. & Vapnik, V. 1995. Support-vector networks. *Machine Learning*, vol.20, pp. 273 – 297.
- Cracknell, M.J. & Reading, A.M. 2014. Geological mapping using remote sensing data: a comparison of five machine learning algorithms, their response to variations in the spatial distribution of training data and the use of explicit spatial information. *Computational Geosciences*, vol. 63, pp. 22 – 33.
- Cudahy, T. & Hewson, R. 2002. ASTER geological case histories: Porphyry-skarn-epithermal, iron oxide Cu-Au and Broken Hill Pb-Zn-Ag. *Annual General Meeting of the Geological Remote Sensing Group: ASTER Unveiled*. London, UK: Burlington house (December 5 – 7, 2002).
- Damaševičius, R. 2010. Structural analysis of regulatory DNA sequences using grammar inference and Support Vector Machine. *Neurocomputing*, vol.73, pp. 633 – 638.
- Debba, P., Carranza, E. J. M., van der Meer, F. D., & Stein, A. 2006. Abundance estimation of spectrally similar minerals by using derivative spectra in simulated annealing. *Geoscience and Remote Sensing*, vol.44, pp. 3649 – 3658.
- European Space Agency, ESA. 2018. Level-2A Prototype Processor for atmospheric-, terrain and cirrus correction of Top-Of-Atmosphere Level 1C input data. Accessed January 2019. URL:<http://step.esa.int/main/third-party-plugins-2/sen2cor/>
- Fal, S., Maanan, M., Baidder, L. & Rhinane, H. 2019. The contribution of Sentinel-2 satellite images for geological mapping in the south of Tafilalet basin (Eastern Anti-Atlas, Morocco). *ISPRS - The International Archives of the Photogrammetry, Remote Sensing and Spatial Information Sciences*, vol.42.
- Feng J., Rivard B., Rogge D. & Sánchez-Azofeifa A. 2013. The long-wave infrared (3–14 μm) spectral properties of rock encrusting lichens based on laboratory spectra and airborne SEBASS imagery. *Remote Sensing of Environment* vol.131, pp. 173 – 181.
- Gidon, M., Moullade, M., Montjuvent C. & Flandrin, J. 1991. Notice explicative, 94 Carte géologique France (1/50 000), feuille Laragne-Montéglin (893) – Orléans : BRGM 84p. Carte géologique par Gidon, M., Moullade, M., Montjuvent C., Flandrin, J. 1991.
- Gomez, C., Delacourt, C., Allemand, P., Ledru, P. & Wackerle, R. 2005. Using ASTER remote sensing data for geological mapping. In Namibia. *Physics and Chemistry of the Earth*, vol. 30, pp. 97 – 108.
- Green, A.A. & M.D. Craig. 1985. Analysis of aircraft spectrometer data, with logarithmic residuals. *Proceedings of the Airborne Imaging Spectrometer Data Analysis Workshop*, pp. 111 – 119.
- Guanter, L., Kaufmann, H., Segl, K., Foester, S., Rogass, C., Chabrillat, S., Kuester, T., Hollstein, A., Rossner, G., Chlebek, C., Straif, C., Fischer, S., Schrader, S., Storch, T., Heiden, U., Mueller, A.,

Bachmann, M., Mühle, H., Müller, R., Habermeyer, M., Ohndorf, A., Hill, J., Buddenbaum, H., Hostert, P., Van der Linden, S., Leitão, P.J., Rabe, A., Doerffer, R., Krasemann, H., Xi, H., Mauser, W., Hank, T., Locherer, M., Rast, M., Staenz, K. & Sang, B. 2015. The EnMAP Spaceborne Imaging Spectroscopy Mission for Earth Observation. *Remote Sensing*, vol.7, pp. 8830 – 8857.

Gupta P.R. 2017, *Remote Sensing Geology*, 3rd. ed., Springer, Berlin.

Guyon, I. 2008. Practical feature selection: From correlation to causality. *Mining Massive Data Sets for Security*.

F. Fogelman-Soulié, D. Perrotta, J. Piskorski, R. Steinberger. *Mining Massive Data Sets for Security – Advances in Data Mining, Search, Social Networks and Text Mining, and their Applications to Security*, IOS Press, Amsterdam, pp. 27 – 43.

Haselwimmer, C.E., Riley, T.R. & Liu, J.G. 2011. Lithological mapping in the Oscar II Coast area, Graham Land, Antarctic Peninsula using ASTER data. *International Journal of Remote Sensing*, vol. 32, pp. 2013 – 2035.

Hastie, T., Tibshirani, R. & Friedman, J.H. 2009. *The elements of statistical learning: data mining Inference and Prediction*, 2nd edition. Springer, New York, USA, pp. 533.

Hunt G.R. 1982. Spectroscopic properties of rocks and minerals. *Handbook of Physical Properties of Rocks*, vol.8(4), pp. 658.

JPL California Institute of Technology Pasadena, California. 2018. HypsIRI Final Report.

URL:https://hyspiri.jpl.nasa.gov/downloads/reports_whitepapers/HyspIRI_FINAL_Report_1October2018_20181005a.pdf

Krishnamurthy, Y. M. & Sreenivasan, G. 2005. Remote Sensing Technology for Exploration of Mineral Deposits with Special Reference to Bauxite and Related Minerals. *Conference: 16th International Symposium of ICSOBA, “Status of Bauxite, Alumina, Aluminium, Downstream Products and Future Prospects”*, vol. 36.

Kruse, F. A., Lefkoff, A.B., Boardman, J.B., Heidebrecht, K.B., Shapiro, A.T., Barloon, P.J. & Goetz A.F.H. 1993. The Spectral Image Processing System (SIPS) - Interactive Visualization and Analysis of Imaging Spectrometer Data. *Remote Sensing of Environment*, vol.44, pp. 145 - 163.

Kruse, F. A. 2010. Mineral Mapping Using Spectroscopy: From Field Measurements to Airborne and Satellite-Based Imaging Spectrometry. *Semantic Scholar*.

Kruse, F. A. 2012. Mapping surface mineralogy using imaging spectrometry. *Geomorphology*, vol.137(1), pp. 41–56.

- Kumar, C., Chatterjee, S., Oommen, T. & Guha, A. 2020. Automated lithological mapping by integrating spectral enhancement techniques and machine learning algorithms using AVIRIS-NG hyperspectral data in Gold-bearing granite-greenstone rocks in Hutti, India. *International Journal of Applied Earth Observation and Geoinformation*, vol. 86.
- Kupidura, P. 2019. The Comparison of Different Methods of Texture Analysis for Their Efficacy for Land Use Classification in Satellite Imagery. *Remote Sensing*, vol.11(10), pp. 1233.
- Louis, J., Debaecker, V., Pflug, B., Main-Knorn, M., Bieniarz, J., Muellen-Wilm, U., Cadau, E. & Gascon, F. 2016. Sentinel-2 Sen2Cor: L2A Processor For Users. *Proc. Living Planet Symposium 2016, Prague, Czech Republic*.
- Mars, J.C. & Rowan, L. C. 2010. Spectral assessment of new ASTER SWIR surface reflectance data products for spectroscopic mapping of rocks and minerals. *Remote Sensing of Environment*, vol.114(9), pp. 2011– 2025.
- Michalski J.R., Kraft M.D., Sharp T.G. & Christensen P.R. 2006. Effects of chemical weathering on infrared spectra of Columbia River Basalt and spectral interpretations of martian alteration. *Earth and Planetary Science Letters*, vol.248(3–4), pp. 822 – 829.
- Mountrakis, G., Im, J. & Ogole, C. 2011. Support vector machines in remote sensing: a review. *ISPRS Journal of Photogrammetry and Remote Sensing*, vol. 66, pp. 247 – 259.
- Murphy, R. J., Monteiro, S. T., & Schneider, S. 2012. Evaluating classification techniques for mapping vertical geology using field-based hyperspectral sensors. *IEEE trans. Geoscience and Remote Sensing*, vol.50, pp. 3066 – 3080.
- Mustard, J. F. & Sunshine, J.M. 1999. Spectral analysis for earth science investigation: investigations using remote sensing data. *Remote Sensing for the Earth Sciences*. 3rd edition. John Wiley & Sons.
- Nahmi-al, F., Saddiqi, O., Hilali, A., Rhinane, H., Baidder, L., El arabi, H. & Khanbari, K. 2017. Application of Remote Sensing in Geological Mapping, Case Study Al Maghrabah Area – Hajjah Region, Yemen. *ISPRS - The International Archives of the Photogrammetry, Remote Sensing and Spatial Information Sciences*, vol. 4.
- Othman, A. & Gloaguen, R. 2013. Automatic extraction and size distribution of landslides in Kurdistan Region, NE Iraq. *Remote Sensing*, vol.5, pp. 2389 – 2410.
- Othman, A.A. & Gloaguen, R. 2014. Improving Lithological Mapping by SVM Classification of Spectral and Morphological Features: The Discovery of a New Chromite Body in the Mawat Ophiolite Complex (Kurdista, NE Iraq). *Remote Sensing*, vol. 6, pp. 6867 – 6896.

Parashar, C., Sharma, R. U., Chatteraj, S. L., Sengar, V. K. & Ray, P. K. C. 2016. Identification and mapping of minerals by using imaging spectroscopy in south eastern region of Rajasthan. *Proceedings In Multispectral, Hyperspectral, and Ultra Spectral Remote Sensing Technology, Techniques and Applications VI*, vol.9880.

Pflug, B., Bieniarz, J., Debaecker V., Louis, J. & Müller-Wilm, U. 2016. Some Experience Using Sen2Cor. *EGU General Assembly 2016, Vienna, Austria*.

Qui, F., Abdelsalam, M. & Thakkar, P. 2006. Spectral analysis of ASTER data covering part of the Neoproterozoid Allaqi-Heiani suture, Southern Egypt, *Journal of African Earth Sciences*, vol.44, pp. 169 – 180.

Rajesh, H. M. 2004. Application of remote sensing and GIS in mineral resource mapping – An overview. *Journal of Mineralogical and Petrological Sciences*, vol. 99, pp. 83 – 103.

Rast, M., Ananasso, C., Bach, H., Dor, E.B., Chabrilat, S., Colombo, R., Del Bello, U., Feret, J-B., Giardino, C., Green, R.O., Guanter, L., Marsh, S., Nieke, J., Ong, C., Rum, G., Schaepman, M., Schlerf, M., Skidmore, A.K., Strobl, P. 2019. Copernicus Hyperspectral Imaging Mission for the Environment - Mission Requirements Document.

URL:http://esamultimedia.esa.int/docs/EarthObservation/Copernicus_CHIME_MRD_v2.1_Issued20190723.pdf

Richards, J.A. & Jia, X. 2006. Remote Sensing Digital Image Analysis, vol. 4, *Springer-Verlag Berlin Heidelberg*.

Rowan, L. C., Crowley, J. K., Schmidt, R. G., & Mars, J. C. 2000. Mapping hydrothermally altered rocks by analysing hyperspectral image (AVIRIS) data of forested areas in the Southeastern United States. *Journal of Geochemical Exploration*, vol.68(3), pp. 145 – 166.

Rowan, I.C. & Mars, J.C. 2003. Lithological mapping in the Mountain Pass, California area using Advanced Spaceborne Thermal Emission and Reflection Radiometer (ASTER) data. *Remote Sensing of Environment*, vol. 84, pp. 350 – 366.

Rudorff, N. de M., Kampel, M. & de Rezende, C. 2011. Spectral mapping of the Paraíba do Sul River plume (Brazil) using multitemporal Landsat images. *Journal of Applied Remote Sensing*, vol.5(1), pp. 1 – 19.

Salehi, S., Mielke, C., Pedersen, C.B. & Olsen, S.D. 2019. Comparison of ASTER and Sentinel-2 spaceborne datasets for geological mapping: a case study from North-East Greenland. *GEUS Bulletin*, vol. 43.

- Shao, Y., Lan, J., Zhang, Y. & Zou, J. 2018. Spectral Unmixing of Hyperspectral Remote Sensing Imagery via Preserving the Intrinsic Structure Invariant. *Sensors*, vol.18(10), pp. 3528.
- Science toolbox exploitation platform (STEP). 2019. Sen2Res, URL: <http://step.esa.int/main/third-party-plugins-2/sen2res/>
- Spectral Evolution. 2012. PSR+ High resolution field portable spectroradiometer. Lawrence, USA.
- Unger, Z. & Sikhegyi, F. 2004. The importance of remote sensing techniques in surface geologic mapping. *Acta Geologica Hungarica*, vol.47(1), pp. 35 – 51.
- Van der Meer, F.D. & de Jong, S. M. 2006. Imaging Spectrometry; basic principles and prospective applications, vol.4, *Springer, Dordrecht: The Netherlands*.
- Van der Meer, F.D., van der Werff, H.M.A. & van Ruitenbeek, F.J.A 2014. Potential of ESA's Sentinel-2 for geological applications. *Remote Sensing of Environment*, vol. 148, pp. 124 – 133.
- Van der Werff, H., Hewson, R. & Meer, F. 2018. Use What is There: What can Sentinel-2 do for Geological Remote Sensing? *38th IEEE International Geoscience and Remote Sensing Symposium 2018*, pp. 8359 – 8362.
- Waske, B., Benediktsson, J.A., Arnason, K. & Sveinsson, J.R. 2009. Mapping of hyperspectral AVIRIS data using machine-learning algorithms. *Canadian Journal of Remote Sensing*, vol. 35, pp. S106-S116.
- Weih, R.C. & Riggan, N.D. 2010. Object-based classification vs. Pixel-based classification: Comparative importance of multi-resolution imagery. *International Archives of the Photogrammetry, Remote Sensing and Spatial Information Sciences, ISPRS*, vol. 38.
- Yang, X. 2011. Parameterizing Support Vector Machines for Land Cover Classification. *Photogrammetric Engineering & Remote Sensing*, vol.77, pp. 27 –37.
- Yamaguchi, Y. & Naito, C. 2003. Spectral indices for lithological discrimination and mapping by using the ASTER SWIR bands. *International Journal of Remote Sensing*, vol. 24, pp. 4311 – 4323.
- Younis, M.T., Gilabert, M.A., Melia J. & Bastida J. 1997. Weathering process effects on spectral reflectance of rocks in a semiarid environment. *International Journal of Remote Sensing* vol.18(16), pp. 3361 – 3377.
- Zhou, K.F & Wang S.S. 2017. Spectral properties of weathered and fresh rock surfaces in the Xiemisitai metallogenic belt, NW Xinjiang, China, *Open Geosciences*, vol. 9 (1).
- Zhu, X.; Zhang, S.; Jin, Z.; Zhang, Z.; Xu, Z. 2011. Missing Value Estimation for Mixed-Attribute Data Sets. *IEEE Transactions on Knowledge and Data Engineering*, vol.23, pp. 110 – 121.

Appendix A - full lithological maps of the study area

This appendix is dedicated to the full scene classification maps derived in the main body of work. Figure 34 is the geological map obtained from French Geological Survey (BRGM). The geological map of the study area is comprised of 4 different geological maps being assembled together. The correlation between the 4 geological sections does not always match and geological units are described using different legends. Despite that, in the majority of the study area map, the dark marls are depicted in various shades of blue, “Berriasian” group is assigned the green colour, with different geological sequences having different shade of green. “Calcaire Tithonique” is assigned a pale grey color.

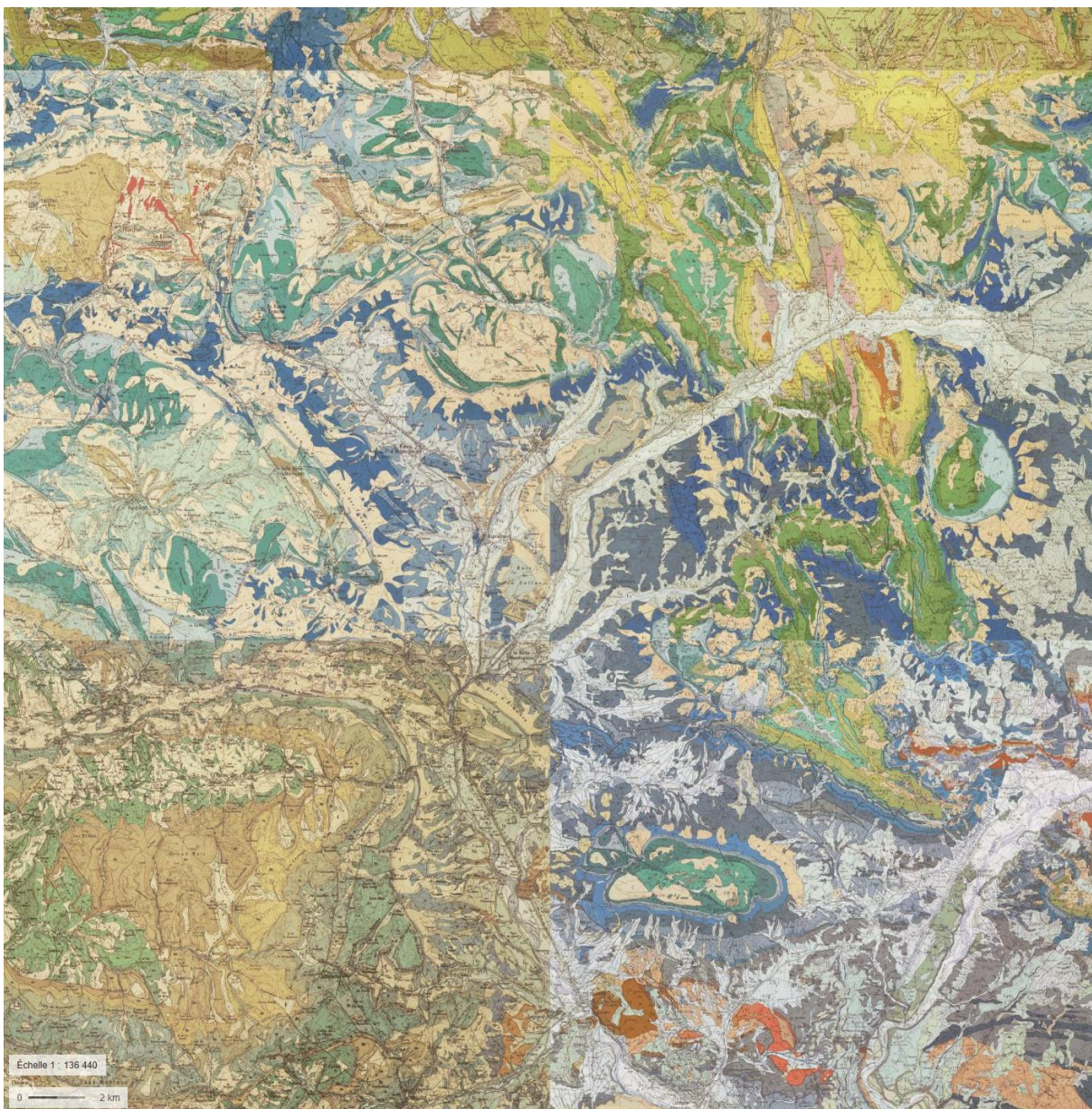


Figure 34: Geological map of the study area (Source: BRGM).

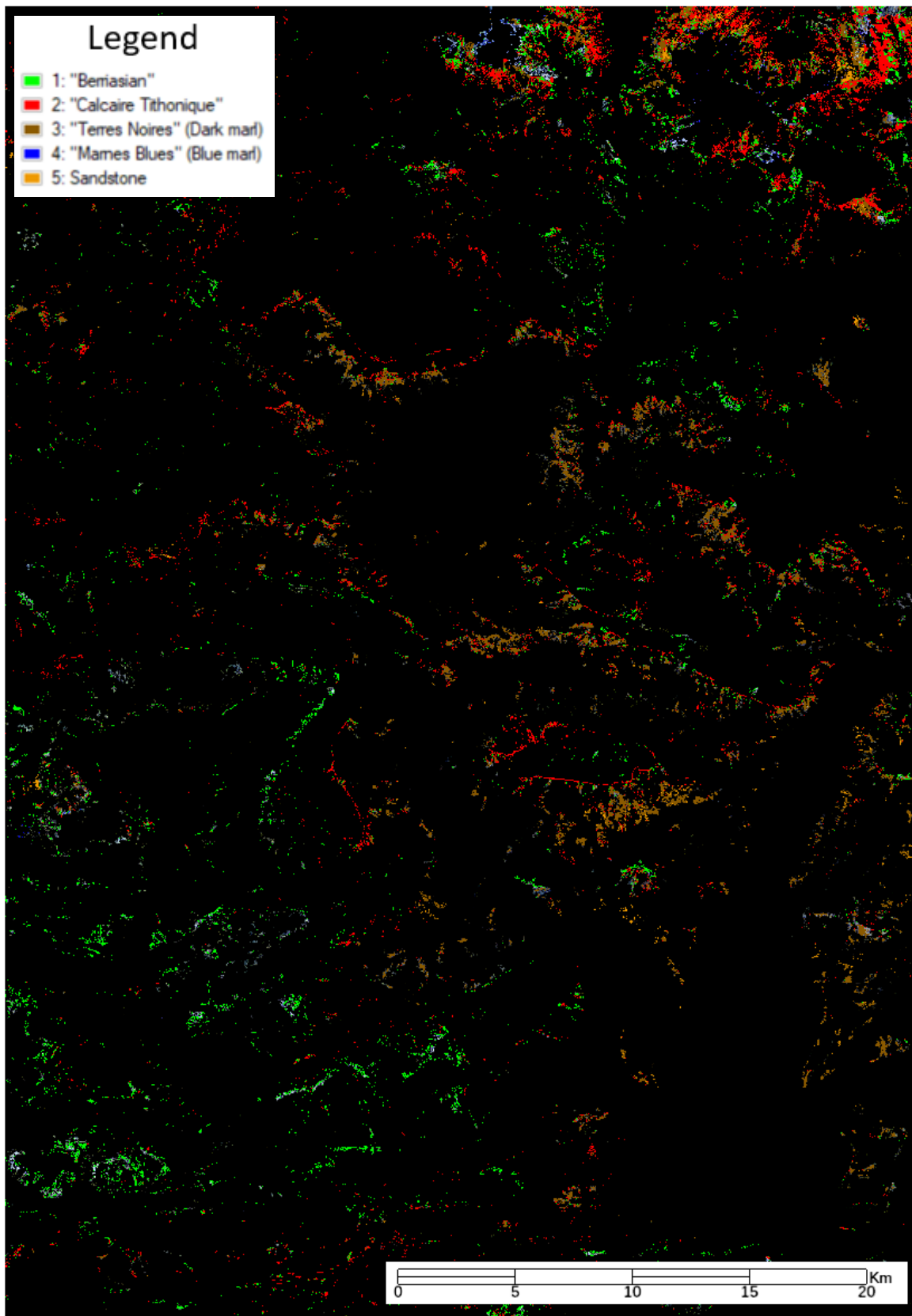


Figure 35: Sentinel-2 SVM classification overlaid on masked raster.

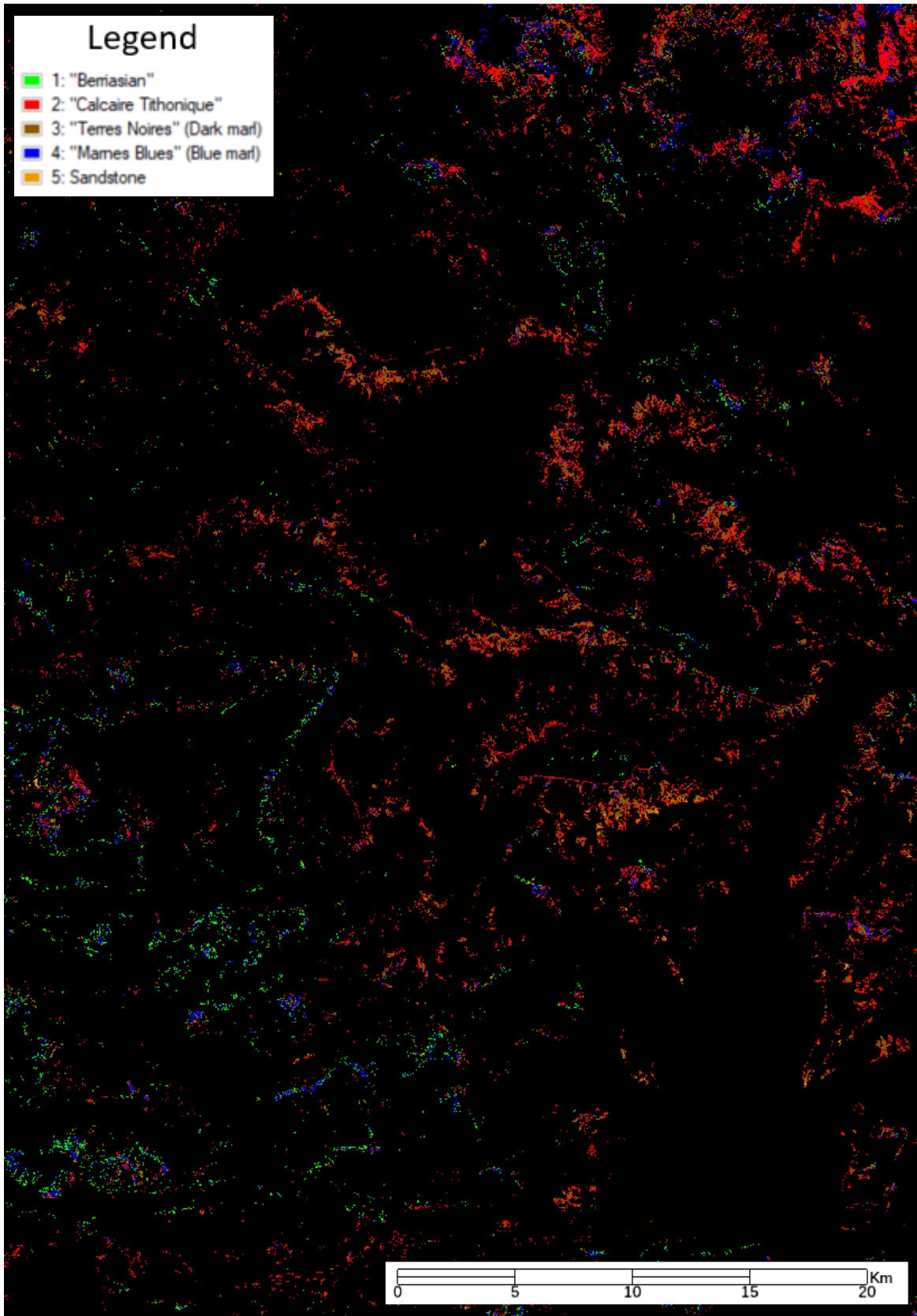


Figure 36: Sentinel-2 SAM classification overlaid on masked raster.

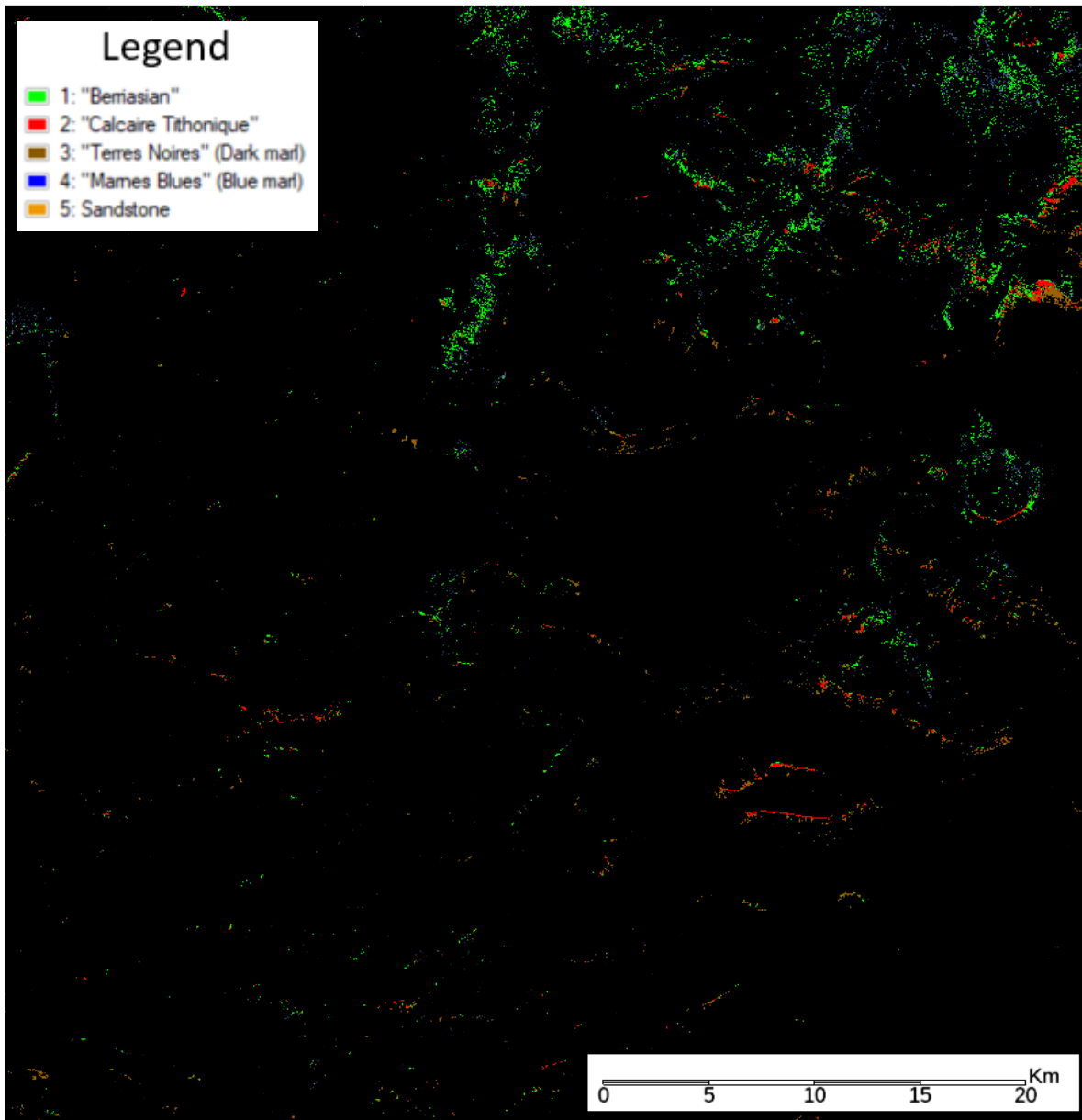


Figure 37: ASTER SVM classification overlaid on masked raster.

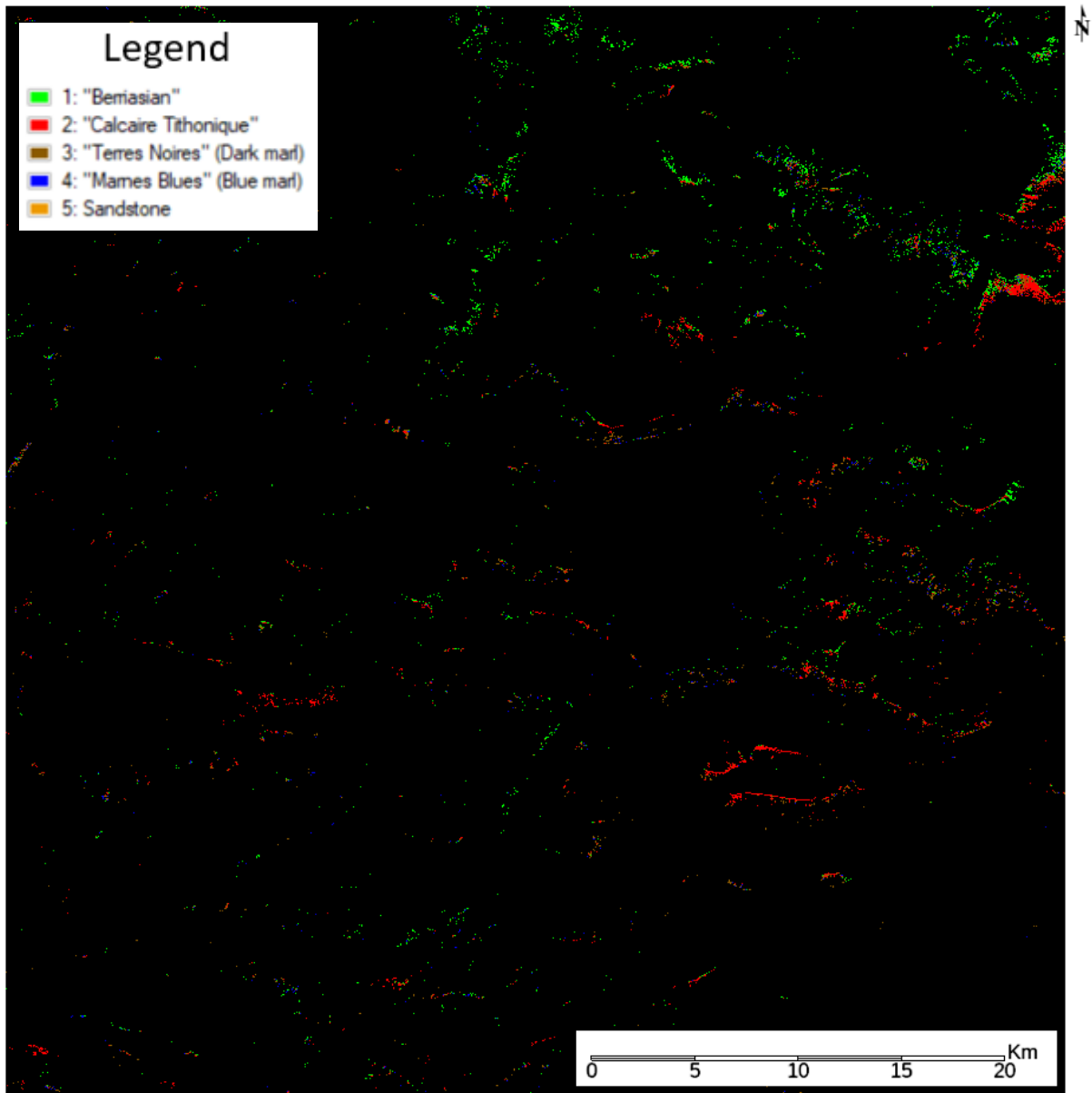


Figure 38: ASTER SAM classification overlaid on masked raster.

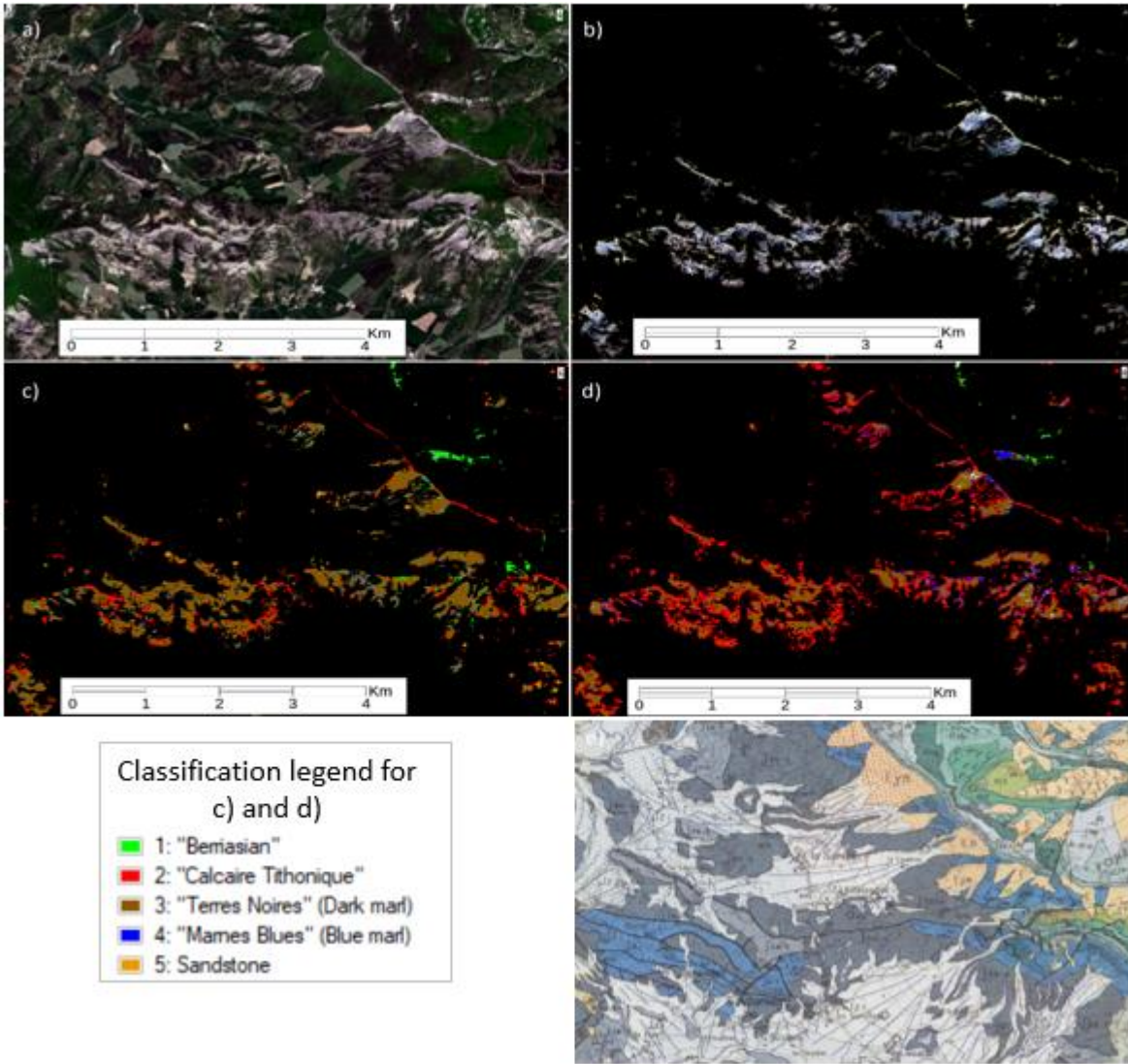


Figure 39: a) Sentinel-2 true color image of Terres Noires outcrops (RGB: [B4,B3,B2]), b) image after applied mask, c) SVM classification image, d) SAM classification image, and e) geological map.

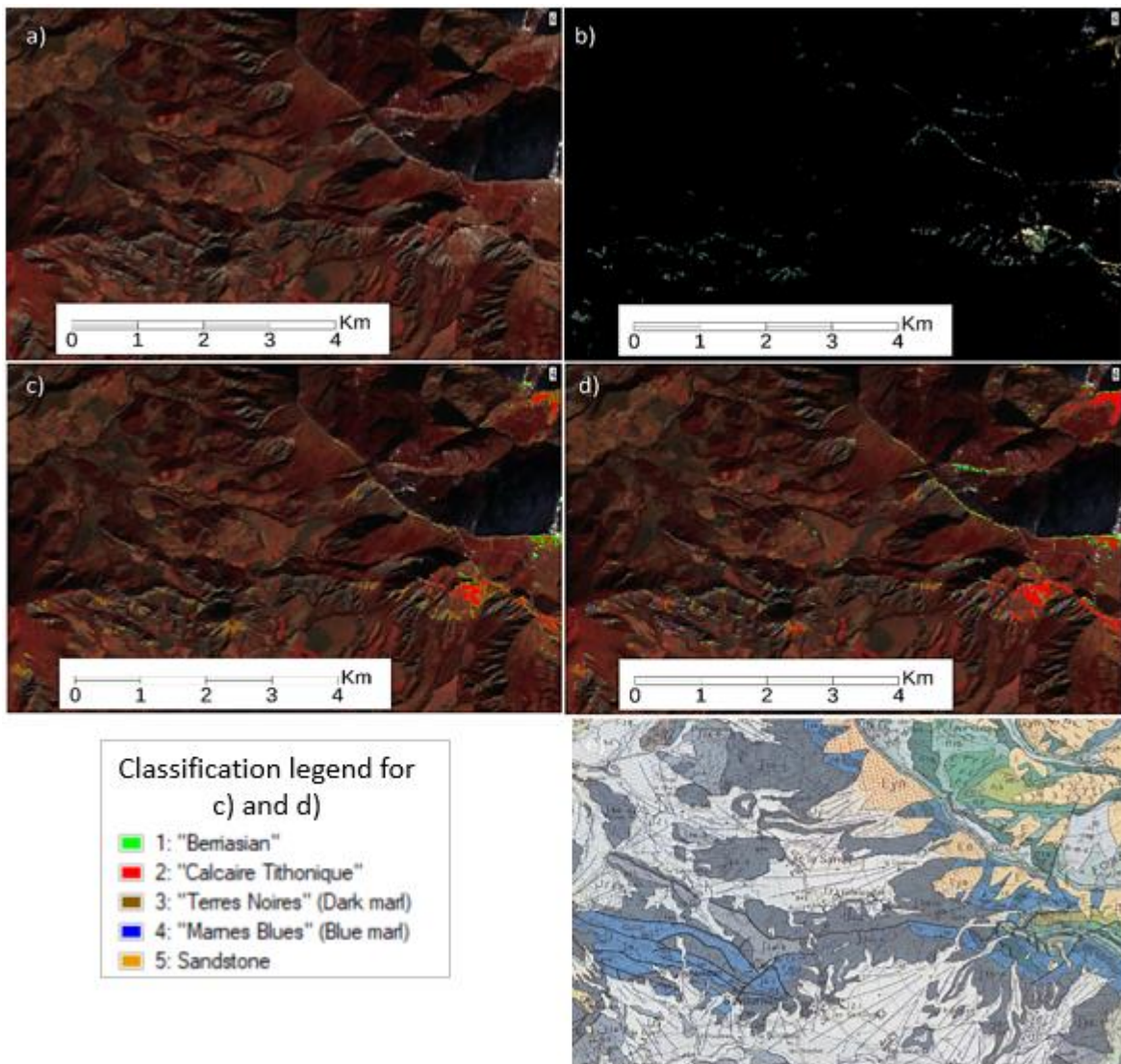


Figure 40: a) ASTER FCC image of Terres Noires outcrops (RGB: [B1,B2,B3N]), b) image after applied mask, c) SVM classification overlaid on FCC, d) SAM classification overlaid on FCC, and e) geological map.

Appendix B - fresh and weathered rocks

The following appendix contains spectral signatures of fresh and weathered rocks sampled in the study area. The figures contain an image of weathered and fresh rock surfaces and the spectral responses from measuring these surfaces.

Examples include samples: #1, #8, #25, #34, #42. For sample locations refer to Figure 7 in the main body of work.

To relate to the project of lithological mapping a table is presented to show which samples fall in which lithological category:

"Calcaire Tithonique"	"Berriasien"	Dark marl	Blue marl	Sandstone
#1,	#34	#8	#42	#25

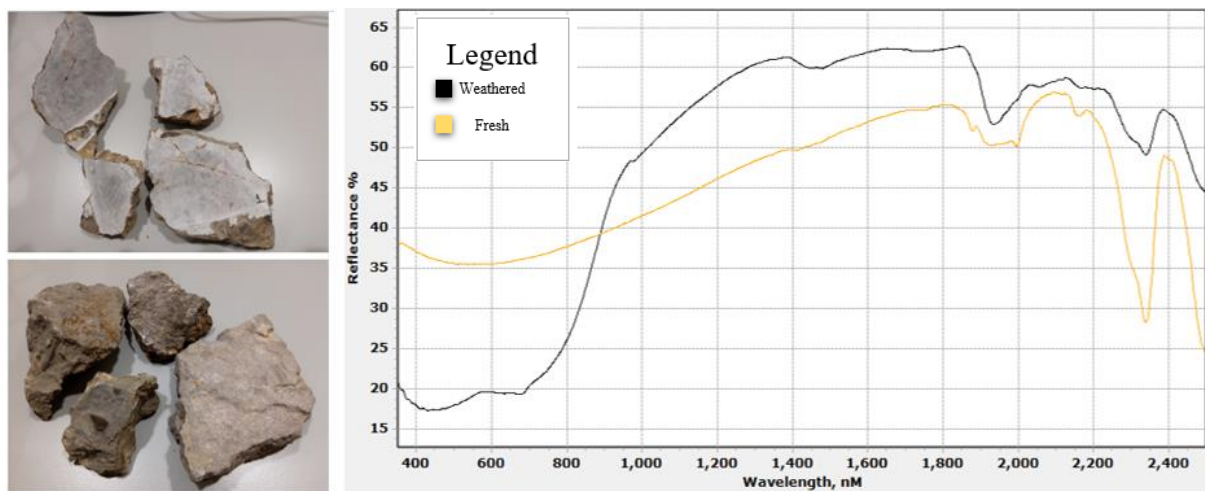


Figure 41: Spectral signatures of fresh and weathered sample #1.

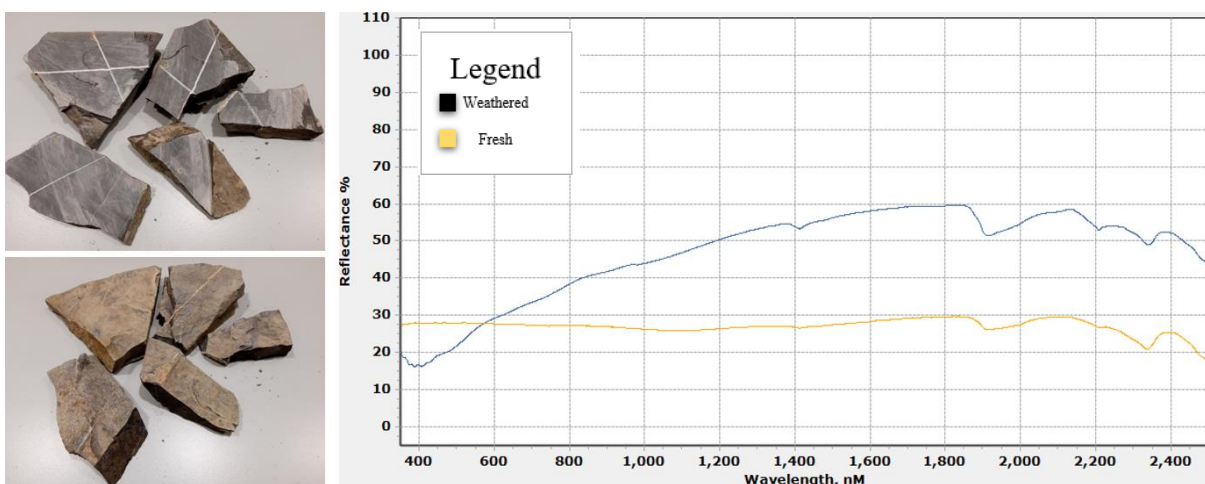


Figure 42: Spectral signatures of fresh and weathered sample #34.

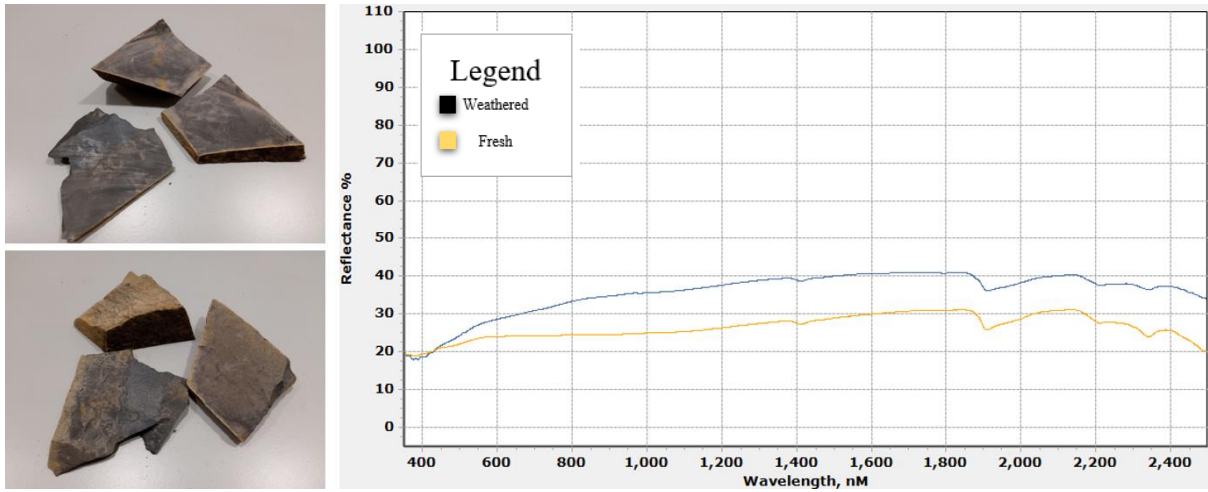


Figure 43: Spectral signatures of fresh and weathered sample #8.

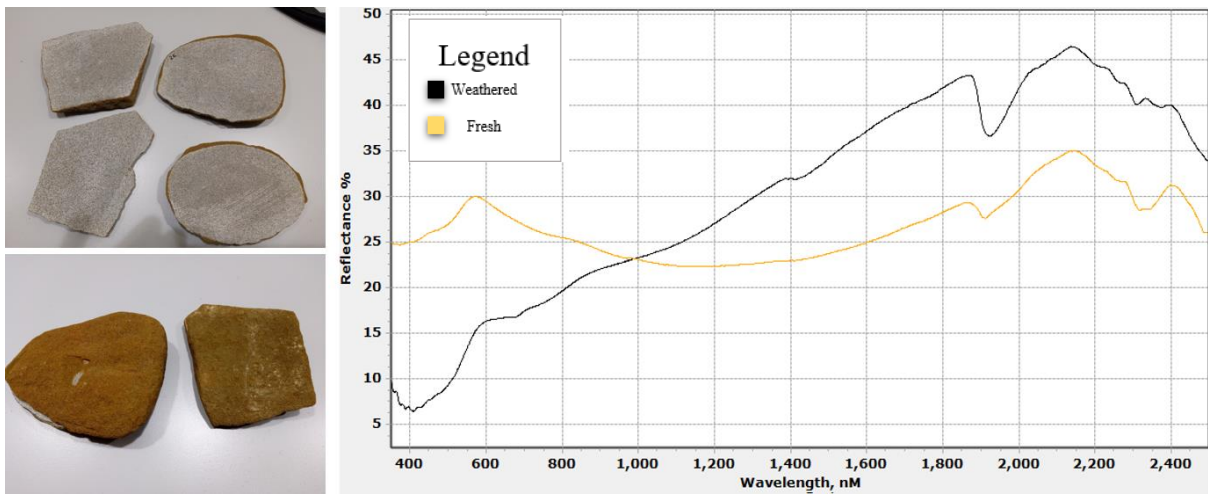


Figure 44: Spectral signatures of fresh and weathered sample #25.

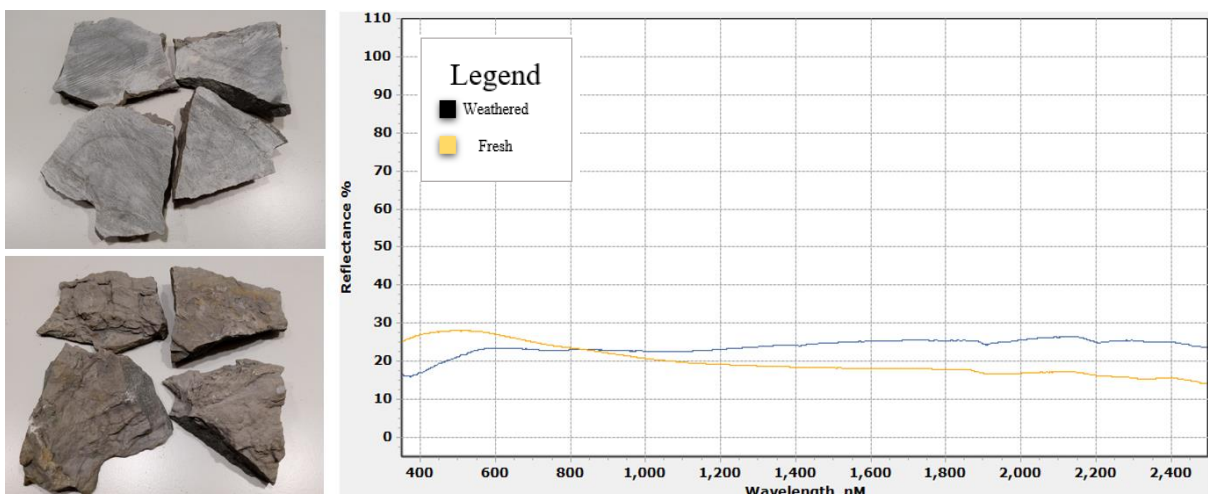


Figure 45: Spectral signatures of fresh and weathered sample #42.

Appendix C - results using different mapping techniques

The following appendix is dedicated to alternative mapping techniques and digital enhancement tools which provided aid in recognition of different classes, were used in similar prior studies or performed well in lithological mapping in this project.

i) RGB band combinations.

Sentinel-2 (B12, B11, B2) combination has been widely used to give contextual information about surface geology. It leverages the Short-Wave InfraRed (B12 & B11) and blue (B2) bands to provide a more contrast image of the lithology. This band combination was applied to masked Sentinel-2 image and the information derived was taken into account when defining the training data for subsequent analysis. The combination performs exceptionally well in discriminating the sandstone outcrop to the West and “Calcaire Tithonique” from the surrounding rock (Figure 44). The false color composite highlights the “Calcaire Tithonique” ridges along the Ear of Serres and provides more contrast to the complex marl outcrops (Figure 45).

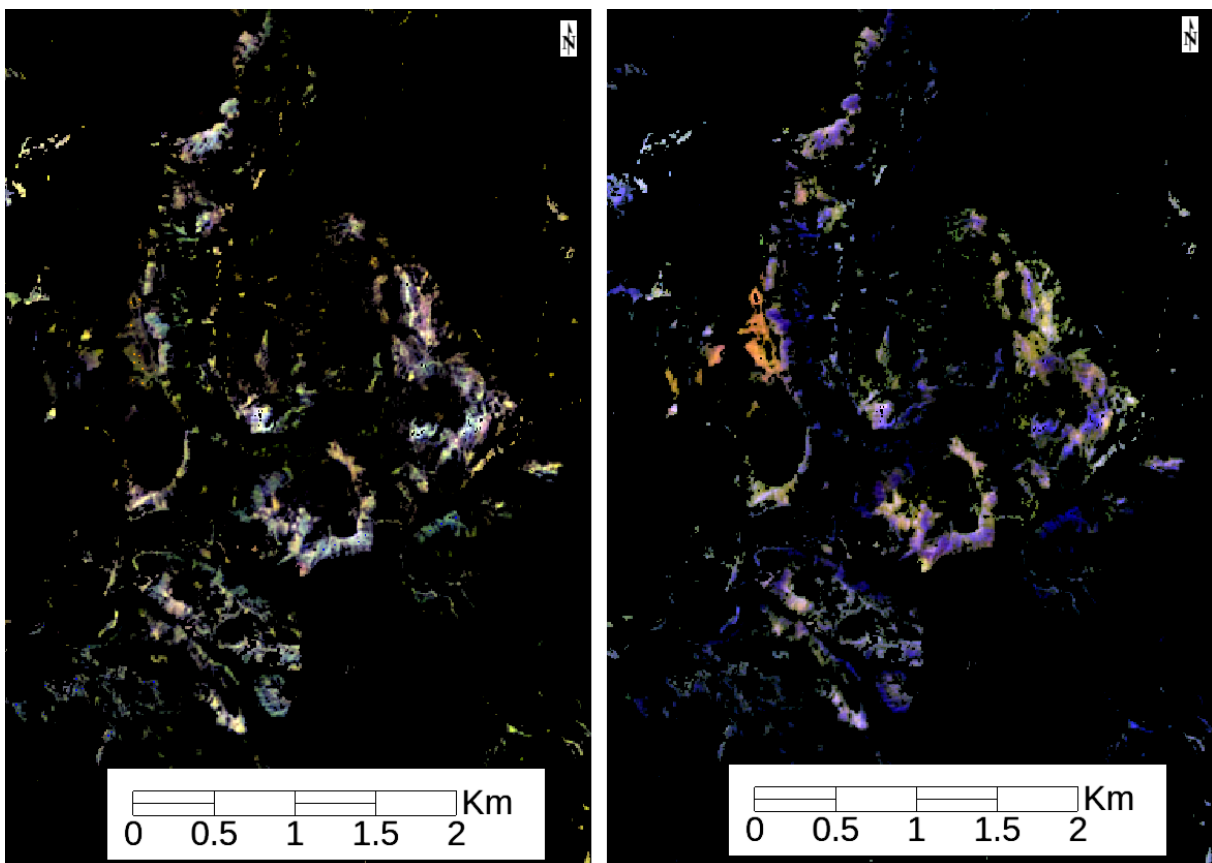


Figure 46: Original masked image over the sandstone and blue marl area to the left and RGB: (B12, B11, B2) image of the same area to the right.

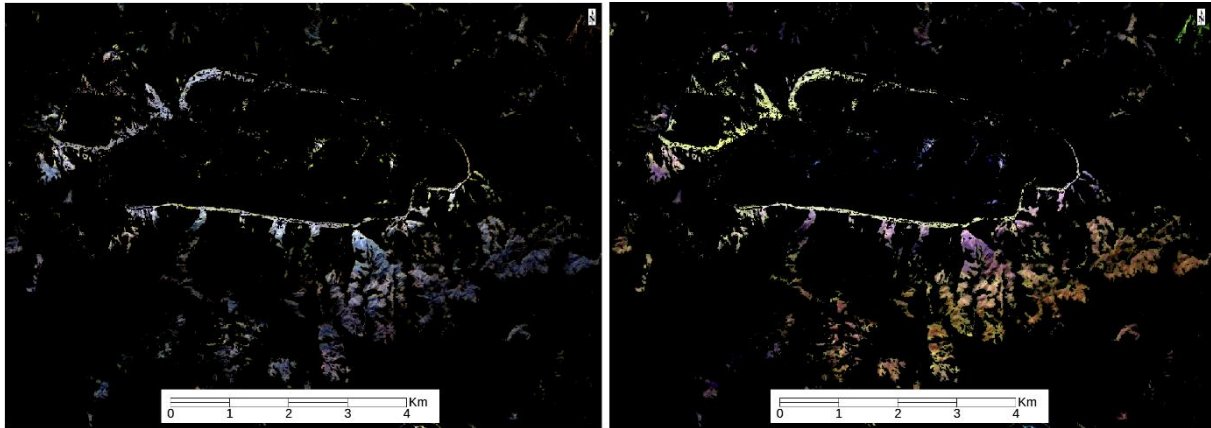


Figure 47: Original masked image of Serres Ear to the left and the same RGB: (B12,B11,B2) image to the right.

ii) Band math

A primary comparison between Sentinel-2 multispectral instrument and ASTER imagery for the purposes of geological remote sensing can be established by a series of band ratios (van der Werff et al., 2018). An array of band ratios can be created using spectral signatures to serve as proxies for mineral compositions (Cudahy & Hewson, 2002). Image-based spectral signatures were taken for each lithological group and representative proxies were derived (Table 5).

Sensor	Sentinel-2	ASTER
“Calcaire Tithonique”	$b6/b4+b9$	$b2+b6+b8/b3+b7$
“Berriasien”	$b3+b6+b9/b4+b8$	$b2+b4+b6+b8/b3+b5+b7$
“Terres Noires”	$b5+b6/b4+b10$	$b2+b8/b3$
“Marnes Blues”	$b3+b6+b9/b4+b8$	$b2+b6+b8/b3+b7$
Sandstone	$b3+b8/b2+b4+b10$	-

Table 5: Aster and Sentinel-2 band ratios for identification of lithological units.

This technique was examined in the case of Serres. Application of band math on Sentinel-2 imagery yields promising results, mainly due to the spectral responses in the VNIR range (Figure 46). Figure shows dark marls being well distinguished from the surrounding rock and “Calcaire Tithonique” having slightly bluish/pinkish colour. Band ratios based on spectral responses of lithological groups show potential and is capable of differentiating limestone-dominated formations from marls. However, due to band ratioing being less of a classification technique and more of an abundance estimate, this method requires intense supervision and detailed post-processing analysis to obtain useful geological information.

Figure 47 shows a case of band ratios being applied to ASTER imagery. Limestone surrounding the Serres Ear is depicted in pink colour, while lighter colours dark marl in the area. Although the appropriate discrimination is seen, without the prior knowledge of the area and background of the geological setting, it would be greatly difficult to interpret the resulting lithological map.

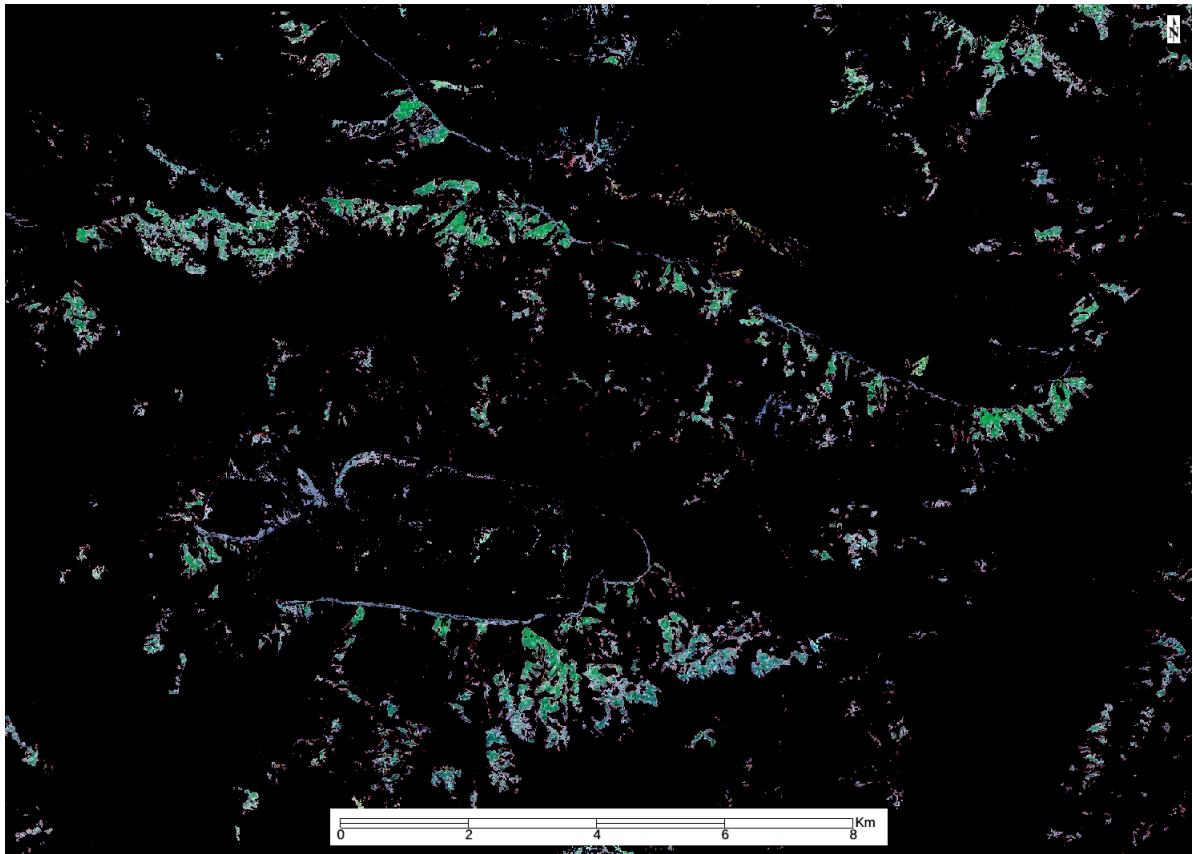


Figure 48: Sentinel-2 image with RGB: ("Calcaire Tithonique", "Terres Noires", sandstone).

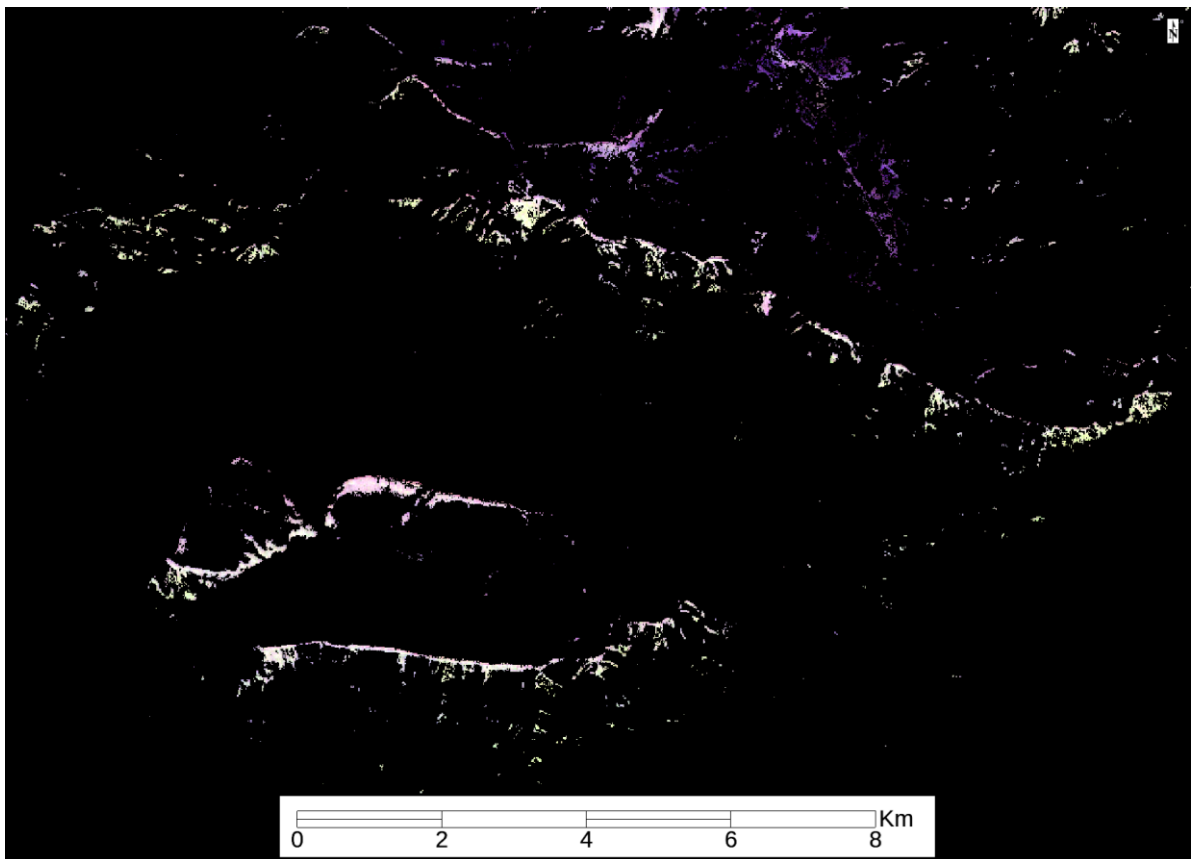


Figure 49: ASTER image with RGB: ("Calcaire Tithonique", "Terres Noires", "Marnes Blues").

iii) Neural Network

Neural Network (NN) is another promising machine-learning classification. Unlike parametric classifiers such as Maximum Likelihood Classification (MLC) or Minimum Distance Classification (MDC), NN is not dependant on statistical relationships. NN and SVM classifiers share numerous similarities. Both have the ability to resolve a difficult, large-scale problem, i.e. pattern recognition and both are content-oriented instead of being location specific. The latter means that pixel content is favoured over pixel location in a scene.

The NN classifier learns the relationship between groups by training to associate target pixels with input reference data. When NN is applied, the reference data pattern is identified, and the algorithm attempts at reproducing the same pattern. An important step occurs when an input is given that does not have any associated output. When this happens, the algorithm assigns the learned input pattern which least differs from the given input to the output.

Application of NN shows that it is fully capable of pattern-recognition and generalizes the training data fairly well. As is the case for SVM classifier, NN does not need *a priori* statistical information and is capable of distinguishing large parts of dark marls from the overlaying limestone formations. “Calcaire Tithonique” and “Berriasian” again provide an issue for this classifier around the ear of Serres (Figure 50 & 51). Slightly more dark marl is identified as sandstone in the bottom parts of the badlands. These areas are where sediment and debris mixes with the eroded marl, thus, providing difficulty for class distinction. While geological thinking and geological map of the area confirm the classification of dark marl in those areas, the real field situation might be different and can only be confirmed by field observation.

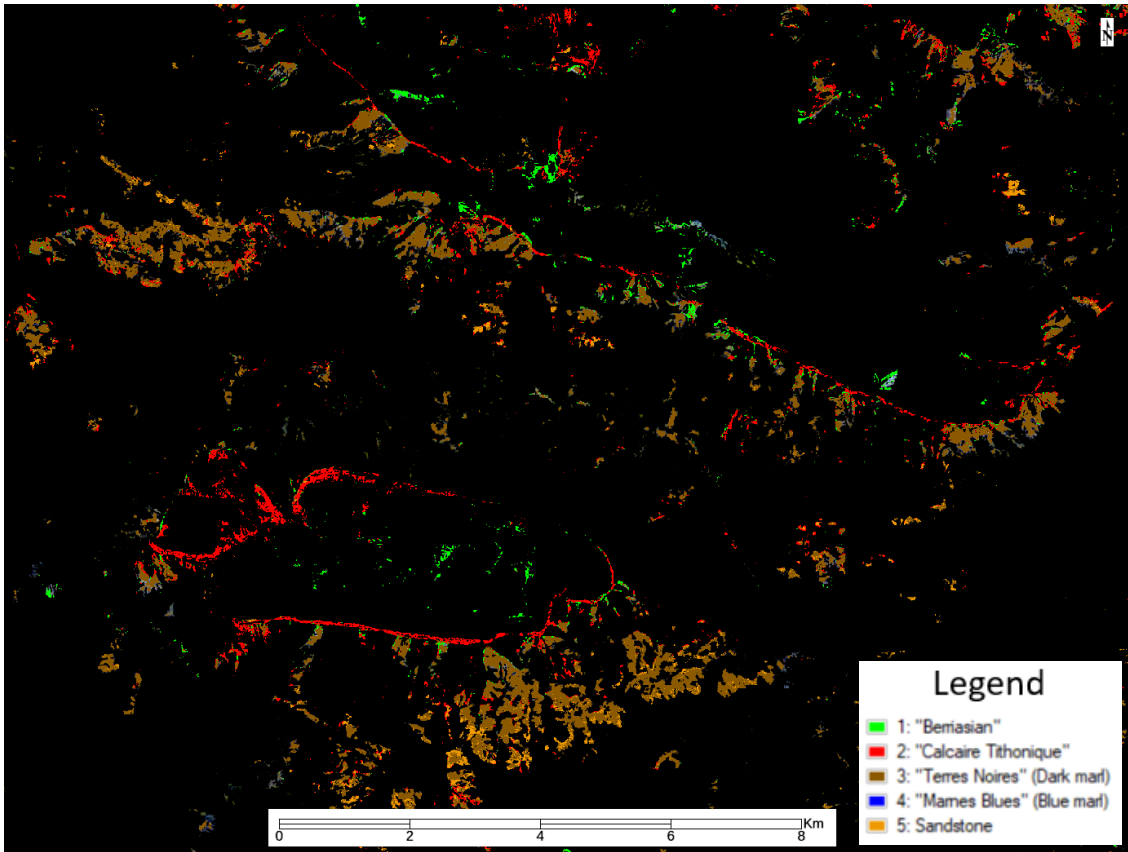


Figure 50: Sentinel-2 NN

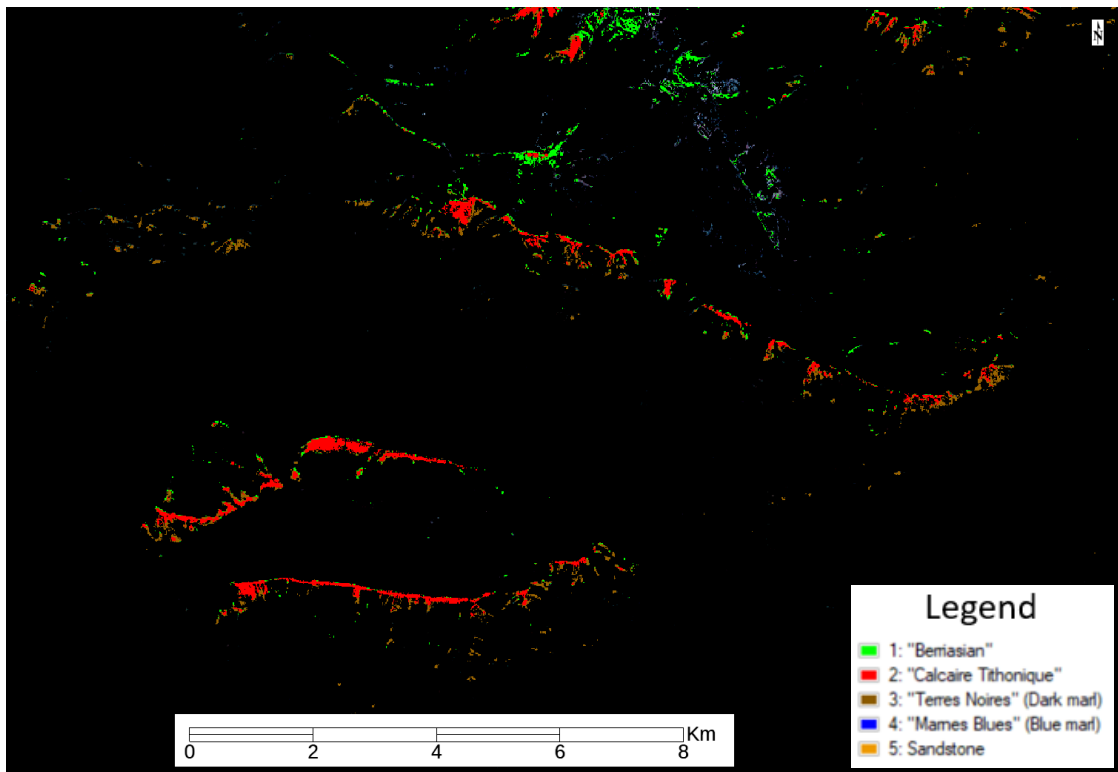


Figure 51: ASTER NN